Dissertation

submitted to the
Combined Faculty for Natural Sciences and Mathematics
of the Ruperto-Carola University of Heidelberg, Germany
for the degree of
Doctoral of Natural Sciences

presented by

Msc. Molecular Cell Biology Carlo Antonio Beretta
born in: Monza, Italy

Oral-examination:
April 26th, 2013

Long-term *in-vivo* analysis of habenular neurocircuit development identifies a thalamic bilateral cluster of early projecting cells (ThEPC) critical for interhemispheric communication and ventral habenula (vHb) formation

Referees: Prof. Dr. Joachim Wittbrodt
Dr. Soojin Ryu

Table of Content

SUMMARY **6**

ZUSAMMENFASSUNG **7**

1 INTRODUCTION **9**

1.1 Brain history and the discovery of brain asymmetry **11**

1.2 DDC system connects the habenulae nuclei in the limbic forebrain with midbrain limbic structures **12**

1.3 Habenular nuclei cell complexity **15**

1.4 Zebrafish as a model system to investigate neuronal networks formation **16**

1.4.1 Habenular cell complexity and main axonal innervations in the DDC system of zebrafish 17
1.4.2 Habenular neurogenesis 18
1.4.3 Asymmetric dHb axonal targeting within the IPN 20

1.5 Axon elongation process during the establishment of brain neuronal networks **22**

1.5.1 Axonal guidance: pioneering neurons and molecular cues 22
1.5.2 Molecular guidance cues are essential for axonal pathfinding 24
1.5.3 Midline immature glia are necessary for interhemispheric axonal communication 24

2 AIM OF THE THESIS **27**

3 RESULTS **29**

3.1 The *Et(1.0otpa:mmGFP)hd1* transgenic embryos express GFP in all habenular subnuclei and their efferent projections during DDC system formation **29**

3.2 Long-term 2-PM *in-vivo* microscopy can be used to follow the DDC system formation between 32 hpf and 5 dpf. **33**

3.3 Function of ThEPC neurons during the dHb network formation **37**

3.3.1 Long-term 2-PM *in-vivo* time-lapse discovers multiple interhemispheric connections during the habenular neuronal circuit establishment 37
3.3.2 ThEPC neurons located in one brain hemisphere are crucial for dHb axon migration and IPN targeting 38
3.3.3 dHb axonal pathfinding errors depend on the number of ablated ThEPC neurons 44
3.3.4 Unilateral dHb neuron ablation does not affect axonal IPN targeting on the contralateral side emphasising the specific importance of short- and long-range communication mediated by the ThEPC network 46

3.4 ThEPC neurons contribute to the ventral habenula architecture **48**

3.4.1 ThEPCs consist of different neuronal populations 48
3.4.2 ThEPC neurons contribute to the vHb subnucleus 50
3.4.3 *Tcf7l2* gene function is required for vHb development 52
3.4.4 The vHb cell subpopulation in ThEPCs is missing in *tcf7l2* mutants 53
Figure legends for Supplementary movies 56

4 DISCUSSION 59

4.1 Combining long-term 2-PM and automatic colour code labelling systems to study neuronal network formation *in-vivo* 60

4.2 dHb axonal pathfinding depends on the ThEPC neuronal network 63

4.3 ThEPC neurons promote brain interhemispheric long distance axonal communication 66

4.4 Unilateral ablation of one habenula does not influence dHb axon elongation and pathfinding on the contralateral brain side 69

4.5 Ventral habenular neurons originate in the thalamus and only develop in the presence of *tcf7l2* 71

5 EXPERIMENTAL PROCEDURES 74

5.1 Fish lines and maintenance 74

5.2 *Tcf7l2*^{exl} *x Et(-1.0otpa:mmGFP)hd1* genotyping 76

5.2.1 Genomic DNA extraction 76
5.2.2 PCR 77
5.2.3 BsajI restriction analysis 78

5.3 *In-situ* hybridization procedures 79

5.3.1 Plasmid preparations 79
5.3.2 *In-situ* probe transcription and purification 80
5.3.3 *In-situ* hybridization labelling 83
5.3.4 Antibody staining 85
5.3.5 Double fluorescence immuno-*in-situ* labellings 87

5.4 Long-term 2 photon (2-PM) *in-vivo* microscopy 88

5.4.1 Embryo embedding 88
5.4.2 Long-term 2-PM *in-vivo* microscopy - Experimental conditions 88
5.4.3 Long-term 2-PM *in-vivo* microscopy vs long-term CLSM *in-vivo* microscopy 89
5.4.4 2-PM laser ablation in *Et(-1.0otpa:mmGFP)hd1* embryos 90
5.4.5 Image colour code analysis 90

5.5 H2B photoswitchable monomeric orange (PSmOrange) subcloning 92

5.6 mRNA *in-vitro* transcription, purification and injection 94

5.6.1 mRNA *in-vitro* transcription 94
5.6.2 mRNA injection in zebrafish embryos 94

5.7 H2B-PSmOrange photoconversion and image analysis 95

5.8 Confocal Laser Scan Microscope (CLSM), image analysis and neuroanatomy 96

6 REFERENCES 97

7 APPENDIX 109

7.1 List of Abbreviations 109

7.2 List of figure and movie legends 112

7.3 Imagej Script: MIP_ColourCode.ijm 114

7.4 NIC Find Maxima Plugin 118

7.5 Imagej Macro: Colocalisation_H2B-PSmOrange.ijm 121

ACKNOWLEDGMENT 123

Summary

In the dorsal diencephalon of all vertebrates, the habenular neurocircuit transfers cognitive information from the forebrain into the ventral mid- and hindbrain via long axon fibers in the stria medullaris (SM) and fasciculus retroflexus (FR) on both sides of the brain. How these axons navigate through the brain and whether communication between brain hemispheres is required during the formation of this neuronal network is still an open question. The bilaterally formed habenulae in the dorsal diencephalon in zebrafish consist of the asymmetrically formed dorsal habenula nucleus (dHb) and the symmetric ventral habenula nucleus (vHb). While development of the dHb has been well described, the origin of the vHb and the genetic cascades underlying its development are not known.

We use the habenular network as a model to investigate how axon elongation is coordinated during embryonic development. This can best be done by recording its development *in-vivo*. As this neural circuit takes at least 4 days to develop and spans about 300 µm in anterior-posterior and dorso-ventral direction, we needed to develop a novel assay to investigate its development in the living zebrafish embryo. In our studies, we identified a transgenic line of zebrafish expressing GFP throughout the habenular neurocircuit development in all subnuclei and their efferent projections. Combining optimised *in-vivo* 2-photon (2-PM) long-term image recording and colour code analysis with focal laser ablation of neurons, we discovered a neuronal network essential for dorsal habenular axon elongation and pathfinding. We present evidence that a bilateral cluster of early projecting neurons in the thalamus (ThEPC) functions as intermediate target for dHb axonal elongation via ipsilateral short- and contralateral long-range axonal communication between the two brain hemispheres. Moreover, we show that a subset of ThEPC neurons contributes to the forming ventral habenula, which development is controlled by *tcf7l2* mediated Wnt/beta-catenin signalling.

Zusammenfassung

Im dorsalen Dienzephalon aller Vertebraten findet sich das habenulare Neuralnetz, das cognitive Informationen vom Vorder- ins Mittel- und Hinterhirn leitet. Dies geschieht über lange Axonbündel, die stria medullaris und den fasciculus retroflexus auf beiden Seiten des Gehirns. Wie genau diese Axone durch das Gehirn navigieren und ob Kommunikation zwischen den Gehirnhälften während der Ausbildung des neuronalen Netzwerks erforderlich ist, ist noch nicht geklärt. Im Zebrafisch bestehen die bilateral geformten Habenulae aus dem asymmetrisch geformten dorsalen habenularen Subnukleus (dHb) und dem symmetrisch ausgebildeten ventralen Subnukleus (vHb). Während viel über die Entstehung und Lokalisation des dHb bekannt ist, weiß man so gut wie nichts über die Entstehung des vHb.

Wir nutzen das habenulare Neuralnetz als Modellsystem, um herauszufinden, wie das Wachstum von Axonen auf beiden Seiten des Gehirns während der Embryonalentwicklung koordiniert wird. Dies kann am Besten im lebenden Organismus beobachtet werden. Da aber die Ausbildung des habenularen Netzwerks 4 Tage andauert und mit 300 µm Spannweite eines der Größten Netzwerke des Gehirns ist, mussten wir ein verfeinertes Imaging System entwickeln, um dessen Entwicklung "*in-vivo*" verfolgen zu können.

In unseren Studien identifizierten wir eine neue transgene Zebrafischlinie, die GFP während der gesamten Entwicklung des habenularen Neuralnetzes in allen Subnuklei und ihren efferenten Projektionen expremiert. Das Kombinieren von optimierten 2-PM Langzeitaufnahmen, der automatischen Farbgebung von Strukturen entlang der Z-Achse und dem Ablatieren von Neuralzellen ermöglichte es uns, ein neues Neuralnetz während seiner Entwicklung zu filmen und zu zeigen, dass es wichtig für das Wachstum und die Orientierung der dHb Axone ist. Wir zeigen weiterhin, dass eine bilateral angelegte Gruppe von Neuronen im Thalamus (ThEPC) als sogenanntes "Intermediate Target" für dHb Axone fungiert und über kurze und lange Distanzen bis auf die andere Seite des Gehirns mit dHb Axonen

kommuniziert. Des Weiteren fanden wir heraus, dass einige dieser ThEPC Zellen die vHb formen und sich nur in der Gegenwart von *tcf7l2* kontrollierter Wnt/beta-catenin Signalgebung ausbilden.

1 Introduction

The zebrafish (*Danio rerio*) dorsal diencephalon is one of the best systems to study brain asymmetry and lateralization. In our studies, we found that the dorsal diencephalic conduction (DDC) system of zebrafish can be used to investigate intra- and interhemispheric communication processes important for coordinated axon elongation during brain development.

The DDC system interconnects different brain structures localised along the anterior-posterior (A-P), dorso-ventral (D-V) and the left-right axis to establish a complex neuronal network implicated in behavior and cognitive function. In the last two decades, a lot of information on DDC system development has been collected using the zebrafish model. However, the lack in specific transgenic lines expressing fluorescent protein during the main events of DDC formation necessary for in vivo studies makes it rather difficult to draw conclusions about the key-dynamic processes important for network formation.

Habenular efferent projections on either brain hemisphere travel in a seemingly coordinated manner about 300 µm far to reach their target in the ventral midbrain. How this is achieved is unknown, but it appears that the axons on either brain hemisphere communicate with each other. Axonal commissures connect brain hemispheres at multiple locations along the neuraxis, which could potentially allow for such exchange of information. However, studies on fixed embryos only revealed a prominent commissure connecting the habenulae themselves but not the ipsilaterally projecting axons. The potential contribution of the habenula commissure and or other components of the DDC system to axon guidance and elongation can best be studied in vivo. Therefore I established an optimised 2-PM based long-term time-lapse assay combined with computational colour coding of z-positions to follow DDC development over 4 days, the time by which habenular axons have innervated their targets.

In the following, I will give an overview on the history of studies on the habenular neural network and our current knowledge with a particular focus on the zebrafish model system.

1.1 Brain history and the discovery of brain asymmetry

The studies of brain anatomy and brain function have fascinated scientists since thousands of years. The earliest evidences for brain research derive from ancient civilisation documents. The word "brain" was mentioned for the first time in an Egyptian papyrus, known as the Edwin Smith Surgical Papyrus, written around the year 1700 BC. This document is the first proof of brain studies in which 48 cases of brain injuries with different recommended treatments were collected (Breasted JH., 1930). Moving from the Egyptian papyrus throughout the scientific history, different hot spots in brain research can be found. The first one to be mentioned concerns the discoveries of Herophilus, “the father of Anatomy”, that wrote between 335 BC and 280 BC at least nine works about human body architecture. In the subsequent 1500 years, many "scientists" described anatomical brain subdivisions, the cranial nerves, some mental diseases but one of the most fertile times for brain discovery was during the Renaissance. At this time, Leonardo da Vinci described with different models the brain structures and introduced the concept of anatomical brain asymmetry (Bell and Sons, 1897). The discovery of a functional brain asymmetry had to wait until the pioneering findings of Paul Broca; in his studies he proved the function of the left brain hemisphere in the language control (Broca, P., 1861). Since then, many anatomical brain structures have been carefully described in human and in many other vertebrate species proving a high conservation of functional brain lateralisation for sensory and cognitive processes. For instance, the discoveries of James Papez (1937) and the subsequent studies of Paul D. MacLean (1950) highlighted the cognitive and sensory function of limbic system making it an excellent model for neuronal networks investigations (Beretta et al., 2012).

1.2 DDC system connects the habenulae nuclei in the limbic forebrain with midbrain limbic structures

The limbic system is a complex of structures in the forebrain and midbrain, which consists of several neurotransmitter pathways involved in behavior, emotion, memory and olfaction (Hikosaka, 2010). The main components of the limbic system are the prefrontal cortex, cingulate cortex, amygdaloid nuclear complex, limbic thalamus, hippocampal formation, nucleus accumbeus, anterior hypothalamus, ventral tegmental area and midbrain raphe nuclei (Figure 1.1); (Morgane PJ et all., 2005). Two major associated networks connect the limbic forebrain with the limbic structures located in the midbrain of vertebrate species. The medial forebrain bundle (MFB) interconnects the anterior olfactory areas (OA) with the lateral preoptic (LPO), lateral hypothalamic (LH) and ventral tegmental area (VTA). The DDC system exchanges information between the medial forebrain bundle and the habenulae nuclei (Hb) through the stria medullaris (SM) and connects the habenulae nuclei with the ventral midbrain area via axons of the fasciculus retroflexus (FR); (Figure 1.1); (Sutherland, 1982; Morgane et al., 2005).

The stria medullaris, also known as stria medullaris thalami or stria habenularis, is part of the epithalamus and it mainly consists of a bundle of habenular afferent projections running along the lateral margin of the third ventricular surface, interconnecting the medial basal forebrain (anterior hypothalamus and septal nuclei) with the habenulae nuclei. The fasciculus retroflexus is a compacted bundle of efferent fibers arising in the habenulae nuclei and mainly target structures in the ventral midbrain/hindbrain, such as interpeduncular nucleus (IPN) and median raphe (MR).

The DDC system functions in association with different limbic forebrain components and it was found that modifications in DDC neuronal network causes psychological alteration such as depression, anxiety, schizophrenia and neuropathological responses to addictive drugs (Caldecott-Hazard et al., 1988; Ellison, 2002; Lecourtier et al., 2004; Yang et al., 2008; Agetsuma et al., 2011). Additionally, investigations on the DDC neuronal network demonstrated a function in the secretion of melatonin hormones, mediated by pineal organ connections, implicating a regulation of sleep and circadian

rhythm (Klein and Moore, 1979; Valjakka et al., 1998; Falcon et al., 1999). Moreover, DDC neurons act as a modulator of dopaminergic and GABAergic neurons and function in behaviors and learning processes (Lisoprawski et al., 1980; Lee and Huang, 1988; Lecoutier and Kelly, 2005).

The identified connections and functions carried out during the processing of stimuli make the DDC neuronal network an suitable model to investigate complex brain processes (Aramaki and Hatta, 2006).

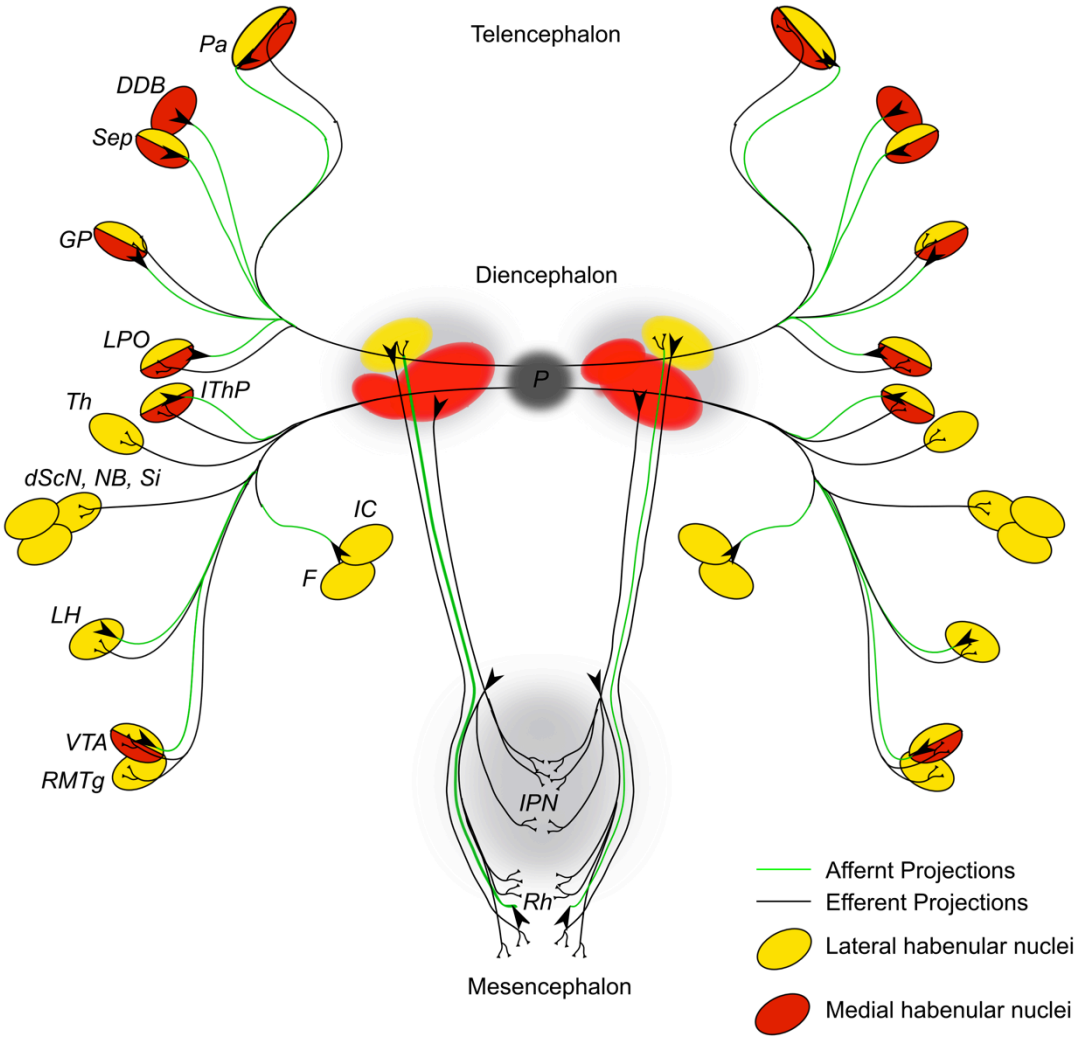

Figure 1.1: DDC neuronal network complexity in the mammalian brain.
Simplified schematic diagram of the main afferent (green lines) and efferent connections (black lines) of the DDC system in the mammalian brain. Targets and origins of axons related to the lateral habenulae are highlighted in yellow; those of the medial habenulae in red.

DDB, nucleus of diagonal band; dScN, dorsal superchiasmatic nucleus; F, fornix; GP, globus pallidus (primate homologue of the teleost entopeduncular nucleus); IC, internal capsule; IThP, inferior thalamic peduncle; LH, lateral hypothalamic area; LPO, lateral preoptic area; NB, nucleus basalis; P, pineal; Pa, pallium; Sep, septum; Si, substantia innominate; Th, thalamic nuclei; VTA, ventral tegmental area of Tsai. (Modified from Beretta et al., 2012).

1.3 Habenular nuclei cell complexity

A highly conserved neuronal networks described in the vertebrate brain is the DDC neurocircuit, which interconnects the habenulae nuclei with different brain targets located in the anterior forebrain and in the ventral midbrain and hindbrain (Figures 1.1,1.2); (Sutherland, 1982). The habenular structure consists of two bilaterally symmetric nuclei located dorsal to the posterior part of the thalamus adjacent to the third ventricle (Guillery, 1959; Cragg, 1961; Morgane et al., 2005). In mammalian, each habenula can grossly be subdivided into a medial and lateral nucleus corresponding to dorsal and ventral nuclei in amphibians, fish and reptiles respectively (Figures 1.1,1.2); (Concha and Wilson, 2001; Amo et al., 2010).

The dorsal habenulae display a left-right asymmetry across the midline with respect to morphology, axonal projections and gene expression and can be subdivided into lateral and medial habenula subnuclei (Figure 1.2); (Goronowitsch, 1883; Concha and Wilson, 2001; Gamse et al., 2003, 2005; Guglielmotti and Cristino, 2006). Contrary to the dorsal habenula, the ventral habenula is symmetric in cell composition, gene expression and in the pattern of innervations in the ventral hindbrain target (Figure 1.2); (Amo et al., 2010).

The efferent axonal targets of habenular nuclei were investigated in different vertebrate species using diverse approaches mainly based on horseradish peroxidase (HRP) injection, radioactive labelling, anterograde fibers degeneration experiments and lipophilic dye labelling (Beretta et al., 2012). Using these systems it was possible to identify the IPN and the MR as the main midbrain targets of habenulae nuclei efferent projections (Figures 1.1,1.2).

1.4 Zebrafish as a model system to investigate neuronal networks formation

In the last two decades, zebrafish became a suitable vertebrate model system to investigate *in-vivo* neuronal network formation. The advantages of zebrafish to follow developmental processes in living animals are related to the possibility to combine its transparency and external development with genetic tools and transgenesis. The availability of the several teleost genome sequences including zebrafish allows for comparative studies between vertebrate species and increases the potential applications of this model system to investigate complex developmental processes also in respect to evolutionary conservation. In zebrafish, DDC establishment requires approximately 4 days of development making the investigation of this system *in-vivo,* over the time, potentially reliable in comparison to other vertebrate models (Altman and Bayer, 1979). Unfortunately, the absence of transgenic tools to label habenular network components throughout their development and appropriate long-term imaging systems made it impossible until now to study its formation in living embryos (Beretta et al 2012). To acquire new knowledge on DDC system development and to understand more about the spatio-temporal events, new transgenic tools and imaging systems are necessary to record its formation *in-vivo*. This would allow to combine long-term imaging with genetic manipulations (Del Bene and Wyart, 2011) to visualise and compare *in-vivo* the DDC neuronal network establishment between wild type and manipulated embryos. This would open avenues to understand and correlate neuronal network function and embryonic behavior.

1.4.1 Habenular cell complexity and main axonal innervations in the DDC system of zebrafish

The habenular neurocircuit is conserved between vertebrate species. In fish, the habenular nuclei are subdivided in the dorsal (dHb) and ventral habenula (vHb) domain (Concha and Wilson, 2001; Amo et al., 2010). Several gene members of the potassium channel tetramerization domain (KCTD) familly are found to be expressed in the dHb asymmetrically across the left-right axis starting from 48 hpf (Gamse et al. 2003, 2005). Combining marker gene analyses with lipophilic dye labellings it was found that the lateral subnucleus is larger on the left brain side and it is manly sending axonal projections into the dorsal part of the IPN (dIPN). Conversely, the medial habenular subnucleus of the dHb is larger on the right hemisphere and its axons predominately target the ventral part of the IPN (vIPN). Therefore, left-right asymmetry displayed in the dHb is transformed during DDC system development into a dorso-ventral asymmetry in the midbrain target (Figure 1.2); (Gamse et al., 2005; Aizawa et al., 2006; Bianco et al., 2009).

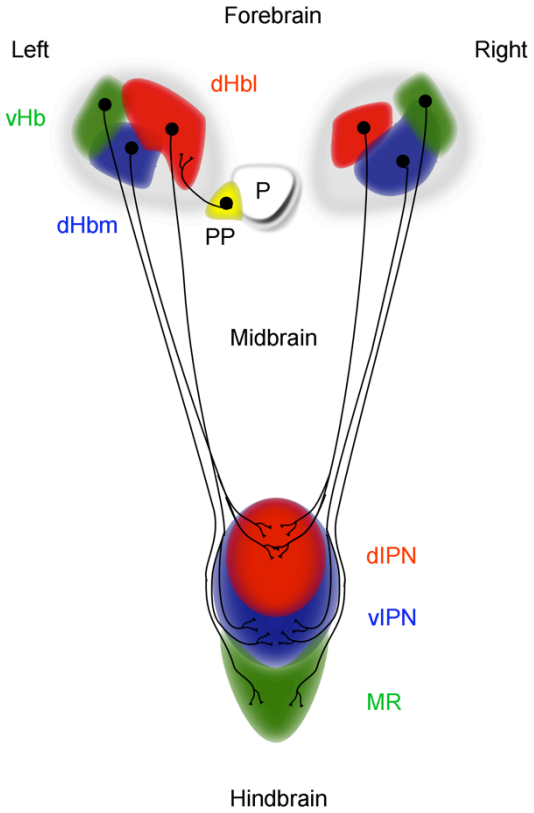

Figure 1.2: Habenular neuronal network in the zebrafish brain.
Schematic of the habenular cell composition and efferent axonal projections innervating the interpeduncular nucleus (IPN) in 4 day old zebrafish embryos. The habenular nuclei are subdivided into lateral (red), medial (blue) and ventral (green) domains. Hb, habenula; dHbl, lateral dorsal habenula; dHbm, medial dorsal habenula; IPN, interpeduncular nucleus; MR, median raphe; P, pineal organ; PP, parapineal organ; d: dorsal; v, ventral.
(Modified from Beretta et al., 2012).

The zebrafish vHb has been discovery recently by applying tract-tracing techniques to identify axons that project to the MR, the main target of mammalian lateral efferent neurons (Herkenham and Nauta, 1979), homologous of vHb (Figure 1.2); (Amo et al., 2010). Gene expression analysis in zebrafish revealed that vHb neurons express symmetrically the cell-cell adhesion marker protocadherin 10a (Hirano et al., 2010). This gene is expressed specifically in the mammalian lateral habenular neurons indicating the evolutionary conservation of the vHb in zebrafish. Supporting this observation, the expression of vHb markers is localised only to neurons that target especially the MR nucleus (Amo et al., 2010). Previous studies performed in the mammalian lateral habenular were showing the serotoninergic character of the axons innervating the MR (Nishikawa T. and Scatton B., 1985). Anti-serotonin antibody stainings on fixed zebrafish embryos showed that the vHb is sending projection in the hindbrain to form serotoninergic synapsis with the MR nucleus (Amo et al., 2010).

1.4.2 Habenular neurogenesis

In the last two decades, the understanding of habenular neurocircuit formation and function increasingly attracted neuroscientists. Most of the data collected on the development of habenulae nuclei, the habenular neuronal network formation and the underlying genetic cascades were obtained mainly through labellings at fixed developmental stages in wild type embryos and in mutant lines (Halpern et al., 2003; Aizawa et al., 2007; Carl et al., 2007; Beretta et al., 2012).
The formation of dHb nuclei starts after somitogenesis from a bilateral symmetric pool of neuroectoderm progenitor cells located in the dorsal

diencephalon adjacent to the pineal organ (Aizawa et al., 2007, Roussigne et al., 2009). Using BrdU labellings it was found that the precursor cells on the left brain side start to proliferate at 24 hpf followed by the progenitor cells on the right brain hemisphere (Aizawa et al., 2007). The location of dHb precursor cells on the left and the right hemisphere was determined using *cxcr4b* as the only dHb precursor marker (Roussigne et al., 2009). *Cxcr4b in-situ* stainings revealed that number of dHb precursor cells is early higher on the left brain hemisphere equalizing subsequently between the left and the right brain side. The reason for the asymmetric proliferation of the dHb precursor cells is unknown. However, these data support the hypothesis that the dHb nuclei formation may depend on an asymmetric proliferation process but do not exclude other possible mechanisms. To investigate, whether differentiation is involved during habenular nuclei neurogenesis, the early expression of lateral and medial marker genes and Brdu labeled embryos at different stages of development were analysed (Aizawa et al., 2007; Roussigne et al., 2009). Around 28 hpf, the progenitor cells located on the left and right brain hemispheres start to acquire the lateral character and build up the lateral subnuclei. Subsequent to the initial steps of lateral habenular (dHbl) formation, the medial habenulae (dHbm) neurons start to differentiate from a sub-cluster of dHb precursor cells to organise the medial habenula subnuclei. This data suggest that left-right asymmetry is not only dependent on asymmetric proliferation but also depends on the differentiation of dHb precursors cells. Indeed, the process of development of dHbl and dHbm cells is asymmetric between the left and the right axis. The entire process of habenular nuclei formation ends around 72 hpf. Simultaneously to the establishment of left-right asymmetry dHb efferent axons elongate starting around 45-48 hpf and innervate the IPN by 4 dpf (Aizawa et al., 2007; Bianco et al., 2008; Roussigne et al., 2009).

Three molecular pathways have been identified involved in dHbl and dHbm formation: the Wnt/beta-catenin pathway (Carl et al, 2007), Notch pathway (Aizawa et al, 2007) and Nodal signaling pathway (Regan et al, 2009). Further investigations are still necessary to completely understand the mechanism underlying the establishment of left-right asymmetry.

Concerning the vHb nucleus neurogenesis nothing is known. The lack in appropriate transgenic tools and early molecular markers made it impossible to investigate the source of progenitor cells and the underlying molecular pathways. Therefore, the study of vHb origin is still a challenging task that neuroscientists have to investigate.

1.4.3 Asymmetric dHb axonal targeting within the IPN

dHb development has been well studied, but we only begin to understand dHb axonal elongation and targeting. In zebrafish, the dHb efferent axons form bundles on both hemispheres and they navigate through the brain for approximately 300 µm to reach the targets in the ventral midbrain. dHb efferent axon labellings using lipophilic dyes have shown that both habenular neurons located in the left and in the right hemisphere target the IPN nucleus. (Aizawa et al., 2005). The dHb efferent axons start to project simultaneously at 45-48 hpf from both habenulae nuclei and elongate in a coordinated process, which is completed at 5 dpf (Bianco et al., 2008). dHb efferent axons realised different types of neurotransmitters in the IPN. For instance, high levels of acetylcholine, choline acetyltransferase, acetylcholine esterase, GABA, monoamines, neuropeptides, serotonins and dopamine were found in the IPN (Hattori et al., 1977; Staines et al., 1980; Bianco and Wilson, 2009).
Different studies on the genetics underlying the development of dHb nuclei asymmetry suggest that habenular efferent axons receive crucial targeting information from their respective unipolar projecting neurons. In wildtype embryos, the lateral subnucleus is larger on the left brain side and it is targeting the dIPN (Aizawa et al., 2005; Gamse et al., 2005). The medial habenular subnucleus of dHb is larger on the right brain hemisphere and its efferent axons are innervating the vIPN. The laterotopic segregation of these axons was shown to be absent in mutants in which dHb left-right asymmetry is converted in a symmetric lateral and medial predominate character (Carl et al 2007, Carl, personal communication). These findings support the hypothesis that dHb neurons specification is primary in the decision of which target will be innervated from their axons. However, the only known molecule

implicated in dHb neuronal pathfinding is neuropilin1a expressed in the left dHb neurons (Kuan et al., 2007). The identification of guidance components involved in dHb efferent axonal pathfinding is essential to understand indeed the entire process of IPN innervation. Unfortunately, our knowledge on development of habenular neural network is almost exclusively derived from the analysis of fixed samples in a wildtype and mutant background. Insights into the dynamic process of dHb neural network establishment for identification of key-events can only be obtained using an *in-vivo* system.

1.5 Axon elongation process during the establishment of brain neuronal networks

During brain development the process of axonal elongation is influenced by a heterogeneous array of components and molecules, which function is essential for axonal guidance and pathfinding. The mechanisms of axonal elongation are well described in different neuronal networks, such as the corpus callosum (Mizuno et al., 2007), olfactory system (Raper and Mason, 2010; Imai and Sakano, 2011; Miyasaka et al., 2012) and the retinotectal axons (Pittman et al., 2008; Raper and Mason, 2010).
The information collected on these neuronal networks may be used to compare and contrast, how the dHb efferent axon navigate through the brain to reach their target in the ventral midbrain.

1.5.1 Axonal guidance: pioneering neurons and molecular cues

The process of axonal guidance was described for the first time in the studies of Ramon y Cajal, in which he recognised that axons grow towards their ultimate targets. He suggested that axonal guidance depends on molecular cues able to attract and guide the growing axons in the direction of their target (Ramon y Cajal, 1892; trans. English 1995). The preliminary results on the function of cues during axonal guidance obtained by Ramon y Cajal found confirmation for instance, in the studies of retinotectal axons, with the identification of the gradient of Ephs and ephrins necessary for axonal pathfinding of retina neurons (Cheng et al., 1995; Feldheim et al., 2000; Hindges et al., 2002; McLaughlin et al., 2003).
The identification of the molecular cues, responsible for axonal guidance and targeting, opened important questions concerning the possible pioneering function of early projecting neurons. Preliminary observations in invertebrate species (Bate, 1976; Edwards, 1977; Keshishian, 1980) and studies performed in chicken (Tello, 1923) and in zebrafish embryos (Chitnis and Kuwada, 1990; Wilson et al., 1990; Ross et al., 1992) suggested that the early axons were growing along stereotyped routes to organise a scaffold for subsequent follower axons. For instance, ablation of pioneer neurons

perturbed the guidance of subsequently growing axons with a delay or misrouting of them (Edwards et al., 1981; Durbin, 1987; Pike et al., 1992; Hutter, 2003). However, in most of the experiments performed in invertebrate and vertebrate models, the follower axons were able to reach their appropriate targets and only in rare cases, a complete miss targeting of subsequently growing axons was observed (Raper and Mason, 2010). These findings suggest that the pioneer neurons are mainly increasing the targeting efficiency of the follower axons.

A crucial question that neuroscientists tried to answer since the discovery of pioneer neurons was how their axons can find the route to reach their appropriate targets. Deflection experiments of pioneer trajectories in the leg of insect embryos demonstrated the essential function of intermediate neurons in the guidance of pioneer axons (Bentley and Caudy, 1983). Indeed, ablation of intermediate targets located on the route of trajectories of pioneer axons, cause abnormalities in their pathfinding suggesting that intermediate targets provide navigational information to the pioneers.

Pioneer neurons are influenced by different molecular cues and construct a basic scaffold between different targets during the early stage of development (Raper et al., 1984; Bastiani et al., 1984). The definition of pioneer trajectories depends on short-range interactions between the pioneer axons and the intermediate targets that provide the navigation cues necessary for their correct pathfinding. Once the pioneer scaffold is organised, the follower axons can elongate on them guided by molecular gradients and by axon–axon interactions with the pioneer axons in the direction of the specific targets. For instance, in fly eye it was found that hemophilic adhesive interactions are essential to assemble axons belonging to the same ommatidial bundle. Conversely, repulsive/antifasciculation interactions between heterotypic bundles allow the segregation of fibers important to reach different targets (Chen and Clandinin, 2008).

1.5.2 Molecular guidance cues are essential for axonal pathfinding

The existence of reproducible pattern of axonal innervation depends on a conserved mechanism able to guide axons in the direction of their targets independently from embryo to embryo. In the last two decades, many *in-vivo* and *in-vitro* assays were developed to identify molecules involved in axonal guidance. These experiments allowed the identification of at least four different categories of cues acting at various levels necessary for axonal guidance and pathfinding:

1. Adhesion cues, such as extracellular matrix components (ECM) and cell adhesion molecules (CAMs) guide axons throughout permissive or nonpermissive substrates (Schmid and Manes, 2008).
2. Trophic cues promote neuronal growth cone mobility, axon out-growth, directionality and neuronal survival (Connolly et al., 1985; O'Connor and Tessier-Lavigne, 1999; Marshak et al., 2007).
3. Tropic cues, such as netrin, are influencing growth cone mobility and directionality (Colamarino and Tessier-Lavigne, 1995).
4. Modulatory guidance cues modulate the axonal response to tropic cues (Dontchev and Letourneau, 2002). In general, these molecules interact with specific receptors located on the membrane of axons modulating the growth (Raper and Mason, 2010).

1.5.3 Midline immature glia are necessary for interhemispheric axonal communication

Midline glia cells are an essential source of molecular cues, necessary for midline axonal crossing for instance in the forebrain, optic chiasm and spinal cord. Glial cells at the midline express different types of molecules attracting or repelling incoming axons. For instance, during optic chiasm formation in mouse, a transient population of pioneer neurons is able to guide retinal axons through the midline (Mizuno et al., 2007). The pioneer axons interact with specialised radial glia cells at the optic chiasm midline promoting or

inhibiting the navigation across the midline of the follower retinal axons (Sretavan et al., 1994; Marcus et al., 1995 and Marcus and Mason, 1995). Several tropic guidance cues were found to be implicated in the attraction and repulsion of crossing axons. *Netrin/unc6* is secreted in the ventral midline of vertebrate and invertebrate species promoting ipsilateral or contralateral axonal migration. In the spinal cord, the Deleted in Colon-rectal Carcinoma (DCC) receptor is expressed in the commissural axons and the interaction between *netrin* ligand and DCC receptors is essential for axonal guidance across the ventral midline (Serafini et al., 1996; Fazeli et al., 1997).

As mentioned above, the midline glia express different molecules important for axonal attraction and repulsion. For instance, in the floor plate, *netrin and shh* genes are expressed in non-neuronal cells regulating the crossing of the incoming axons. An interesting aspect is how the crossed axons proceed in the direction of their target instead of crossing back again the midline. Data collected in fly show that the temporary regulation of protein compositions at the axonal tip before and after the crossing is essential to determine the axonal fate. For instance, in the floor plate pre-crossing axons express a functional form of Robo receptors that are immediately degraded after midline crossing (Keleman et al., 2002). A second mechanism identified in the ventral midline of vertebrate species is the silencing of netrin-mediated attraction. In the early stages of development, *netrin* is expressed in the ventral midline allowing midline crossings of DCC positive axons. Later in the development *netrin* is silenced and this inhibits axonal midline crossings (Nawabi and Castellani, 2011). These findings suggest that midline crossing is influencing the nature of pre-crossing and post-crossing axons, mainly regulating transcriptional and post-transcriptional levels. Moreover, midline properties can change over the time of embryonic development controlling the ipsilateral and contralateral axonal elongation behavior (Nawabi and Castellani, 2011).

In summary, the successful establishment of neuronal networks across the midline depends on coordinated spatio-temporal expression of molecular cues and guidance receptors over the embryonic developmental time.

In our studies, we combined long-term *in-vivo* 2 photon microscopy (2-PM) and colour code analysis to follow habenular neuronal network formation in a

novel enhancer trap transgenic line of zebrafish expressing GFP between 32 hpf and at least 5 dpf. We identified a bilateral cluster of early projecting neurons with a thalamic origin, which neurons contribute to the vHb architecture under the influence of Wnt signialing, mediated by *tcf7l2* gene activity.

Additionally, we discovered that dHb efferent axons cross during DDC system formation a subset of ThEPC neurons. We suggest that ThEPC neurons function as intermediate target essential for axonal guidance of dHb efferent axons. For instance, unilateral ablation of ThEPC neurons followed by long-term *in-vivo* 2-PM highlight the arrestment in the elongation of dHb efferent axons in both brain hemispheres. Our results are consistent with a model based on ThEPC interhemispheric axonal communication across the midline crucial for axonal elongation and pathfinding. We speculate that ThEPC axonal interhemispheric crossings may influence the midline proprieties influencing the ThEPC located in the bran counterpart and consequently the dHb axon elongation and pathfinding in both brain hemispheres.

2 Aim of the thesis

Interhemispheric communication in the brain is one of the most fascinating fields in neuroscience. The identification of long-range guidance molecules and axonal commissures connecting the left and right brain hemispheres brought up the idea that brain hemispheres integrate incoming stimuli before responding to them. For instance, the brain hemispheres can be compared with computer disk driver systems composed of different logical units, in which every element functions on its own but also in concert with other units to generate a specific response to a certain stimulus. How these units/interhemispheric networks are organised and whether the communication between the two forming brain hemispheres influences the final architecture and function of the brain are fundamental questions.

In my project, I overcame the limitations of analyzing fixed developmental stages by imaging a novel zebrafish *Et(1.0otpa:mmGFP)hd1* transgenic line labelling the habenular neural network throughout its development. I developed a new protocol for long-term image recording to follow the formation of DDC neuronal network in living transgenic embryos using 2-photon microscopy (2-PM). Combing the 2-PM and focal laser cell ablation with a new automatic colour code algorithm, I identified a so far unknown hemisphere spanning neuronal network essential for dorsal habenular (dHb) axon elongation and pathfinding mediated by a bilateral cluster of early projecting cells located in the thalamus (ThEPC). Using 2-PM, colour code analysis and laser ablation, I investigated the following aspects:

- Spatial and temporal sequence of events during DDC formation in living embryos
- ThEPC neural network formation and nature of ThEPC neurons
- ThEPC neuron function in ipsilateral short- and contralateral long-range axonal communication for dHb axonal elongation and pathfinding

- Interhemispheric communication within the dHb network important for efferent axon elongation and targeting.

The analysis of *Et(1.0otpa:mmGFP)hd1* transgenic embryos provided a detailed description of the main events of DDC system formation and highlighted the crucial role of ThEPC long-range interhemispheric axonal communication for dHb axonal elongation and pathfinding. Moreover, ThEPCs consist of a heterogeneous assembly of neurons, some of which contribute to the ventral habenula (vHb). I established the photoswitchable mOrange protein system for the zebrafish and combined it with a newly colocalisation ImageJ macro to investigate the following aspects:

- The origin of vHb neurons
- Involvement of Wnt/beta-catenin pathway signalling in vHb formation

Using this approach, I identified the source of vHb neurons in the ThEPCs and Wnt pathway gene *tcf7l2* as the first gene involved during vHb development.

3 Results

3.1 The *Et(1.0otpa:mmGFP)hd1* transgenic embryos express GFP in all habenular subnuclei and their efferent projections during DDC system formation

Available transgenic lines start to express GFP in the DDC (dorsal diencephalic conduction) system when the main events have already occurred and are not suitable to investigate *in-vivo* habenular network formation (Aizawa et al., 2007; Wen et al., 2008). In an enhancer trap screen in the laboratory of Soojin Ryu, Max Planck Institute Heidelberg, a novel transgenic line was identified, in which GFP is strongly expressed in the habenulae and their efferent projection.

We initially analyzed GFP expression in the *Et(1.0otpa:mmGFP)hd1* line at 4 dpf (day post fertilization) by co-labelling GFP and α-acetylated tubulin. In these preliminary studies, we found that GFP positive neurons overlap with the habenular neuropil marker suggesting that GFP is potentially expressed in all habenular domains (Figure 3.1A). We further labeled the *Et(1.0otpa:mmGFP)hd1* transgenic embryos with other habenular markers specific for the different habenular subpopulations. The dorso-lateral (dHbl) *kctd12.1*, the dorso-medial (dHbm) *kctd8* (Gamse et al., 2003, 2005) and the ventral (vHb) *kisspeptin-1* (Servili et al., 2011; Ogawa et al., 2012) habenular marker all overlap with *hd1:GFP* transgene expression, demonstrating that all habenulae sub-domains are labeled (Figures 3.1B-D).

At 4 dpf, Hb axons innervate the interpeduncular nucleus (IPN) and the median raphe (MR) located in the mesencephalon and rhombencephalon respectively (Bianco et al., 2009 and Beretta et al., 2012). To investigate the innervation of these two targets, we imaged *Et(1.0otpa:mmGFP)hd1* embryos using 2 photon microscopy (2-PM). Our experiments show axonal innervations of both structures confirming that GFP is expressed in all the

habenular subpopulations and in the major habenulae efferent axons (Figures 3.1E-G).

It is known that the dHb neurons start to differentiate around 32 hpf (hour post fertilization) from a *cxcr4b* expressing pool of progenitor cells located on both sides of pineal complex, in the center of the epithalamus (Aizawa et al., 2007; Roussigne et al., 2009). To assess GFP expression in the dHb precursor neurons in *Et(-1.0otpa:mmGFP)hd1* transgenic embryos, confocal stacks were acquired at 32 hpf. Our analysis shows that GFP starts to be expressed at this stage in a bilateral cluster of projecting neurons posterior and lateral to the dHb cells domain (Figure 3.4A and movies S1,S2). To characterise this bilateral cluster of neurons, co-stainings using different diencephalic markers were performed at 32 hpf. These cells express the prosomere 2 marker *lhx2b* (Seth et al., 2006; Peukert et al., 2011), but not the prosomere 1 (pretectum) markers *lhx1a* (Toyama et al., 1995) and *nr4a2a* (Filippi et al., 2007; Blin et al., 2008) or Calretinin expressed in the nucleus of the medial longitudinal fascicle (Nmlf); (Castro et al., 2006); (Figure 3.1H and Figures 3.2A-C). Additional images acquired later during the DDC system development show that GFP starts to be expressed in the dHb domain around 45 hpf (Figure 3.4C). To characterize these cell clusters, immuno *in-situ* stainings for *cxcr4b* and GFP were carried out and showed that GFP is expressed dorsally adjacent to *cxcr4b* positive dHb progenitor cells. This region has been shown to contain differentiated dHb cells (Gamse et al., 2003, 2005). These data indicate that in *Et(-1.0otpa:mmGFP)hd1* transgenic embryos GFP is expressed in differenced cells of the dHb at this stage of development (Figures 3.2E-E'').

All these observations make the *Et(-1.0otpa:mmGFP)hd1* transgenic line an excellent readout system to investigate the habenular neuronal circuit formation *in-vivo*. Moreover, we discovered a cluster of neurons which develops before and during the DDC system organisation. In agreement with the location of these neurons and the fact that they start projecting axons earlier than dHb axons, we refer to them as thalamic-epithalamic early projecting cluster (ThEPC).

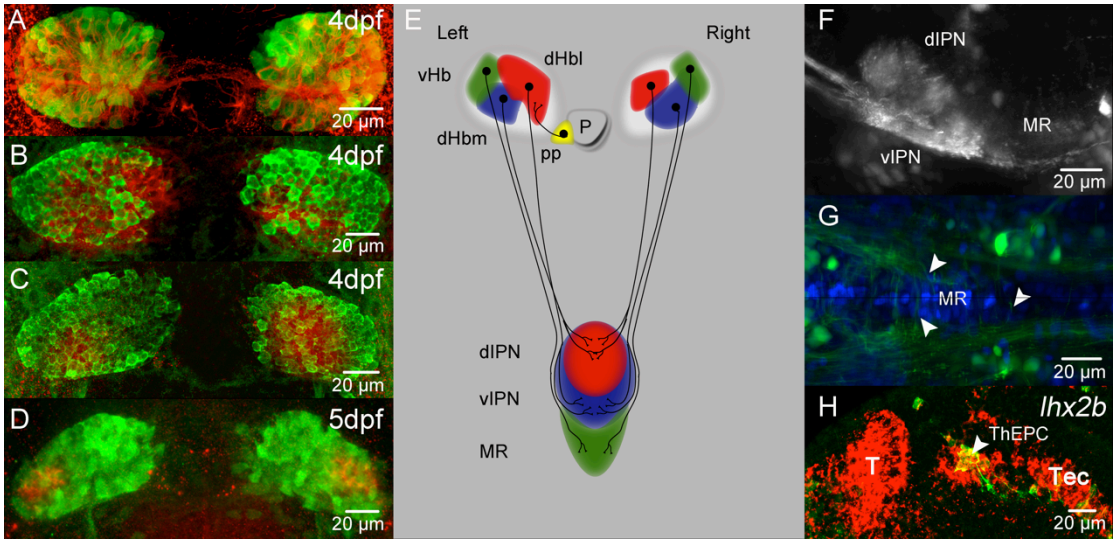

Figure 3.1: All habenular domains and efferent projections innervating the ventral mid- and hindbrain are labelled in *Et(-1.0otpa:mmGFP)hd1* transgenic embryos.

(A-D) Dorsal views, MIP, anterior to the top, focussed on the habenular nuclei in the *Et(1.0otpa:mmGFP)hd1* transgenic line. At 4 dpf, GFP expression overlaps with (A) acetylated tubulin, (B) the dHbl marker *kctd12.1*, (C) the dHbm marker *kctd8* and (D) at 5 dpf with the vHb marker *kisspeptin-1*.

(E) Scheme of habenular cell complexity and efferent axonal projections innervating IPN and MR in 5 dpf old embryos. The habenular nuclei are subdivided into lateral (red), medial (blue) and ventral (green) domains.

(F) Lateral view, anterior to the left, MIP, of habenular efferent projections innervating their targets in the ventral midbrain at 4 dpf in *Et(1.0otpa:mmGFP)hd1* transgenic embryos.

(G) Dorsal view, anterior to the left, MIP, of MR innervating axonal projections in 3 dpf *Et(1.0otpa:mmGFP)hd1* embryos. The nuclei (blue) are labelled with H2A-CFP; the arrowheads highlight axons entering in the MR.

(H) Lateral view, anterior to the left, MIP, immuno/*in-situ* labelling of *Et(1.0otpa:mmGFP)hd1* transgenic embryos at 32 hpf. ThEPCs (arrowhead) are labelled in green. The thalamic marker *lhx2b* (red) colocalises with the GFP expressing ThEPC cells.

(A-D, F-H) For all images, the scale bar is displayed in the right bottom corner. The gamma was corrected to values between 0.80 and 0.60 for display purposes.

d, dorsal; dHbl, lateral dorsal habenula; dHbm, medial dorsal habenula; dpf, days post fertilization; hpf, hours post fertilization; IPN, interpeduncular nucleus; MR, median raphe; MIP, Maximum Intensity Projection; P, pineal; pp, parapineal; T, telencephalon; ThEPC, thalamic early projecting cluster; v, ventral.

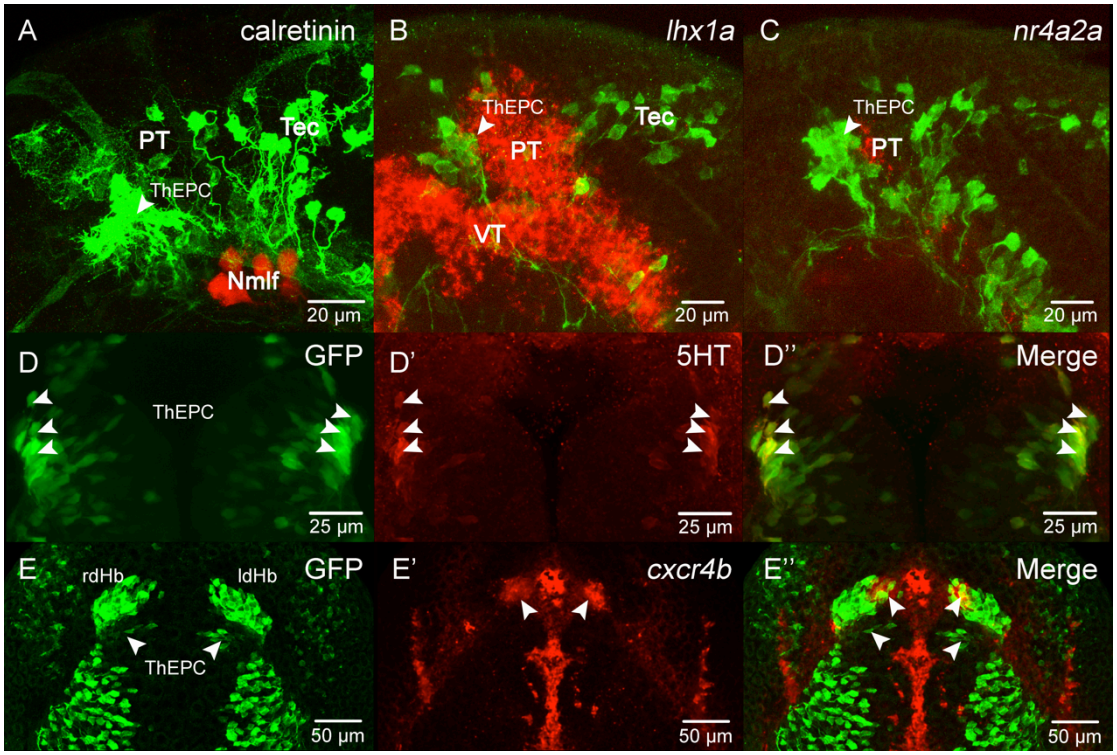

Figure 3.2: Marker gene analysis of the ThEPC.
(A-C) Lateral view focussed on the thalamic area, MIP of 32 hpf *Et(-1.0otpa:mmGFP)hd1* transgenic embryos co-labelled with (A) the calcium binding protein *calretinin* (Castro et al., 2009) and the pretectal markers (B,C) *lim1* and *nurr1* in red. Arrowheads highlight the position of the ThEPC.
(D-D'') Dorsal view focussed on the thalamic area, MIP, anterior to the top, of a 48 hpf *Et(-1.0otpa:mmGFP)hd1* embryo stained for the serotonergic marker 5-HT (in red). From left to right: GFP channel, far-red channel and merged channels. White arrowheads highlight the co-labelled ThEPC 5HT positive neurons.
(E-E'') Dorsal view with anterior to the top, MIP, of a 52 hpf *Et(-1.0otpa:mmGFP)hd1* embryo labelled with *cxcr4b* expressed in dHb progenitor cells (in red). From left to right: GFP channel, FITC channel and merged channels. Arrowheads mark the ThEPCs and the *cxcr4b* positive cells located in the ldHb and rdHb nuclei.
The scale bar is displayed in the right bottom corner of each image. The gamma was corrected to values between 0.60 and 0.80 using the software Fiji for display purposes.
d, dorsal; Hb, habenula; l, left; MIP, Maximum Intensity Projection; Nmlf, nucleus of the medial longitudinal fascicle; PT, pretectum; r, right; ThEPC, thalamic early projecting cluster; VT, ventral thalamus.

3.2 Long-term 2-PM *in-vivo* microscopy can be used to follow the DDC system formation between 32 hpf and 5 dpf

In zebrafish, the establishment of habenular nuclei and axonal projections requires around 4 days of development. The network extends over about 300 µm in dorso-ventral direction and approximately 200 µm anterior-posteriorly (Bianco et al., 2009; Beretta et al., 2012). To investigate *in-vivo* the DDC formation in the *Et(1.0otpa:mmGFP)hd1* transgenic line, we initially applied the CLSM (confocal laser scan microscopy). The key problems for the use of the CLSM are the phototoxicity due to the pinhole setting limitations and high laser power necessary to record habenular neurocircuit development in a Z-range of several hundred micrometers (Squirrell et al., 1999). As a consequence of these technical/anatomical limitations, we were just able to follow the DDC system formation for less than 30 hours (Figure 3.3A-D); (Beretta et al., 2012).

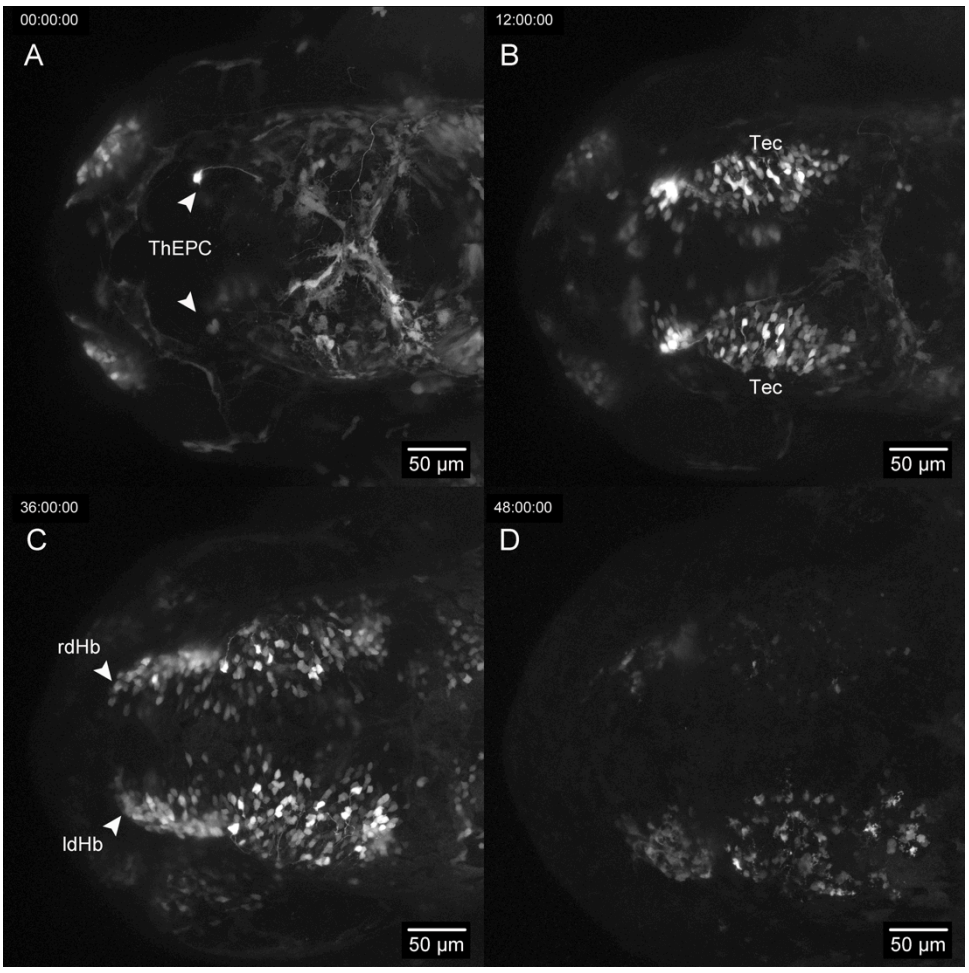

Figure 3.3: CLSM cannot be used to follow DDC system formation for more then 30 hours.
(A-D) Dorsal view, anterior to the left, of four developmental stages acquired by *in-vivo* CLSM of *Et(-1.0otpa:mmGFP)hd1* transgenic embryos. The time of recording (hh:mm:ss) is always shown in the left upper corner. The original stacks were cropped and the gamma was corrected between 0.45 and 0.65 for display purposes.
(A-C) Arrowheads show the location of ThEPCs at 32 hpf and the bilateral expression of GFP in dHb neurons at 68 hpf.
(C-D) CLSM imaging of the brain development results in the embryo dying after approximately 30 hours of recording due to phototoxicity.
d, dorsal; Hb, habenula; l, left; r, right; Tec, optic tectum; ThEPC, thalamic early projecting cluster.

To circumvent these problems and to elucidate *in-vivo* the spatio-temporal events during habenular network formation, we applied 2-PM in collaboration with the Nikon Imaging Center (NIC) of Heidelberg (Helmchen and Denk, 2005; Svoboda and Yasuda, 2006). Using this approach, we were able to perform long-term time-lapse imaging on living *Et(1.0otpa:mmGFP)hd1* embryos between 32 hpf up to at least 5 dpf (movies S1,S2). 2-PM microscopy turned out to be far superior to CLSM and we developed a refined protocol to follow the entire DDC development using multi photon excitation.
A main disadvantage of long-term imaging is the large amount of data obtained from each recording with a strong limitation in 3D visualisation and analysis. Therefore, to efficiently overcome this problem and to be able to follow and track single axons in a 3D volume, we developed an automatic script based on a depth colour coding algorithm. The first part of the script is detecting the first and the last slide in each stack containing useful information and saving them as slide and maximum intensity projection (MIP). The second part of the algorithm is applying a different colour code LUT (look up table) table to the MIP according to the depth of the recorded data (Figure 3.4; movie S1 and Appendix 7.3,7.4).
This combination allowed us to describe the formation of DDC system in the living *Et(1.0otpa:mmGFP)hd1* embryos in detail. Indeed, the bilateral dHb neurons start to express GFP around 45 hpf and their axons cross the ThEPCs before to elongate to the IPN. The tip of each dHb efferent axonal bundle defasciculate before to reach the IPN and at 5 dpf the IPN connections are established (Figures 3.4D-G and movies S1,S2); (Bianco et al 2009;

Beretta et al., 2012). Additionally, we observed the expression of GFP anteriorly bilateral in the olfactory bulb (OB), olfactory epithelium (OE) and posteriorly in the optic tectum (Tec) and spinal cord neurons (SCNs); (Figures 3.4A,B,G).

In summary, combining the 2-PM with the newly automatic ImageJ script, we were able to follow for the first time *in-vivo* the DDC development providing a detailed description in relation to space and time. Moreover, our time-lapse analysis identifies a connection between the habenular neuronal circuit and the bilateral cluster of early projecting neurons located in the thalamus (th); (Figure 3.4C).

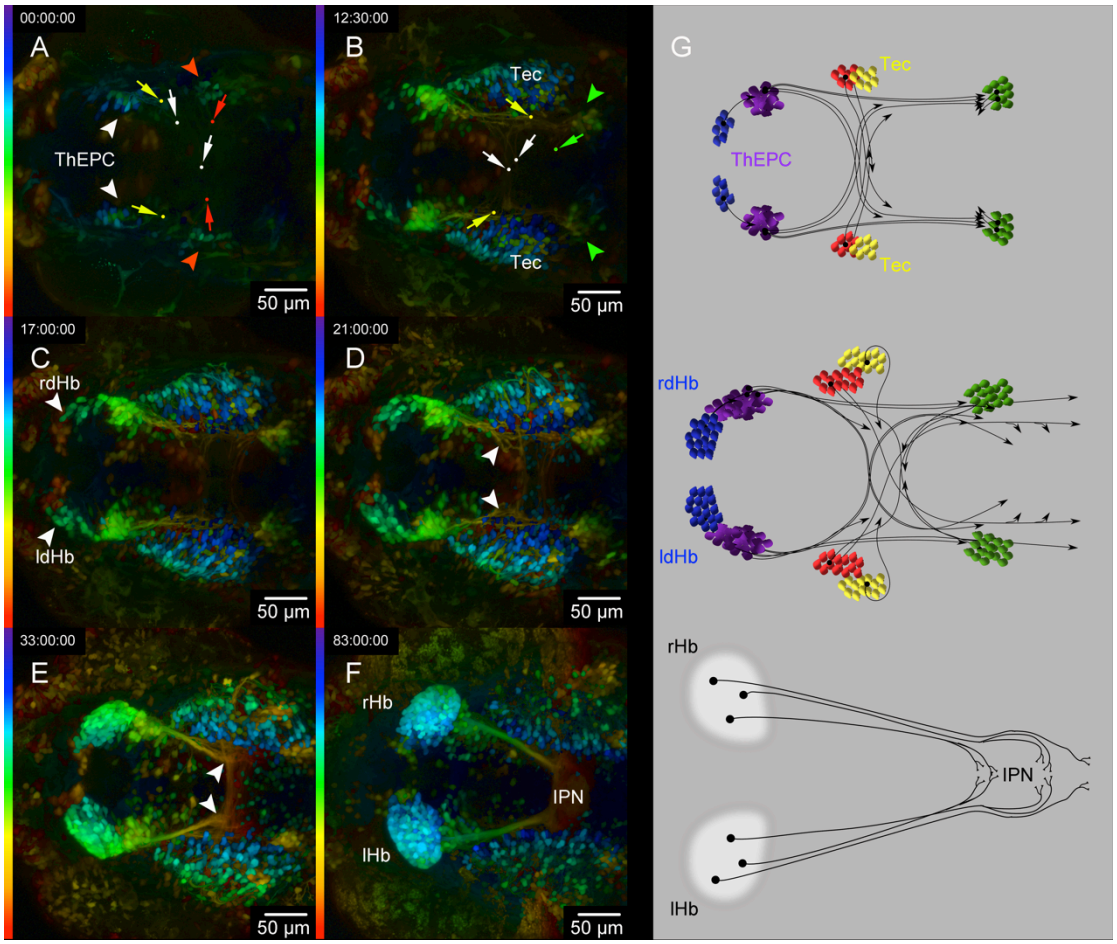

Figure 3.4: Long-term 2-PM *in-vivo* recording identifies interhemispheric axonal connections during habenular neural circuit development.
(A-F) Dorsal view, anterior to the left, automatic Colour Code MIP, of six developmental stages acquired by *in-vivo* 2-PM of *Et(-1.0otpa:mmGFP)hd1* transgenic embryos. Left side, Colour Code Scale LUT displays the Z colour code table according to the depth of each slice. The time of recording (hh:mm:ss) is

always shown in the left upper corner. The original stacks were cropped and the gamma was corrected to 0.45 for display purposes.
(A-B) Arrowheads show the location of ThEPCs at 32 hpf; red and green arrowheads mark two posterior bilateral clusters of projecting neurons. White and yellow dots and arrows mark the tips of ThEPC derived axons projecting contra- and ipsilaterally respectively. Red and green dots and arrows highlight tips of axons from the second and third cluster of contralaterally projecting neurons.
(C) White arrowheads highlight the bilateral expression of GFP in dHb neurons at 49 hpf.
(D-E) White arrowheads highlight dHb efferent projections (D) navigating towards the midline before IPN innervation at 53 hpf and (E) thereafter at 65 hpf.
(F) Architecture of the habenular neuronal circuit at 5 dpf; GFP is expressed in the lHb, in the rHb and in the Hb efferent projections innervating the IPN and MR.
(G) Summary of the events during habenular neural circuit development between (top to bottom) 32 hpf and 44.5 hpf, 32 hpf and 53 hpf and 32 hpf and 5 dpf: ThEPCs (violet); Tec (yellow); second cluster of projection neurons (red); third cluster of projection neurons (green); ldHb/rdHb (white) and the main axonal projections tracked (black lines).
d, dorsal; Hb, habenula; IPN, interpeduncular nucleus; l, left; LUT, Look Up Table; MR, median raphe; P, pineal; pp, parapineal; r, right; Tec, optic tectum; ThEPC, thalamic early projecting cluster; v, ventral.

3.3 Function of ThEPC neurons during the dHb network formation

3.3.1 Long-term 2-PM *in-vivo* time-lapse discovers multiple interhemispheric connections during the habenular neuronal circuit establishment

ThEPC neurons start to express GFP at 32 hpf and send their axonal projections ipsilaterally posteriorwards organising axonal bundles in the left and in the right brain hemisphere (Figures 3.4A,B and movies S1,S2). Concurrently, some ThEPC efferent axons migrate towards the midline to reach the ThEPC axon bundle in the contralateral brain side and follow their track (Figures 3.4A,B and Figure 3.5). These ThEPC axons slow down before to cross the midline to speed up again thereafter and apparently intermingle with the ThEPC axons on the contralateral side (Figure 3.5 and movies S1,S2). On their way posteriorly and down in the direction of the spinal cord, the ipsilateral axons pass two other GFP expressing neuronal clusters sending axons across the midline (Figures 3.5A,B; Figures 3.5C,D; Figures 3.7C,D and movies S1,S2). These axons intermingle with the ThEPC derived axons on the contralateral side as well and follow their track (Figures 3.4B-D,G). In detail, the first bilateral cluster of neurons is located approximately 80 µm posterior to the ThEPCs and starts to send axons at 32 hpf (Figures 3.5A-C; Figures 3.7A-C and movies S1,S2). The most posterior cluster is placed at 200 µm of distance from the ThEPCs and around 100 µm from the first cluster of projecting neurons (Figures 3.4A) and it is starting to send axons around 44 hpf (Figures 3.5E,F and movies S1,S2).

In summary, the discovery of the three axonal projecting clusters suggests the existence of multiple intrahemispheric and interhemispheric axonal connections in at least three different regions of the brain as part of the ThEPC neural network. Our transgenic line does not label any potentially existing axonal connection within the habenular network.

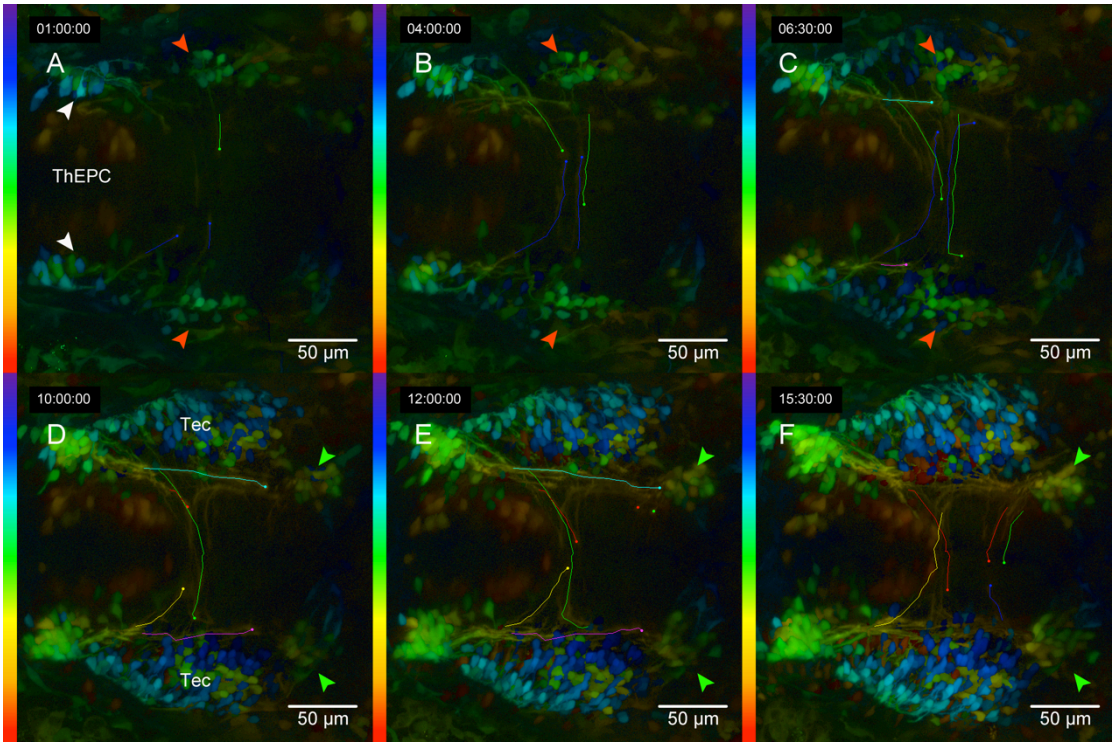

Figure 3.5: ThEPC early axonal tracking.
Dorsal view with anterior to the left, Colour Code MIP obtained from a total Z-height of 300 µm focussed on the ThEPC crossing axons in a *Et(-1.0otpa:mmGFP)hd1* transgenic embryo. Time points between 33 hpf and 49.5 hpf. Left side, Colour Code Scale LUT displays the Z colour code table according to the depth of each stack. The time of recording (hh:mm:ss) is shown in the left upper corner. The original stacks were cropped and the gamma was corrected to 0.45 for display purposes.
(A,F) White arrowheads show the location of ThEPCs at 33 hpf; red and green arrowheads mark two posterior bilateral clusters of projecting neurons. Manual tracking, overlay of dots and lines was used to highlight the position of ThEPC axonal network and the axons originating from the second and third cluster of neurons.
LUT, Look Up Table; Tec, optic tectum; ThEPC, thalamic early projecting cluster.

3.3.2 ThEPC neurons located in one brain hemisphere are crucial for dHb axon migration and IPN targeting

Through the analysis of *Et(1.0otpa:mmGFP)hd1* transgenic embryos, we discovered a new cluster of cells, ThEPC, which seems to be interconnected with the later forming dHb efferent projections during the DDC system organisation. Consistently with what was found in other neuronal networks (Burrill and Easter, 1995; Chalupa et al., 1996; Whitlock and Westerfield, 1998, 2000), we hypothesized that the ThEPC cells may function as pioneer neurons or intermediate structures in a short-range axonal communication

process necessary for dHb axonal guidance. To study the potential function of these cells, we performed 2-PM laser ablation experiments of ThEPC neurons on one side of the brain keeping the contralateral brain hemisphere as a control side. In our experiments, we unilaterally removed the ThEPC neurons at 32 hpf when the GFP positive cells can be easily detected and next, we monitored the neuronal network formation up to 6 dpf. ThEPCs on the ablated side cannot recover during the 5 days of recording, contrarily the contralateral ThEPC cells apparently developed unperturbed during the initial steps of network formation (Figure 3.6A and Figure 3.7A').

Our time-lapsis show that unilateral removal of one ThEPC causes dramatic consequences on the migration of dHb axons with the arrest of them on both brain hemispheres (Figures 3.6A-G and movies S3,S4).

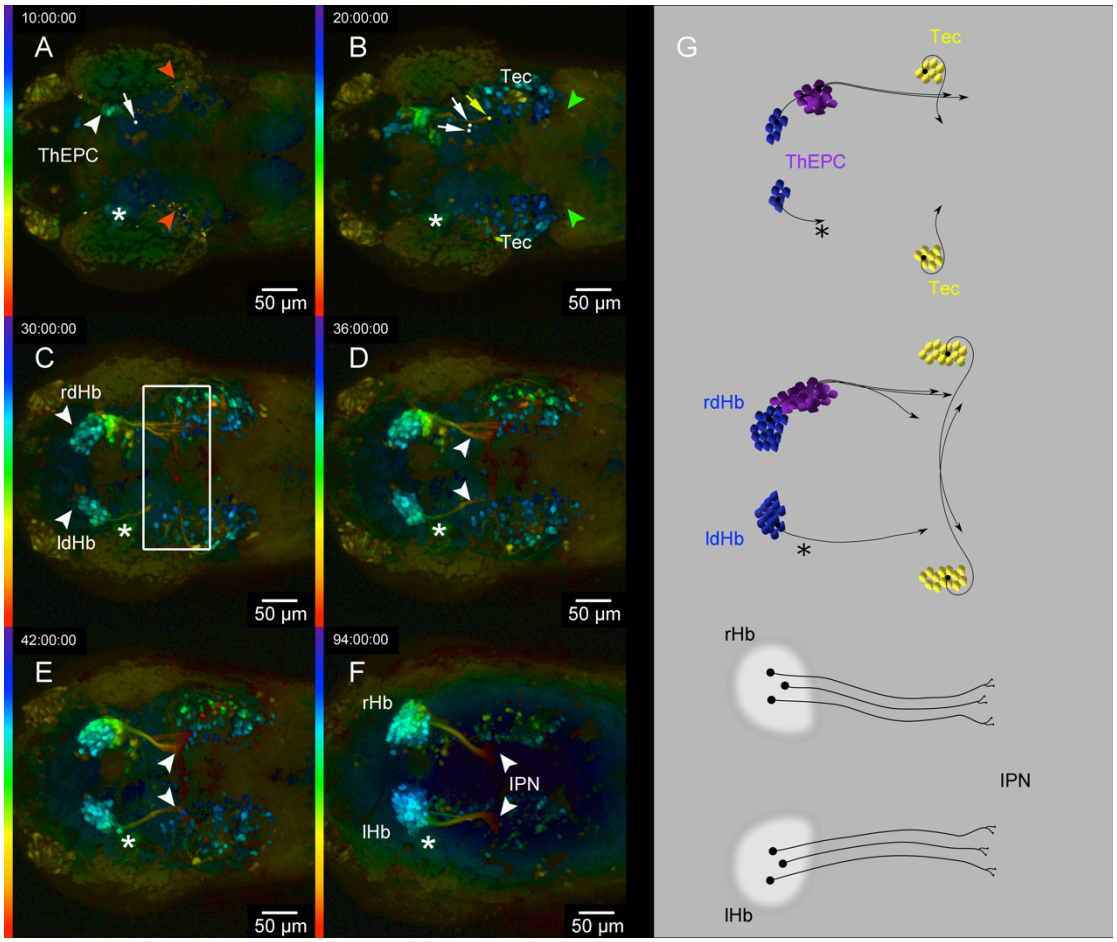

Figure 3.6: Unilateral ThEPC cell ablation causes the arrest of dHb efferent axons on both brain hemispheres.
(A-F) Dorsal view, anterior to the left, automatic Colour Code MIP, of six developmental stages acquired by *in-vivo* 2-PM after complete unilateral ThEPCs

ablation at 32 hpf in an *Et(-1.0otpa:mmGFP)hd1* transgenic embryo. Left side, Colour Code Scale LUT displays the Z colour code table in according to the depth of each slice. The original stacks were cropped and the gamma was corrected to 0.60 for display purposes.
(A-G) Asterisk marks the location of the ablated ThEPC cells between 32 hpf and 5 dpf.
(A-B) Yellow dot and arrow mark the tip of an ipsilaterally projecting ThEPC axon. White dots and arrows mark tips of axons starting to migrate towards the midline, but regress subsequently. Red and green arrowheads highlight the predicted position of the second and the third cluster of usually contralaterally projecting neurons.
(C) White arrowheads show the bilateral expression of GFP in the dHb. The white square highlights the area, in which dHb axon migration arrest as landmarked by tectal axons crossing the midline.
(D-E) White arrowheads highlight the position of dHb efferent axons on the ablated side and on the contralateral hemisphere, which start to migrate towards the midline.
(F) Architecture of the habenular neuronal circuit after left sided ThEPC cell ablation at 5 dpf. White arrowheads mark the ends of dHb efferent axons bundles on both sides of the brain.
(G) Summary of events during habenular neural circuit development after complete unilateral ThEPC ablation between (up to bottom) 42 hpf and 52 hpf, 42 hpf and 62 hpf and 42 hpf and 5 dpf. ThEPCs (violet); Tec (yellow); ldHb/rdHb (blue); rHb/lHb (white) and DDC axonal projections (black lines).
d, dorsal; Hb, habenula; IPN, interpeduncular nucleus; l, left; r, right; Tec, optic tectum; ThEPC, thalamic early projecting cluster.

Analyzing habenula neurocircuit formation in detail, we noticed that the dHb neurons start to express GFP normally in both brain hemispheres and their efferent axons pass unaffected the site of ablation (Figures 3.6B,C and Figures 3.7B',C'). Similar to not ablated embryos, the left and the right dHb axonal bundles defasciculate at the tip, with the difference that axonal elongation is arrested for the remaining time of recording. Peculiarly, not only the dHb axons on the ablated side show the stop in their elongation but also the dHb axonal bundle located on the not ablated side (Figures 3.6D-G). Indeed, after the crossing of the ThEPC neurons, the dHb axons on the not ablated brain hemisphere arrested their migration at approximately the same A-P level such as dHb efferent projections located on the ablated side (Figures 3.6C-F). These data may suggest a guidance function of ThEPC neurons based on the existence of short-range axonal communication between ThEPC neurons and dHb cells. Furthermore, we observed that the ThEPC derived axons on the not ablated side fail to migrate to the contralateral side and regress after only few micrometers (Figures 3.7B-C').

Therefore, we speculate that the impaired inter-hemisphere communication is the reason for dHb efferent axons elongation arrest in the control brain side.

A second intriguing consequence of unilateral ThEPC ablation is related to the two posterior axonal clusters described in the subchapter 3.3.1. ThEPC unilateral ablations cause a partial reduction of GFP expression in the second and a complete absence of the third cluster of GFP positive neurons on both hemispheres and a reduction or absence of any midline crossing axons (Figures 3.7C-E'; movies S3,S4).

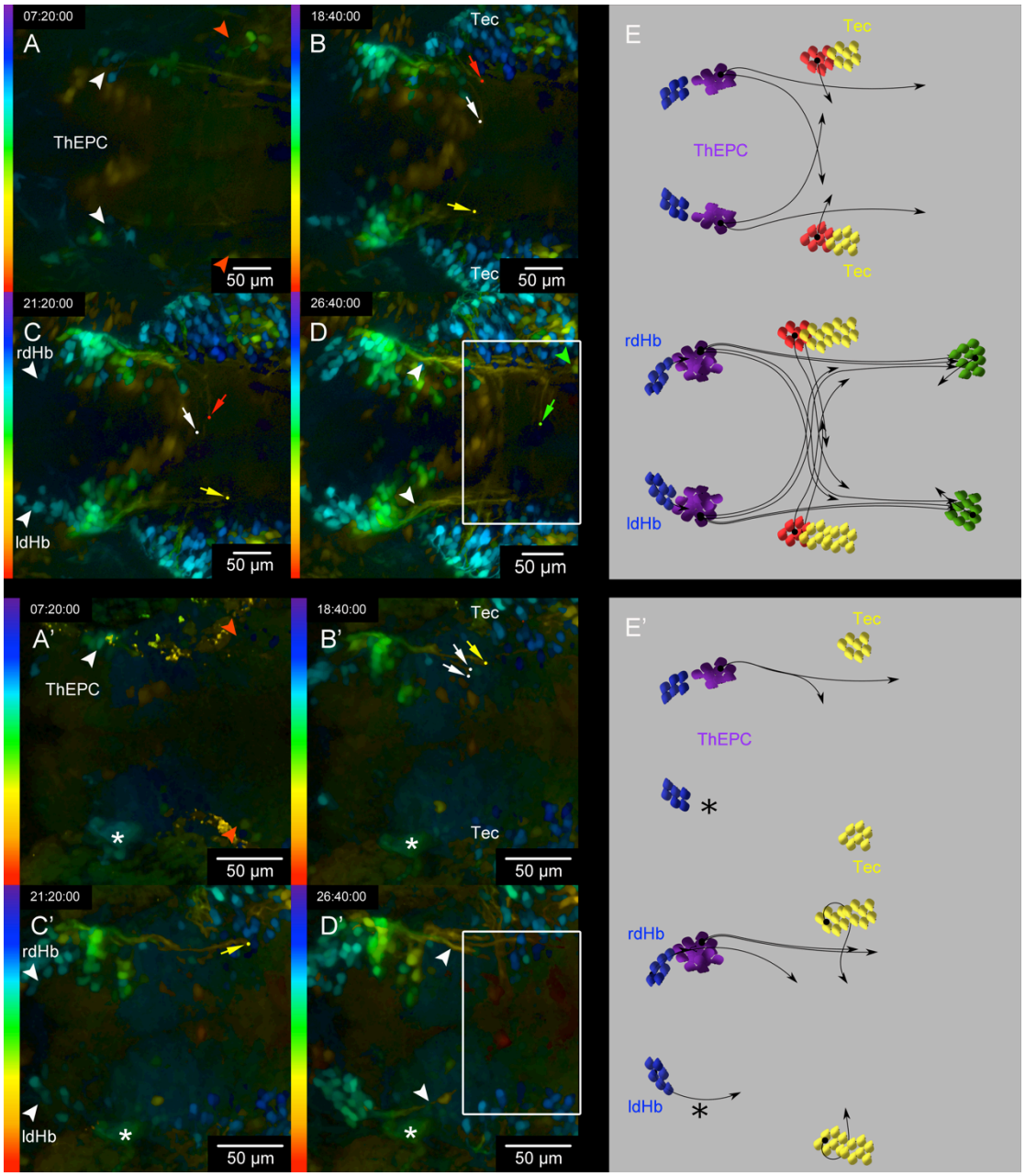

Figure 3.7: Habenular neuronal circuit development in normal and ThEPC ablated embryos.
(A-D') Dorsal view, anterior to the left, automatic Colour Code MIP, of four developmental stages acquired by *in vivo* 2-PM in (A-D) non-ablated and (A'-D') unilateral ThEPC cell ablated *Et(-1.0otpa:mmGFP)hd1* transgenic embryos – asterisk marks the ablated area.
(A-D') Left side, Colour Code Scale LUT displays the Z colour code table according to the depth of each stack. The original stacks were cropped and the gamma was corrected to 0.60 for display purposes.
(A,A') White arrowheads show the location of the ThEPCs, red arrowheads highlight the position of the second cluster of projection neurons.
(B-C') White dots and arrows mark the tips of ThEPC neuron derived contralaterally projecting axons, not present in C'. Yellow dots and arrow label the tips of ipsilaterally projecting ThEPC axons, while red dots and arrow mark axonal tips originating from the second cluster of projecting neurons, not seen in ablated embryos. White arrowheads show the location of the left and right dHb.
(D-D') White arrowheads highlight dHb efferent axons, green arrowheads and the green spot highlight the third cluster of projecting neurons and the axonal tip, not present in D'. The box marks the region at which dHb axon migration is arrested in D'.
(E-E') Summary of events observed during habenula neuronal circuit development in the non-ablated embryo and after unilateral removal of one ThEPC between 39.2 hpf and 58 hpf, 39.2 and 66 hpf. ThEPCs (violet); Tec (yellow); ldHb/rdHb (blue); rHb/lHb (white) and DDC axonal projections (black lines).
d, dorsal; Hb, habenula; l, left; r, right; Tec, optic tectum; ThEPC, thalamic early projecting cluster.

The results described above are based on 5 independent ThEPC ablation experiments with 4 of them resulting in similar phenotypes (n_{left} = 2/2; n_{right} = 2/3; Figure 3.9H) indicating consistency of the phenotype, which develops independently of the side of ablation.

To further assess whether the guidance function is specific for the ThEPC neurons, we performed ablation experiments in the surrounding area of ThEPC cells. The failed ablation of ThEPC neurons does not affect the dHb efferent axonal migration and the ThEPC neuronal network itself suggesting that specifically ThEPC neurons function in short- and long-range axonal communication process required for the dHb axons elongation and targeting (Figure 3.8).

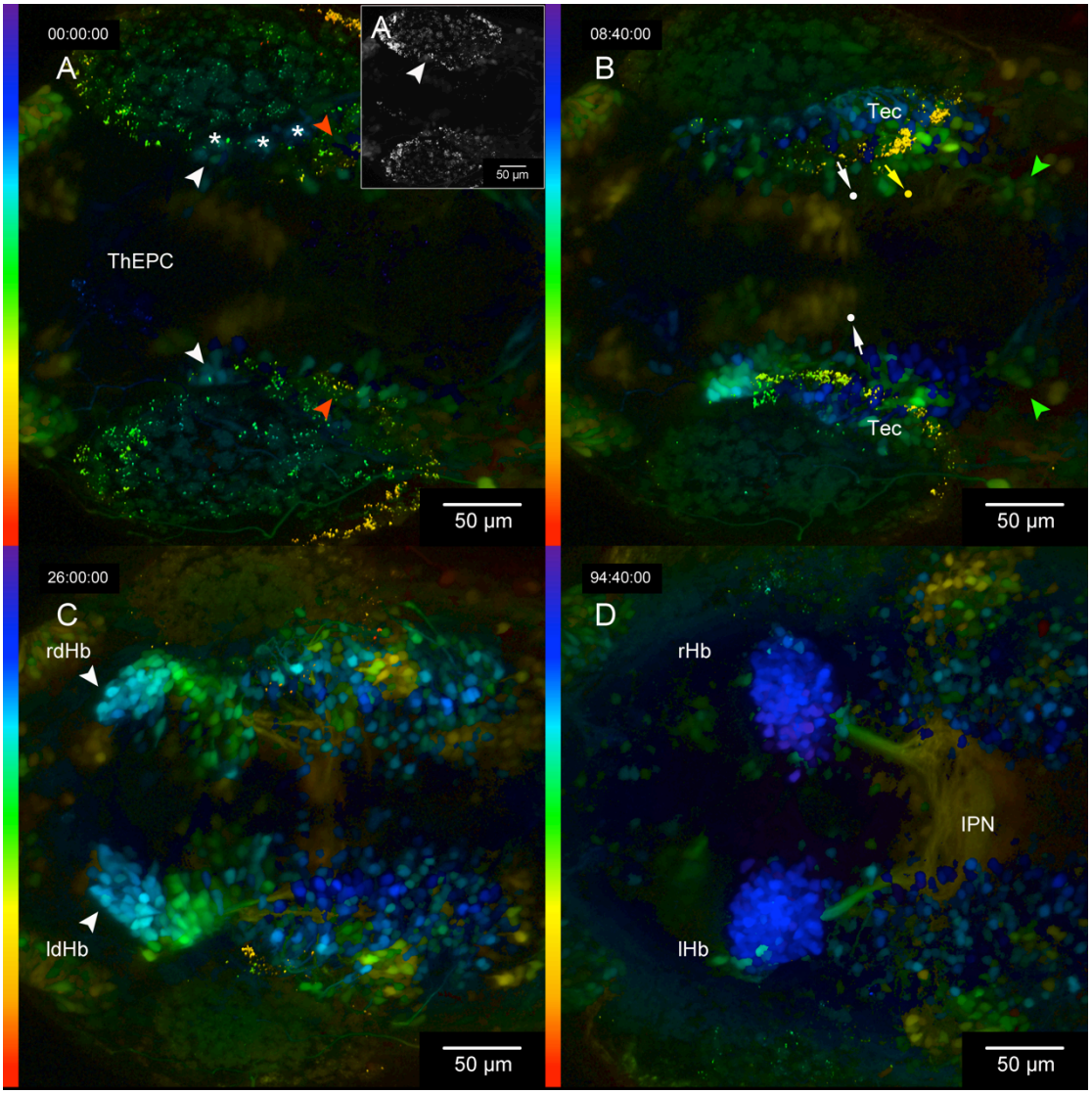

Figure 3.8: Failed ThEPC ablation does not affect ThEPC and dHb axon pathfinding.

(A-D) Dorsal view, anterior to the left, automatic Colour Code MIP, of four developmental stages acquired by *in vivo* 2-PM after failed ThEPC cell ablation at 32 hpf in an *Et(-1.0otpa:mmGFP)hd1* transgenic embryo. Left side, Colour Code Scale LUT displays the Z colour code table according to the depth of each stack. The recording time (hh:mm:ss) and the scale bar are displayed in the left upper and the right bottom corner respectively. The original stacks were cropped and the gamma was corrected to 0.60 using the software Fiji for display purposes.

(A,A') White and red arrowheads show the bilateral location of ThEPC neurons and the second cluster of projecting neurons respectively. The asterisks mark the ablated area next to the ThEPC neurons. (A') The inset shows the position of ThEPC cells before failed ablation.

(B) White dots and arrows highlight the axonal tips of contralateral projecting ThEPC axons and the yellow dot and arrow marks the tip of a ThEPC axon projecting ipsilaterally. Green arrowheads show the location of the third cluster of projecting neurons.

(C) White arrowheads highlight the position of the ldHb and rdHb.

(D) DDC system architecture at 5 dpf. The IPN is normally innervated by dHb axons. d, dorsal; Hb, habenula; IPN, interpeduncular nucleus; l, left; LUT, Look Up Table; MIP, Maximum Intensity Projection; r, right; Tec, optic tectum; ThEPC, thalamic early projecting cluster.

3.3.3 dHb axonal pathfinding errors depend on the number of ablated ThEPC neurons

Most of the data collected on axonal guidance were based on the discovery of pioneer neurons in the olfactory system (Whitlock and Westerfield, 1998, 2000) and in the retina (Meissirel and Chalupa, 1994; Burrill and Easter, 1995). In these studies were found out that the severity of axonal pathfinding errors is correlated to the number of pioneer neurons ablated independently of the neuronal system examined. To assess whether incomplete ablation of ThEPC cells affects the pathfinding of dHb efferents, we performed incomplete ablations of ThEPC neurons checking each time for potential alterations in dHb axonal elongation and IPN pathfinding. To manipulate consistently the ThEPC neuronal network, we ablated each time between 2 and 4 cells, immediately after the onset of GFP expression, in four consecutive experiments. Each round of ablation was performed always between 32 hpf and 40 hpf and to ensure the successful removal of ThEPC cells a stack was acquired after each ablation. After the ablations, newly GFP expressing neurons emerge in the ThEPC of the ablated side during DDC system formation. They projected axons ipsilaterally and contralaterally across the midline and the dHb efferent axons start to elongate normally in the direction of their ventral midbrain target (Figures 3.9A-D). By using 2-PM we acquired high-resolution stacks of IPN innervations at 4 dpf. We found that dHb axonal targeting was perturbed on the ablated side and in accordance with the dHb axon innervation phenotypes, we sorted embryos into two different categories: IPN reduced innervation (n=6/28) and IPN disorganisation (n=10/28; Figures 3.9E-H). Only in 2 of 28 independent experiments, we monitored a complete lack of IPN innervations (data not show).

By following the DDC system formation in 3 ablated embryos, we discovered that ThEPC axons crossing the midline are affected in the ablated side and

slightly perturbed in the not ablated side. Moreover, we observed a reduction of GFP expression in the two posterior clusters with apparently modification of their crossing axons (Figures 3.9A-B; movies S5,S6). Consistent with our previous hypothesis, these data support the idea that ThEPC mediated short-range communication is highly necessary for the correct pathfinding of dHb axonal on the ablated side. In addition, only in the absence of ThEPC derived commissures axon elongation is stalled on both hemispheres upon unilateral cell ablation. Incomplete ablations, which allow commissures to form does not evoke axon elongation defects.

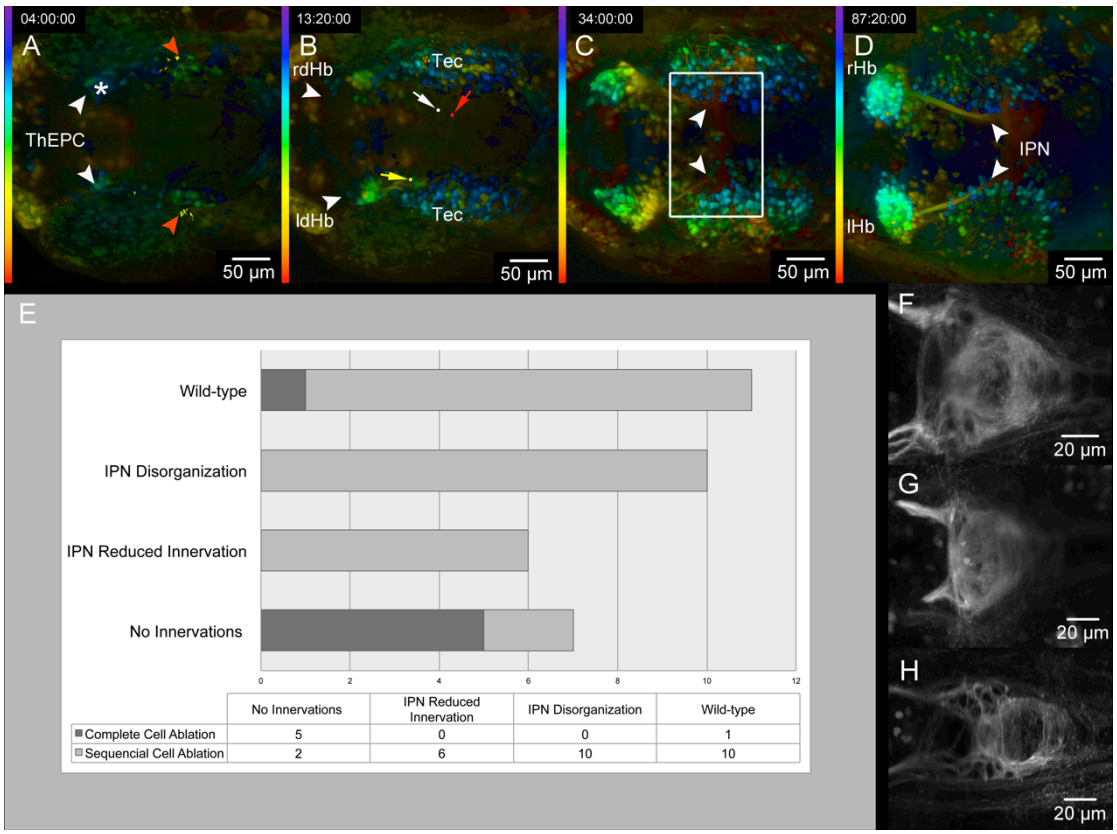

Figure 3.9: Incomplete unilateral ThEPC cell ablation causes dHb axon pathfinding errors.
(A-D) Dorsal view, anterior to the left, automatic Colour Code MIP, of four developmental stages acquired by *in vivo* 2-PM after sequential, incomplete unilateral ThEPC cell ablation at 32 hpf in an *Et(-1.0otpa:mmGFP)hd1* transgenic embryo. Left side, Colour Code Scale LUT displays the Z colour code table according to the depth of each stack. The original stacks were cropped and the gamma was corrected to 0.60 for display purposes.
(A) White arrowheads mark the ThEPC neurons; red arrowheads mark the second posterior bilateral cluster of projecting neurons. Asterisk marks the ablated side.

(B) White arrowheads mark the left and the right dHb domain. White and yellow dots and arrows mark the tips of ThEPC neuron derived crossing axons and those projecting ipsilaterally, respectively; red dot and arrow marks an axon originating from the second cluster of projecting neurons.
(C) White arrowheads show the dHb efferent projections entering the IPN. The white square highlights the area, in which dHb axon migration is arrested upon complete ThEPC cell ablation as landmarked by tectal axons crossing the midline (see Figure 4).
(D) Architecture of the habenular neuronal circuit at 5 dpf; GFP is expressed in the lHb, in the rHb and in the Hb efferent projections (white arrowheads).
(E) The graph shows the classification of the different IPN innervation phenotypes observed after 28 independent sequential ThEPC cell ablations.
(F-H) Dorsal views with anterior to the left focussed on the IPN. (F) Wildtype IPN innervation, (G-H) disorganisation and axons overshooting the IPN after unilateral sequential ThEPC neuron ablations.
d, dorsal; Hb, habenula; IPN, interpeduncular nucleus; l, left; r, right; Tec, optic tectum; ThEPC, thalamic early projecting cluster.

3.3.4 Unilateral dHb neuron ablation does not affect axonal IPN targeting on the contralateral side emphasising the specific importance of short- and long-range communication mediated by the ThEPC network

To support our findings on the role of ThEPC neuronal network and to understand the importance of interhemispheric communication between the ThEPC cell clusters in dHb axonal pathfinding, we performed dHb ablation experiments on one brain hemisphere.

We unilaterally ablated dHb neurons in the presence of the ThEPCs at 2 dpf and acquired high-resolution IPN stacks at 4 dpf (Figure 3.10). MIP and 3D reconstructions do not show any obvious difference in IPN innervations with axons from the contralateral side in the absence of IPN innervations with axons from the ablated side. Indeed, the left side dHb ablated embryos display a normal pattern of innervations from the rdHb (right dorsal habenula) in the ventral part of IPN (Figures 3.10A-C). Consistently, in the right side dHb ablated embryos the dHb efferent projections from the not ablated side mainly target the dorsal part of the IPN (Concha and Wilson, 2001), (Figures 3.10A'-C').

The data obtained from dHb unilateral ablation experiments suggest that dHb axonal pathfinding does not depend on interhemispheric dHb axonal

communication. dHb neurons and axons do not require the other hemispheric counterpart for axonal elongation, targeting and shaping of dHb axons. Furthermore, our findings support the specific role of ThEPC neurons short- and long-range communication for dHb axon elongation and IPN targeting.

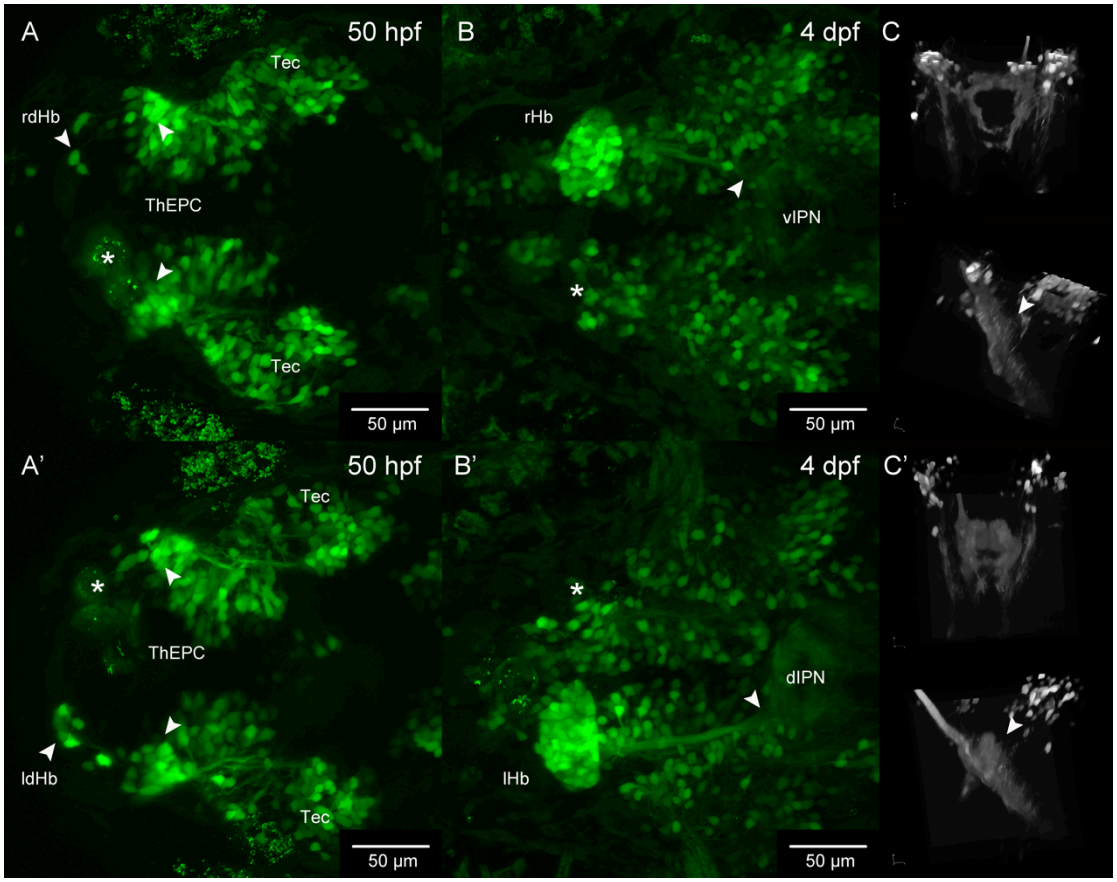

Figure 3.10: Unilateral dHb cell ablation does not affect axonal targeting on the contralateral side.
(A-B') Dorsal view, anterior to the left, MIP of *Et(-1.0otpa:mmGFP)hd1* transgenic embryos after complete dHb cell ablation. (A-A') Asterisks mark the site of ablation, the anterior white arrowheads mark the not ablated dHb cells and the posterior arrowheads mark the ThEPC neurons.
(B-B') White arrowheads mark the habenula efferent projections entering the IPN on the non-ablated side.
The original stacks were cropped and the gamma was corrected to 0.80 for display purposes.
(C-C') 3D reconstructions of dHb efferent projections innervating the IPN at 4 dpf from (up) dorsal and (down) lateral. White arrowheads highlight dHb efferent projections entering the (C) ventral IPN after ldHb cell ablation and the (C') dorsal IPN after rdHb cell ablation. Note the characteristic crown shaped structure of dIPN innervating axons in C'.
d, dorsal; Hb, habenula; IPN, interpeduncular nucleus; l, left; r, right; Tec, optic tectum; ThEPC, thalamic early projecting cluster; v, ventral.

3.4 ThEPC neurons contribute to the ventral habenula architecture

3.4.1 ThEPCs consist of different neuronal populations

To further characterise the early ThEPC neurons expressing GFP, high-magnification time-laps images were acquired between 32 hpf and 52 hpf. Colour code MIP and manual cell tracking analysis revealed a mixture of dividing cells and postmitotic neurons sending out axonal projections (movie S7). In support of the idea that ThEPCs consist of a heterogeneous mixture of neuronal cell types, we found that both ipsilateral and contralateral axonal projections arising from these neurons (see above, Figure 3.5). Indeed, a subset of them express serotonin (see above, Figures 3.2D-D''), while others are serotonin negative.

As shown in subchapter 3.1, the *Et(1.0otpa:mmGFP)hd1* transgenic line marks at 4/5 dpf the dorsal and the ventral habenular subpopulation. While the origin of the dorsal subpopulation has been well described, nothing is known about the early development of the ventral subpopulation (Aizawa et al., 2007; Roussigne et al., 2009). Looking at our time-lapse movies in detail, it appeared as if some ThEPC neurons migrate anteriorly towards the dHb region (Figures 3.4,3.5 and movies S1,S2). To investigate the potential contribution of ThEPC cells to the final habenular architecture, we initially analyzed at 4 dpf the overall habenula shape after unilateral ThEPC ablation. Comparing the left and the right habenula domains, we observed a reduction in the Hb size on the ablated side when compared with the control side. This preliminary evidence supports the hypothesis that ThEPC neurons may contribute to the final habenula architecture (Figure 3.11D). Therefore, to validate this observation, we analyzed at 4 dpf the habenular cell complexity after the unilateral ablation of the developing dHb using a nuclei marker for a better visualization of habenula morphology. Intriguingly, on the ablated side of each embryo (n_{left} = 3/3; n_{right} = 3/3), we found a number of GFP expressing neurons localised in the lateral part of the habenula, precisely in the reported position containing the vHb neurons (Figure 3.11A-C); (Amo et al., 2010).

In summary, these first evidences support the potential contribution of one of the ThEPC neuronal sub-cluster to the final habenular architecture and in particular to the vHb domain. Unfortunately, no transgenic lines for the vHb neural population are currently available. Therefore, we developed a fate mapping system for GFP-transgenic zebrafish based on the photoconvertible fluorescent protein PSmOrange to further explore the origin of vHb neurons (Subach et al., 2011); (Figures 3.12A-D).

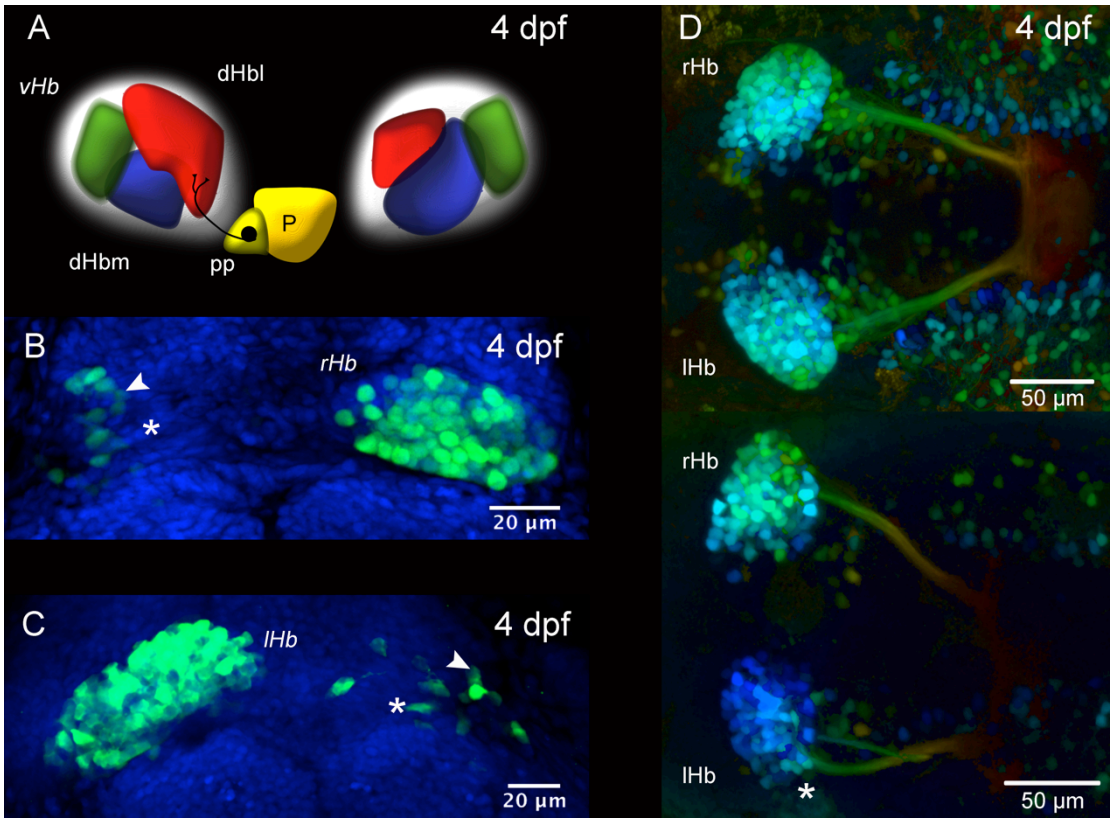

Figure 3.11: Unilateral dHb and ThEPC ablation experiments suggest a contribution of ThEPC cells to the final habenula architecture.
(A) Habenular nuclei organisation at 4 dpf. dHbl, lateral dorsal habenula (red); dHbm, medial dorsal habenula (blue); vHb, ventral habenula (green); P, pineal; pp, parapineal (yellow).
(B,C) Dorsal view, MIP, anterior to the top, focussed on the habenular nuclei of 4 dpf embryos, after left and right dHb ablation at 2 dpf. Asterisk marks the ablated side and white arrowheads highlight neurons located in the predicted position of the vHb domain. The nuclei (in blue) are labelled with Sytox Orange for better orientation.
(D) Dorsal view with anterior to the left, Colour Code MIP, showing habenula formation at 4 dpf in normal (top) and in ThEPC ablated *Et(-1.0otpa:mmGFP)hd1* embryos (bottom). The asterisk marks the ablated side. The habenula on the ablated side is reduced.

The gamma was corrected to 0.80 (B-C) and 0.45 (D) using the software Fiji for display purposes. l, left; r, right; ThEPC, thalamic early projecting cluster.

3.4.2 ThEPC neurons contribute to the vHb subnucleus

To investigate a potential contribution of ThEPC neurons to the vHb, we used the photoswitchable mOrange fluorescent protein (Subach et al., 2011). The main advantage of H2B-PSmOrange is related to the possibility to change the emission from orange to far-red upon a blue-green light illumination making this protein suitable for cell tracking in a GFP background. To evaluate the protein expression levels and the protein stability before and after photoconversion, we subcloned and injected the *H2B-PSmOrange* mRNA in wild type zebrafish embryos. We found that the not photoconverted form of the protein is highly expressed and stabled for at least 3 days. Moreover, we observed that after photoconversion the PSmOrange protein can be visualized for at least 2 days making it an excellent tool for cell tracking in living *Et(1.0otpa:mmGFP)hd1* transgenic embryos.

For our purpose, we photoconverted the protein in and around the ThEPC GFP positive neurons at 2 dpf and we analyzed the location of ThEPC cells in the brain of zebrafish after 2 days post photoconversion (4dpf). To unambiguously identify ThEPC neurons expressing both GFP and the photoconverted H2B-PSmOrange, we generated an automatic colocalisation ImageJ macro (Appendix 7.5). The macro is designed to detect all the ThEPC far-red photoconverted GFP positive cells and display them as a yellow region of interest (ROI) on the orange channel for a better orientation (Figure 3.12C). To avoid colocalisation mistakes and to understand the location of all GFP positive neurons and photoconverted cells, we additionally used green and red ROIs in the orange channel to locate not overlapping cells (Figures 3.12A-C). Using our generated colocalisation tool, we found an average of 8 photoconverted GFP expressing neurons (n=10) in the vHb domain (Figures 3.12A-D and movie S8). Our data suggest that ThEPC neurons contribute to the final habenula architecture and in particular to the vHb domain.

In support of our results, a co-staining for 5HT marker was performed at 2 dpf highlighting a cluster of ThEPC neurons positive for the serotoninergic marker

5HT consistent with the serotoninergic character of the vHb neurons (see above, Figures 3.2D-D''); (Beretta et al., 2012).

In summary, using the PSmOrange protein in combination with our colocalisation macro, we were able to confirm the preliminary ablation data and prove the contribution of ThEPC neurons to the vHb domain.

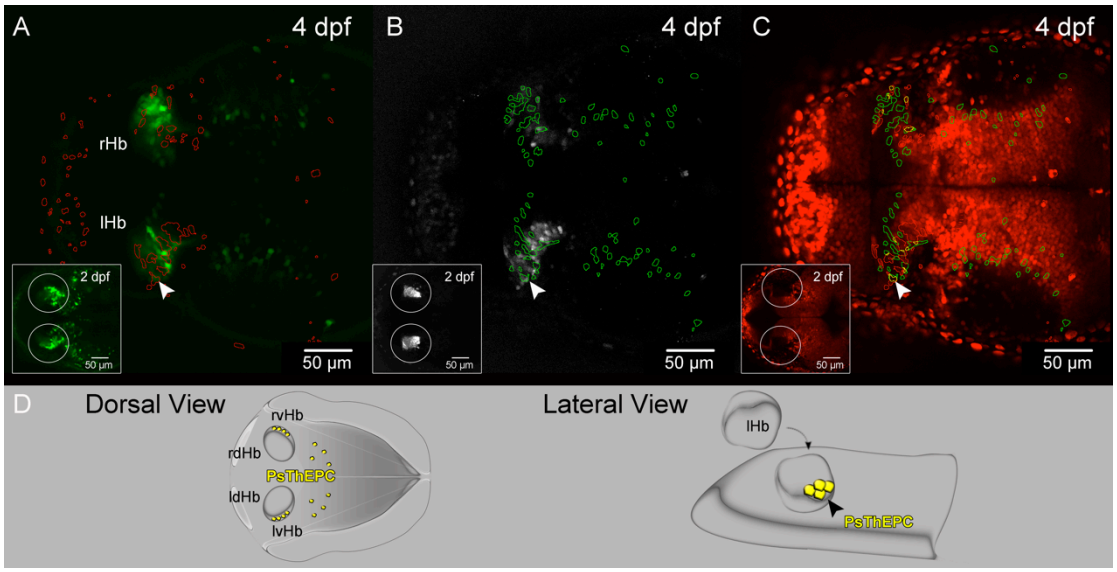

Figure 3.12: ThEPC neurons contribute to the vHb architecture.
(A-C) Dorsal views with anterior to the left of an image from a stack showing at 4 dpf the location of ThEPC neurons in *Et(-1.0otpa:mmGFP)* embryos after photoswitching of H2B-PSmOrange. Left corner to the bottom shows the MIP after ThEPCs photoconversion at 2 dpf; the circles in the insets highlight the area of photoconversion. The gamma was corrected after image analysis between 0.60 and 0.90 for display purposes. Colocalisation studies were performed using a custom-written automatic ImageJ Macro to identify the position of the photoconverted GFP positive ThEPC cells in the entire Z-stack.
(A) Red ROIs show the position of the photoconverted cells in the green channel.
(B) Green ROIs display the location of GFP positive cells in the far-red channel.
(C) Red and green ROIs were combined in the red channel to visualise the position of GFP photoconverted ThEPC neurons in the habenular nuclei in yellow.
(D) Model showing the contribution of ThEPC cells to the final vHb architecture in wild type embryos.
(A-C) White arrowheads mark the position of a photoconverted ThEPC derived GFP positive cells in the wild type habenula.
Hb, habenula; l, left; Ps, photoswitched; r, right; ROI, region of interest; ThEPC, thalamic early projecting cluster; v, ventral.

3.4.3 *Tcf7l2* gene function is required for vHb development

Most of the current understanding regarding the molecular mechanisms responsible for habenular neurocircuit establishment is related only to dHb development and still nothing is known about the signaling pathways involved during vHb formation (Aizawa et al., 2007; Carl et al., 2007; Doll et al., 2011).
Recent results obtained in our lab were suggesting that Wnt/beta-catenin transcriptional regulator *tcf7l2* is necessary for regulating dHb subnuclei asymmetry (M. Carl, personal communication). Based on this discovery and the widespread early *tcf7l2* expression pattern in prosomere 2 of zebrafish, we speculate that this gene might also be required for the development of vHb (Young et al., 2002). To understand whether the *tcf7l2* gene is contributing to vHb formation, we initially analyzed the expression of the vHb cell marker *kisspetidin-1* (*kiss-1*) (Servili et al., 2011; Ogawa et al., 2012;) in the vHb at 5 dpf in wild type and *tcf7l2* homozygote mutant background (Muncan et al., 2007; Figures 3.13A,C). Our stainings show that the expression of *kiss-1* is lost in the absence of *tcf7l2* function (Figure 3.13C). Moreover, the analysis of the main target of vHb efferent axons, the MR in the ventral hindbrain, shows the absence of innervations in the *tcf7l2* mutants (Figure 3.13C'). *tcf7l2* is a context dependent regulator of Wnt signaling, but ongoing studies in the lab indicate that the gene acts as an activator of Wnt signaling in the context of habenula development (M. Carl, personal communication).
Therefore our data suggest that *tcf7l2* is required for vHb formation and down regulation of the Wnt pathway causes the loss of vHb neurons. To test if also the down regulation of Wnt/beta-catenin signalling affects the establishment of the vHb sub-domain, we checked for *kiss-1* expression and MR innervations in *axin1/masterblind* mutant embryos (Heisenberg et al., 2001). In contrast to what we observed in the *tcf7l2* mutant, the up regulation of Wnt signaling does not influence vHb neuron formation and axonal innervations of the MR (Figures 3.13B,B').
In summary, our data suggest that down regulation of *tcf7l2* mediated Wnt/beta-catenin signaling causes the loss of vHb neurons.

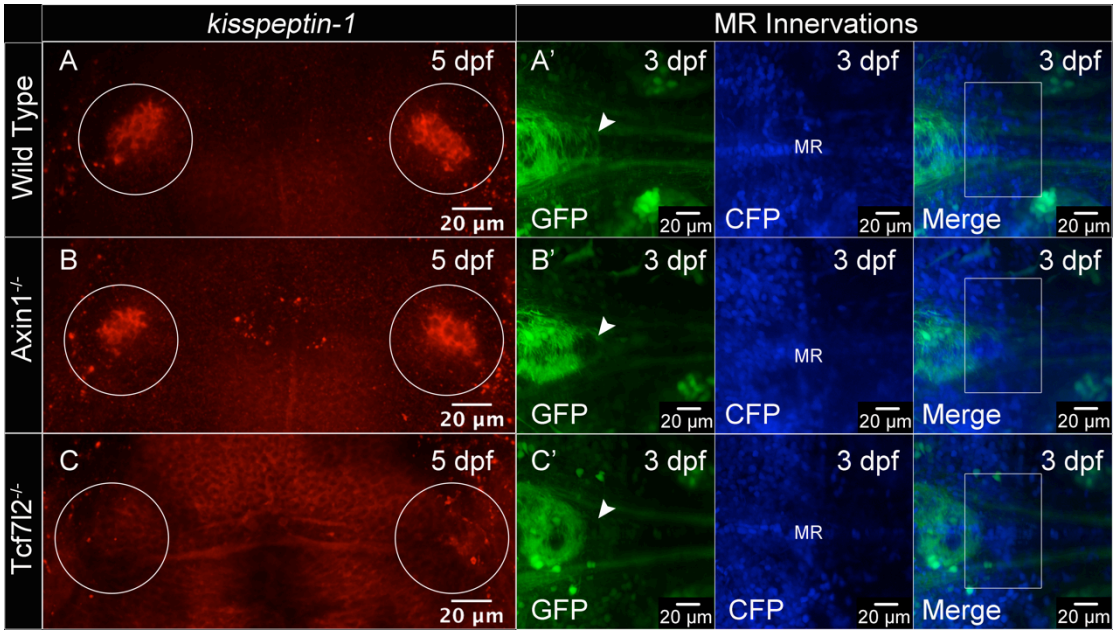

Figure 3.13: *Tcf7l2* mediated Wnt/beta-catenin signaling is required for vHb development.
(A-C) Dorsal views, anterior to the top. *kisspeptin-1* expression in the vHb (circle) is not affected by the upregulation of Wnt/beta-catenin signalling in (A,B) *Axin1/masterblind* mutant embryos, but absent in (C) *tcf7l2* mutants.
(A'-C') Dorsal views with anterior to the left, MIP, focussed on axonal innervation of the MR in *Et(1.0otpa:mmGFP)hd1* transgenic embryos at 3 dpf. H2A-CFP marks the cell nuclei for orientation. (B') Upregulation of Wnt signalling in *Axin1* mutants does not affect MR innervation by vHb efferent axons. (C') In *tcf7l2* mutants, the MR are not innervated. White arrowheads and white squares highlight the location of MR innervating axons, absent in C'.
The gamma was corrected between 0.70 and 0.80 for display purposes.
Hb, habenula; MIP, Maximum Intensity Projection; v, ventral; MR, median raphe.

3.4.4 The vHb cell subpopulation in ThEPCs is missing in *tcf7l2* mutants

In the subchapter 3.4.2, we discussed the contribution of ThEPC neurons to the vHb domain and in the last subchapter we collected evidences that vHb neuron formation depends on Wnt/beta-catenin pathway activity mediated by the *tcf7l2* gene. These findings led us speculate that the *tcf7l2* gene may influence early vHb neuron development within the ThEPCs.

To corroborate our hypothesis, we photoconverted ThEPC/H2B-PSmOrange GFP positive neurons at 2 dpf in the *tcf7l2*$^{-/-}$ x *Et(-1.0otpa:mmGFP)hd1* transgenic line and we checked the location of photoswitched GFP expressing ThEPC neurons in the vHb region at 4 dpf. In our studies, we observed that

the number of GFP expressing ThEPC cells appears largely unaffected but consistent with our hypothesis the double fluorescent ThEPC neurons did not localise in the region of the vHb domain (Figures 3.14A'-D' and movie S8).

Our data indicate that vHb cells originate in the thalamus from a cluster of ThEPC neurons and that *tcf7l2* mediated Wnt signaling is required for their formation.

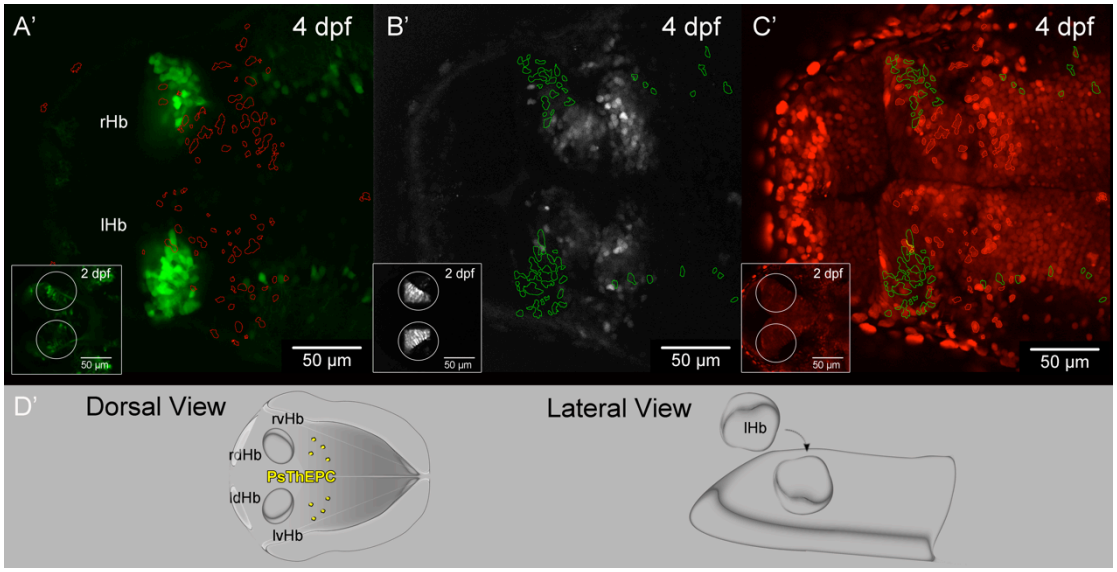

Figure 3.14: ThEPC neurons contribute to the vHb architecture under the influence of Wnt/beta-catenin pathway activity, tcf7l2 mediated.
Dorsal views with anterior to the left of an image from a stack showing at 4 dpf the location of ThEPC neurons in *Et(-1.0otpa:mmGFP)* embryos after photoswitching of H2B-PSmOrange. Left corner to the bottom shows the MIP after ThEPCs photoconversion at 2 dpf; the circles in the insets highlight the area of photoconversion.
(A'-C') Dorsal views with anterior to the left of an image from a stack showing at 4 dpf the location of photoswitching H2B-PSmOrange positive cells in the thalamus of *tcf7l2*$^{-/-}$ x *Et(-1.0otpa:mmGFP)hd1* embryos thalamus. Left corner to the bottom shows the MIP after ThEPCs photoconversion at 2 dpf; the circles in the insets highlight the area of photoconversion. The gamma was corrected after image analysis between 0.60 and 0.90 for display purposes. Colocalisation studies were performed using a custom-written automatic ImageJ Macro to identify the position of the photoconverted GFP positive ThEPC cells in the entire Z-stack.
(A') Red ROIs show the position of the photoconverted cells in the green channel.
(B') Green ROIs display the location of GFP positive cells in the far-red channel.
(C') Red and green ROIs were combined in the red channel to visualise the position of GFP photoconverted ThEPC neurons in the habenular nuclei in yellow.
(A'-C') Photoconverted GFP positive ThEPC cells are not found in the habenulae of *tcf7l2* mutants.
(D') Model showing the absence of ThEPC cells in vHb region in *tcf7l2* mutants.

Hb, habenula; l, left; Ps, photoswitched; r, right; ROI, region of interest; ThEPC, thalamic early projecting cluster; v, ventral.

Figure legends for Supplementary movies

MovieS1: Long-term 2-PM *in-vivo* recording of habenular neuronal circuit development, related to Figure 3.4 and 3.5.
Dorsal view with anterior to the left, Colour Code MIP obtained from a total Z-height of 300 µm focussed on the diencephalon in a *Et(-1.0otpa:mmGFP)hd1* transgenic embryo. Time-lapse between 32 hpf and 5 dpf. Left side, Colour Code Scale LUT displays the Z colour code table according to the depth of each stack. The stacks were acquired every 30 minutes with Z-depth of 1.0 µm. Laser power correction was used to compensate for increasing depth.
The MIPs and the colour coded MIPs were generated with our novel automatic MIP_ColourCode script for Fiji software (Gamma = 0.45).
White arrowheads mark the ThEPCs, lHb, rHb, and dHb efferent projections; red and green arrowheads highlight the second and the third cluster of projecting neurons, respectively.
d, dorsal; Hb, habenula; IPN, interpeduncular nucleus; l, left; r, right; Tec, optic tectum; ThEPC, thalamic early projecting cluster.

MovieS2: Long-term 2-PM *in-vivo* recording of habenular neuronal circuit development (black and white), related to Figure 3.4 and 3.5.
Original time-lapse movie from 32 hpf to 5 dpf (see movieS2) using black and white MIP.
ThEPC, thalamic early projecting cluster.

MovieS3: Complete unilateral ThEPC laser ablation followed by long-term 2-PM *in-vivo* recording of habenular neuronal circuit development, related to Figure 3.6.
Dorsal view with anterior to the left, Colour code MIP obtained from a total Z-height of 240 µm after complete unilateral ThEPC ablation on the left brain hemisphere followed by 2-PM *in-vivo* recording of habenular network development between 32 hpf and 5 dpf. Left side, Colour Code Scale LUT displays the Z colour code table in according to the depth of each stack. The ablation was carried out using laser power of 200 to 300 mW at the objective output. The MIPs were generated with our novel automatic MIP_ColourCode Script for Fiji software (Gamma = 0.60). Each stack was acquired every 40 minutes with a Z-step of 1.0 µm. Laser power correction was used to compensate for increasing depth.
The first time point shows the position of ThEPC cells at the onset of GFP expression before ablation. After ablation, the scar remains visible due to the auto-fluorescence of the dead cells.
Asterisk marks the ablated side. White arrowheads mark the ThEPCs, lHb, rHb, and the dHb efferent projections; red and green arrowheads highlight the predicted position of the second and the third cluster of projecting neurons, respectively.
d, dorsal; Hb, habenula; IPN, interpeduncular nucleus; l, left; r, right; Tec, optic tectum; ThEPC, thalamic early projecting cluster.

MovieS4: Complete unilateral ThEPC laser ablation followed by 2-PM *in-vivo* recording of habenular neuronal circuit development (black and white), related to Figure 3.6.
Original time-lapse movie from 32 hpf to 5 dpf (see movieS3) using black and white MIP.
MIP, Maximum Intensity Projection; ThEPC, thalamic early projecting cluster.

MovieS5: Sequential unilateral ThEPC cell laser ablation followed by 2-PM *in-vivo* recording of habenular neuronal circuit development, related to Figure 3.7.
Dorsal view with anterior to the left, Colour Code MIP obtained from a total Z-height of 250 µm. 2-PM *in vivo* recording of habenular network formation between 32 hpf and 5 dpf after sequential unilateral ThEPC cell ablation on the right brain hemisphere. Left side, Colour Code Scale LUT displays the Z colour code table according to the depth of each stack. 2-4 cells were ablated as they started to express GFP for 4 times over a period of 4 hours using 300 mW of laser power at the objective output.
A stack was acquired every 40 minutes with a Z-depth of 1.08 µm. Laser power correction was used to compensate for increasing depth. The MIPs and the ColourCodeMIPs were generated using the automatic MIP_ColourCode Script for Fiji software (Gamma = 0.40).
The first time point shows the position of ThEPC cells at the onset of GFP expression before ablation. Upon ablation, the scar remains shortly visible due to the auto-fluorescence of the dead cells, but is covered subsequently by GFP expressing neurons. Note that the dHb axon bundles migrate more peripherally and the IPN innervations are “disorganised” (Figure 5).
Asterisk marks the ablated side. White arrowheads mark the ThEPCs, lHb, rHb, Hb efferent projections; red and green arrowheads highlight the second and the third cluster of projecting neurons, respectively.
d, dorsal; Hb, habenula; IPN, interpeduncular nucleus; l, left; r, right; Tec, optic tectum; ThEPC, thalamic early projecting cluster.

MovieS6: Sequential unilateral ThEPC cell laser ablation followed by long-term 2-PM *in-vivo* recording of habenular neuronal circuit development, related to Figure 3.7.
Original time-lapse movie from 32 hpf to 5 dpf (see movieS5) using black and white MIP.
MIP, Maximum Intensity Projection; ThEPC, thalamic early projecting cluster.

MovieS7: The ThEPCs are composed of mixed populations of deviding cells and postmitotic neurons, related to Figure 3.1 and 3.2.
Dorsal view with anterior to the left, Colour Code MIP obtained from a total Z-height of 200 µm. High magnification time-lapse focussed on the ThEPC located in the left brain hemisphere between 32 hpf and 52 hpf. Left side, the LUT shows the Z colour code table according to the depth of each stack. Stacks were acquired every 10 minutes with a Z-step of 1.0 µm. Laser power correction was used to compensate for increasing depth.
The MIPs were generated using the automatic MIP_ColourCode Script for Fiji software (Gamma = 0.60). The cells were tracked using the Fiji manual tracking

plugin and displayed as an overlay of dots and lines. The manual tracking identifies deviding ThEPC cells, while other GFP positive neurons send out efferent projections.
ThEPC, thalamic early projecting cluster.

MovieS8: A population of ThEPC cells contribute to the vHb and is absent in embryos mutant for *tcf7l2*, related to Figure 3.12 and 3.14.
Dorsal view with anterior to the left, Z-stacks of *Et(-1.0otpa:mmGFP)hd1 and tcf7l2*$^{-/-}$ x *Et(-1.0otpa:mmGFP)hd1* transgenic embryos at 4 dpf after photoconversion of the H2B-PSmOrange protein in the ThEPC region at 2 dpf. Each stack was acquired using the sequential scanning mode with a Z-step between 1.0 µm and 2.0 µm. The scale bar is displaye in the right bottom corner of each image and the gamma was corrected for display purposes for each channel between 0.60 and 0.90 using the software Fiji.
The colocalisation studies were performed using an automatic ImageJ Macro for Fiji to identify the GFP positive, photoconverted ThEPC cells in the entire Z-stack. The red channel is used to visualise the habenular morphology due to the nuclear expression of not photoconverted H2B-PSmOrange protein at 4 dpf. Red ROIs display the location of the photoswitched positive cells, while green ROIs show the position of the GPF positive cells. Red and green ROIs were combined to display the position of ThEPC cells expressing both GFP and the photoconverted protein in yellow.
Minor corrections and compression were performed using the software iMovie and Wondershare Video Converter Ultimate.
Hb, habenula; ROI, region of interest; ThEPC, thalamic early projecting cluster; v, ventral.

4 Discussion

Investigating dynamic processes during development of large structures over a long period of time *in-vivo* has been very challenging in the past. In our studies, we present a new method based on optimised 2-PM time-lapse imaging and automatic image code colouring analysis to follow DDC system development for more than 4 days. We identified in the new *Et(-1.0otpa:mmGFP)hd1* enhancer trap transgenic line of zebrafish a thalamic bilateral cluster of early projecting neurons (ThEPC) with a previously uncharacterized function. The ThEPC clusters are connected to habenula axons and project ipsilaterally posterior and contralaterally forming a hemisphere spanning neural network prior to the formation of the dHb neural circuit. To investigate the role of ThEPC neurons during habenular neuronal network formation, we combined the advantages of our method with unilateral 2-PM laser ablation. In according to the number of ThEPC neurons ablated, we observed perturbation of dHb axonal elongation and dHb axonal misrouting in the ablated hemispheres and intriguingly also in the contralateral brain side. Our data show the importance of short- and long-range inter hemispheric axonal communication for DDC neural network formation.

The ThEPC cluster is constituted of different cell sub-types. To follow the hypothesis that one of these subsets participate in the formation of vHb, we successfully developed for zebrafish a new system to track automatically photoconverted ThEPC neurons in a GFP background. The tracking of ThEPC neurons in wild type embryos and embryos mutant for the Wnt pathway gene *tcf7l2* reveals the thalamic origin of vHb neurons, which only form in the presence of *tcf7l2* gene activity.

4.1 Combining long-term 2-PM and automatic colour code labelling systems to study neuronal network formation *in-vivo*

In the last two centuries, much progress has been made in the field of neuronal network formation during embryonic brain development (Beretta et al., 2012). However, most of the current knowledge is derived from data collected from fixed samples and cell culture experiments. Advances in the study of the highly dynamic processes during neuronal network formation under physiological conditions have been hampered due to missing labelling systems and imaging tools. To overcome these limitations and to understand more about the dynamic time sequence of events during DDC system formation, we combined the advantages of the rapidly developing transparent zebrafish embryo and 2-PM (Svoboda and Yasuda, 2006).

The accessibility of the DDC system (Aramaki and Hatta, 2006) and the high GFP expression levels in all major components from early to late developmental stages in *Et(-1.0otpa:mmGFP)hd1* transgenic embryos make it possible to use the habenular neural network as a model to investigate the formation of large neuronal networks *in-vivo*. However, the DDC system spans several hundred micrometers in A-P, D-V and left-right direction and the development of the entire neurocircuit requires a time of approximately 96 hours (Bianco et al., 2009; Beretta et al., 2012). In our studies, we show that CLSM appears inefficient to acquire long-term high-resolution images of the entire DDC system development over a long period of time (Figure 3.3). The prerequisite to acquire high-resolution images using CLSM is related to the pinhole setting, which, in according to the aperture, can only allow fluorescent signal originating within a thin focal plane to reach the detector (Minsky M., 1957). To just excite fluorescent molecules in a single plane, a small confocal pinhole has to be fixed and generally this causes inefficient fluorescence collection when imaging deeper into a thick tissue (Centonze and White, 1998; Conchello and Lichtman, 2005). Laser power correction can be used to overcome this problem and to acquire images with good signal-to-noise ratio. However, high laser power accelerates photobleaching and phototoxicity (Squirrell et al., 1999) making the acquisition of images for long-term time-lapse on living specimen impossible. To circumvent the limits of CLSM and to

be able to follow the DDC system formation, we successfully applied 2-PM confocal microscopy for long-term high-resolution time-lapse (Figure 3.4). Many reports show that 2-PM can be applied to follow different development biological processes occurring in thick tissue overcoming the main limitations discussed for the classical one-photon excitation microscopy (Squirrell et al., 1999; Stosiek et al., 2003; Kamei and Weinstein, 2005; Kobat et al., 2009). Indeed, 2-PM is based on a non-linear excitation process with the quasi-simultaneous absorption of two less energetic photons of longer wavelength. The advantage of this system is that the fluophores are only excited within a diffraction-limited of a spot, without out-of-focus stimulations (Denk et al., 1990). The restricted excitation volume causes a reduction in background with an improvement of signal-to-noise ratio and thus also achieves the reduction of photobleaching and photodamage (Centonze and White, 1998). Since the 2-PM excitation is localised in the focal plane, all the photons emitted by the fluophores represent valuable signal reaching the detector, without any pinhole constrictions. Moreover, the excitation of GFP with a longer wavelength (940 nm) reduced scattering and absorption by endogenous chromophores with a deeper penetration of the light in thick tissue (Helmchen and Denk, 2005).

Combining all 2-PM features discussed above with the *Et(-1.0otpa:mmGFP)hd1* transgenic line, we were able to efficiently overcome the CLSM limitations to investigate *in-vivo* the DDC system formation for more than 4 days.

The data size of each time-lapse acquired makes it generally rather difficult to investigate them and to display all the different structures imaged in a three dimensional space. To visualise our data, we initially developed an ImageJ script to build automatic the MIP obtained from each stack. The system allowed us to quickly process and display in 2D the large amount of data generated after each 2-PM recording. Furthermore, to be able to visualise each time lapse in 3D, we implemented our ImageJ script to automatically apply a colour code LUT in according to the Z-depth to each stack. Alternative methods are already published to generate in ImageJ pseudo-3D views however, we found them inefficiently for our purpose. Indeed, these scripts convert a stack to RGB colour and then compute a projection. The

consequences are not only an increment of the memory necessary for each analysis but also lead to unexpected results by creating an output image that combines maxima found within each colour channel individually, rather than from the original image intensities.

In summary, this method overcomes time constrictions for data analysis and permits a fast two-dimensional reconstruction of 2-PM time-lapse stacks increasing the 3D perception of each image.

4.2 dHb axonal pathfinding depends on the ThEPC neuronal network

Long-term *in-vivo* 2-PM and colour code imaging analysis allowed us to identify a bilateral cluster of neurons located in the thalamus (ThEPC) and to investigate their function during DDC system development.

We find that ThEPC neuronal network establishment takes place before dHb axon migration. dHb axons cross the ThEPCs on either side of the brain before elongating towards their medially positioned target. This observation raised the possibility that ThEPCs might play a role in dHb axon growth and/guidance. Indeed, unilateral complete removal of ThEPC neurons followed by 2-PM time-lapse analysis reveals the arrest of dHb axon elongation and the absence of IPN innervations. Further, the unilateral incomplete ablation of ThEPC neurons causes misrouting of dHb axons, dependent on the number of neurons removed.

The discovery of a connection between the dHb axon and the ThEPC cluster evokes a possible pioneering function of ThEPC neurons during the establishment of DDC system. Pioneering neurons are reported to be essential for axonal pathfinding during the development of retinotectal projections and olfactory system innervations (Whitlock and Westerfield, 1998, Pittman et al., 2008; Imai and Sakano, 2011). In general, this specialised class of neurons provides guidance cues necessary for proper axonal pathfinding of follower axons. Deletion of pioneering neurons often induces perturbations in the guidance of their follower axons with a consequent delay or misrouting of them (Raper and Mason, 2010; Imai and Sakano, 2011; Miyasaka et al., 2012). For instance, the olfactory placode of zebrafish contains a transient class of neurons, which establishes the initial connection with the olfactory bulb to guide the follower olfactory neuronal axons in the direction of their target. Ablation experiments performed on the olfactory pioneering neurons demonstrated that they are necessary for the correct targeting of the incoming sensory neurons (Whitlock and Westerfield, 1998). The absence of the olfactory transient neurons frequently causes the misrouting of olfactory neuronal axons and just in rare cases the complete mistargeting of them (Whitlock and Westerfield, 1998; Raper and Mason,

2010). This data show the essential function of pioneering neurons for axonal pathfinding during the development of a specific neuronal network.

In accordance to the similarity between the olfactory pioneering neurons and the results obtained after ThEPC neurons ablation, we initially speculated on a possible pioneering function of ThEPCs. Indeed, the partial removal of ThEPC cells causes dHb axonal misrouting with the identification of two consistent categories of phenotypes within the IPN: delayed/IPN reduced innervation and IPN disorganisation. Conversely, the complete unilateral ThEPC ablation results in the stop of dHb axon elongation before reaching the IPN. These results are similar to less frequent observations in other neuronal network systems and highlight the crucial function of ThEPC neurons for dHb axonal pathfinding (Whitlock and Westerfield, 1998; Pittman et al., 2008; Raper and Mason, 2010).

All the data collected are consistent with a possible pioneering function of ThEPC neurons. However, even with high magnification time-lapse images, we were not able to unambiguously demonstrate whether the ThEPC neurons guide the dHb axon in the direction of their target (data not shown). It appears that dHb axons contact the ThEPC neurons and/or axons only within the cluster but then follow their own way in the direction of IPN (Figure 3.4 and movies S1,S2). Therefore, we hypothesise that ThEPC neurons are unlikely to function as pioneering neurons but as intermediate targets involved in the sorting and topographic organisation of dHb axons, like reported for the thalamocortical system (Dufour et al., 2003; Bonnin et al., 2007; Powell et al., 2008). Indeed, after incomplete unilateral ablation of ThEPC neurons, dHb axons start to project normally and just after the crossing of ThEPC ablated side, some of them become disorientated. Consistently, the complete unilateral ThEPC neurons ablation causes dHb axon arrest.

In summary, ThEPC cells could be the intermediated target of dHb efferent axons, responsible of dHb axonal sorting and orientation. Therefore, ThEPC neurons may act as a local source of information necessary for dHb axon elongation and guidance.

Our findings provide new functional evidences for a role of thalamic neurons during dHb axonal migration, but several questions still remain open for future

studies. For instance, which are the molecular signaling pathways in the thalamus that may mediate the function of ThEPC cells?

In our studies we found that ThEPC neurons express the *lhx2b* gene. The *Lhx2* transcription factor family has been reported to be essential for axonal guidance in zebrafish and in mice (Seth et al., 2006; Wilson et al., 2008; Nawabi and Castellani, 2011). In the *foxd1* mutant mouse (Herrera et al., 2004) and the *Bella-donna/lhx2b* mutant zebrafish, ipsilateral axons are increased due to the misexpression of genes such as *slits*, *ephs*, *zic2* and *foxg1* in the embryonic midline preventing axonal crossing in the optic chiasm. We may speculate that *lhx2b* gene function could be necessary for ThEPC neuron function and consequently influence dHb axonal migration. Studies performed on pioneering neurons located in the ventral telencephalon of *lhx2*$^{-/-}$ mutant mice reported a perturbation in thalamic efferent axon guidance towards their telencephalic targets (Lekhina et al., 2007). Therefore, we support the hypothesis that *lhx2b* may regulate the intermediate target function of ThEPC neurons and consequently the dHb axon migration. This potentially makes *lhx2b* gene an attractive candidate for future investigation.

4.3 ThEPC neurons promote brain interhemispheric long distance axonal communication

The brain is an extraordinary machine able to efficiently process and integrate information between the two brain hemispheres (Lindell, 2011; van der Knaap and van der Ham, 2011). The establishment of interhemispheric connections is well studied in the corpus callosum in which long-range efferent fibers derived from cortical neurons connect the left and the right cerebral hemispheres. During brain development, the callosal axons take a route to the midline and cross it to migrate through the white matter (WM) to precisely reach the contralateral target area of the neocortex (Mizuno et al., 2007). With our 2-PM *in-vivo* time-lapse, we acquired evidences that also during habenular neuronal circuit development, interhemispheric communication plays an essential role. Indeed, we discovered the existence of midline crossing axons originated from both ThEPC clusters. Intriguingly, the complete unilateral ablation of ThEPC neurons causes the loss of the ThEPC axonal crossing on the contralateral side. These axons regress after having elongated a short distance towards the midline. Moreover, on the ablated side and frequently on the not ablated side, we observed a lack of GFP expression in the two posteriorly bilateral clusters and their axonal bundles (Figures 3.6,3.7,3.9 and movies S3,S4,S5,S6). This does not prove the absence of interhemispheric connections between them. However, this evidence may suggest that the contact between the ThEPC axons influences the genetic program within the neurons of these clusters on both brain hemispheres.

As previously discussed, the unilateral complete ablation of ThEPC neurons causes the arrest of dHb efferent projection elongation evocating a possible function as intermediate target for these neurons during the early habenular neurocircuit development. In the unilateral absence of one ThEPC dHb elongation is affected on both sides of the brain. Since the communication between the ThEPC clusters located in the two brain hemispheres is affected earlier than dHb elongation and due to the functional evidences collected on the intermediate role of ThEPC neurons, we argue that the absence of long-range interhemispheric ThEPC axonal communication is likely the reason for dHb axon elongation perturbations in the not ablated brain side.

Further, the unilateral incomplete ThEPC ablation experiments are consistent with our hypothesis. In the presence of a reduced number of ThEPC neurons, which connect to the contralateral side, dHb axons on the ipsilateral side are misrouted. ThEPC axons from the contralateral side cross the midline normally and the dHb axon targeting is unaffected. Additionally, we show that ThEPC neurons unilateral failed ablation does not affect, neither the short-range intrahemispheric axonal communication, nor long-range interhemispheric axonal communication. These data are consistent with short-range intrahemispheric communication between the ThEPC neurons and the dHb axons and a long-range interhemispheric axonal communication between the two bilateral ThEPC clusters.

The identification of a long-range axonal communication during the habenular neurocircuit formation opens up a new challenging field for the investigation of the function of interhemispheric connections. It is still unclear how the ThEPC neurons transmit information to the other side of the brain.

As mention above, the early establishment of cortical connections in mouse involved guidance factors and molecular cues allowing axons to cross properly the midline and reach their target in the contralateral neocortex (Lindwall et al., 2007). Recent progress in long distance axonal communication in the mammalian forebrain has demonstrated the key role of midline glia structure in commissural formation (Seth A. et al., 2006; Nawabi and Castellani, 2011). For instance, the formation of post-optic commissure in zebrafish depends on the function of *sonic hedgehog* (*shh*) and *slit* that regulate the expression of glia fibrillary acidic protein (GFAP) in the midline glia (Barresi MJ et al., 2005). Disrupting the *slit* signaling cascade causes disorganisation in the midline glia and several commissural axons are affected. Additional evidences demonstrating the importance of midline glia genes have been reported analysing the *belladonna* zebrafish mutant. The disruption of *lhx2* gene function in this mutant causes a disorganisation of midline glia with a consequent disruption of post-optic and anterior commissure axonal crossing (Seth A. et al., 2006). Nawabi and Castellani reviewed that the embryonic midline glia express attracting and repulsive molecules, such as *netrin* used to discriminate between crossing axons and ipsilateral running axons (Nawabi and Castellani, 2011). Moreover, they

highlight that the midline properties change over the time in according to the input received from the incoming axons. Consistent with our observations, one may speculate that ThEPC crossing axons express different guidance receptors, such as DCC (Deleted in Colon-rectal Carcinoma) and Robo. The ablation of ThEPC neurons causes the absence of midline axonal crossing and this influences the glia midline properties. The consequent changes of glia midline gene expression, such as of *netrin*, *shh*, *slit* or *lhx2*, could affect the ThEPC axonal migration on the contralateral brain side. Modification in ThEPC neuron long-range axonal communication may cause changes in ThEPC gene expression on the contralateral side with a consequent effect on ThEPC neuronal network establishment. Since dHb axons cross the ThEPC neurons during the establishment of habenular neurocircuit, the change in ThEPC neuron properties may affect correct dHb axonal elongation and consequently axonal pathfinding. Alternatively, ThEPC neuron derived cues may send signals to or across the midline independently of axon commissures. The identification of molecules involved will shed light on this issue in the future.

Our system allowed us to overcome the limitations studying developmental processes on fixed embryos and to follow the formation of DDC neuronal network for 4 days. Using high-resolution long-term *in-vivo* 2-PM, we identified a crucial role of long distance interhemispheric ThEPC communication for bilateral dHb axon elongation and targeting. However, the molecular mechanism responsible for long-range axonal communication during the DDC system development is still unknown and awaits future investigation.

4.4 Unilateral ablation of one habenula does not influence dHb axon elongation and pathfinding on the contralateral brain side

The development of brain asymmetries is one of the most fascinating fields in neuroscience and it is not clear whether exchange of information between the two brain hemispheres is important for the formation of neuroanatomical asymmetries (Taylor et al., 2010). In the vertebrate brain, one of the best described systems used to study brain asymmetry is the habenular neuronal network of zebrafish (Aramaki and Hatta, 2006). The habenular commissure connects the asymmetric habenular nuclei located in the left and the right brain side and allows interhemispheric exchange of information (Hendricks and Jesuthasan, 2007).

The dHb nuclei are subdivided in the lateral (dHbl) and medial habenula (dHbm), which show asymmetry in their cell composition, gene expression and neuropil density between the left and the right side of the brain (Gamse et al., 2003, 2005). During the formation of the DDC system, left-right dHb asymmetry is converted into a dorso-ventral asymmetry in that efferent habenular projections target dorso-ventrally distinct regions of the IPN (Concha and Wilson, 2001; Gamse et al., 2003; Aizawa et al., 2006; Bianco et al., 2009).

The establishment of interhemispheric axonal connections between the habenulae could be a possible mechanism used to facilitate the asymmetric cell type organisation in the dHb and the coordinated elongation of their efferent projections. We show that unilateral ablation of early dHb neurons at the onset of axonal elongation (2dpf) does not influence the development of the contralateral habenular, the axon elongation and the targeting of their efferent axons. Indeed, high-resolution images of IPN innervation at 4 dpf show the characteristic shape of the axonal arbors within the IPN (Figure 3.10). The absence of changes in IPN innervations after unilateral dHb ablation highlights the specific importance of ThEPC neurons for habenular neurocircuit formation. Therefore, interhemispheric dHb communication processes are not necessary for dHb axon elongation and pathfinding at least after 2 dpf. However, we cannot exclude that early steps of dHb development

may influence habenular nuclei formation and axonal targeting. Indeed, the establishment of dHb subnuclei starts around 28 hpf (Aizawa et al., 2007) with the initial differentiation of dHbl sub-nucleus follow by dHbm development (Roussigne et al., 2009). Therefore, at the time of unilateral dHb ablation, many events responsible for dHbl and dHbm formation have already occurred.

The first commissures between the habenular nuclei have been reported at 2 dpf (Hendricks and Jesuthasan, 2007; Hendricks et al., 2008). However, we cannot completely preclude earlier communication events between the habenular neurons. One way to exclude the early contribution of interhemispheric dHb nuclei communication to dHb axonal elongation and pathfinding could be through the unilateral ablation of the dHb precursor cells. Unfortunately, the lack of transgenic lines expressing fluorescent proteins in the dHbl and dHbm precursor cells makes this investigation currently unrealistic.

4.5 Ventral habenular neurons originate in the thalamus and only develop in the presence of *tcf7l2*

The mammalian habenular nuclei can be grossly subdivided into medial and lateral subnuclei mainly in according to the marker gene analysis, the sources of afferent axons and to the main targets innervated in the brain. The teleost dHb is homologous to the mammalian medial habenula and in the last two decades a lot of information has been collected about its origin and the underlying molecular pathways (Bianco et al., 2009; Beretta et al., 2012). In contrast, the teleost vHb, homologous to the mammalian lateral habenula, has been poorly characterised (Amo et al., 2010), although it recently became a model to investigate reward regulatory systems (Bromberg-Martin and Hikosaka, 2011; Matsumoto and Hikosaka, 2007, 2009a, b). The origin, development and the underlying genetic pathways are still completely unknown.

We show that the *hd1:mmGFP* transgene is expressed in vHb neurons and their efferent axons innervating the MR. We observed that ThEPC clusters are composed of different types of neurons with differences in the mitotic activity and axonal targets. In accordance to the ThEPC neuron nature and to the expression of 5HT serotoninergic marker within a few ThEPC neurons, we investigated the ThEPC neuronal fate during the DDC system formation. Combining the photoswitchable PSmOrange with our automatic ImageJ colocalisation macro, we demonstrated that all the habenular neurons originate within the prosomer 2. Compared to the origin of dHb neurons in the proximity of the pineal complex (Roussigne et al., 2009), vHb cells originate in a more posterior and ventral part of prosomere 2. A fairly small number of cells co-expressing GFP and the photoconverted protein ended up in the vHb (Figure 3.12). However, other photoconverted cells did not coexpress the *hd1:GFP* transgene. This indicates on one hand that probably all vHb neurons originate in the posterior-ventral thalamic area. On the other hand not all the vHb neurons are initially labeled with GFP in the *Et(-1.0otpa:mmGFP)hd1* transgenic line.

One of the most characterised pathways required for the specification of dHb is the Wnt/beta-catenin pathway (Carl et al, 2007). The up- or downregulation

of Wnt pathway activity results is the loss of asymmetry of dHb nuclei. Recent results obtained in our lab have shown that the loss of function in the *tcf7l2* gene causes modifications in the dHb nucleus and in the dHb efferent projections innervating the IPN (M. Carl, personal communication). The transcriptional regulator *tcf7l2* acts as an activator during the establishment of habenular asymmetry and the loss of *tcf7l2* gene causes an increment in the number of dHbl on the right brain hemisphere. Moreover, in *tcf7l2* loss of function embryos, the dHb efferent axons innervate only the dorsal part of the IPN with a consequent alteration of dorso-ventral asymmetry (M. Carl, personal communication).

Since nothing is known about the genetic pathways underlying the vHb neurons, we investigated whether the *tcf7l2* gene has some functions during the vHb formation. Combining the PSmOrange with the automatic ImageJ macro in *Et(-1.0otpa:mmGFP)hd1* line *tcf7l2*$^{-/-}$ mutant background (Muncan et al., 2007), we show that *tcf7l2* functional gene is necessary for vHb development. Additionally, the analysis of the vHb axons innervation within the MR supports the role of Wnt/beta-catenin pathway during vHb development, mediated by *tcf7l2* gene activity (Figures 3.13,3.14).

In our studies, we have identified the source of vHb neurons in the thalamus and the first gene required during their development. Furthermore, ThEPC short-range and long-range axonal communication seems not to be affected in the *tcf7l2* mutant (Muncan et al., 2007) and dHb axons target the IPN (M. Carl, personal communication). These findings indicate that ThEPC neurons responsible of the vHb origin are not required for dHb axon elongation and targeting.

In conclusion, the application of techniques, such as the 2-PM to investigate neuronal network formation in living animals provides a better understanding of the spatio-temporal sequence of developmental events. We show a detailed description of DDC system neuronal network formation *in-vivo* and uncovered the importance of interhemispheric long-range axonal communication mediated by intermediate targets for dHb axons in the thalamus. These ThEPCs consist of different cell types. Combining the photoconvertible PSmOrange fluorescent protein with a new automatic

ImageJ Macro, we identified one subpopulation being vHb neurons. These only develop in the presence of *tcf7l2* gene activity.

5 Experimental Procedures

5.1 Fish lines and maintenance

The zebrafish lines were maintained and bred according to standard procedures (Westerfield, 1995). AB and *tupl* wild-type lines and the *Et(-1.0otpa:mmGFP)hd1*, *tcf7l2*^{exl} (Muncan et al., 2007) x *Et(-1.0otpa:mmGFP)hd1* and *masterblind/Axin1*^{tm213} (Heisenberg et al., 2001) x *Et(-1.0otpa:mmGFP)hd1* lines were used.

The zebrafish embryos were raised in E3 medium and to inhibit pigmentation 0.2 mM 1-phenyl-2 thiourea (PTU, Sigma) was added after gastrulation. The medium was changed twice per day.

To collect different embryonic developmental stages, the embryos were anesthetized using 0.02% of ethyl 3-aminobenzoate methansulfonate (Tricaine, Sigma) and fixed in 4.0% paraformaldehyde (PFA, Sigma) in PBS at room temperature for 3 hours or at 4° C over night. After fixation, the embryos were washed three times in 1X PBST (PBS + 0.01% Tween 20, Sigma) and placed in a sterile petri dish under a light binocular microscope. The chorion was removed with tweezers (No. 5 Dumont & Fils), the larvae were rinsed two times for 5 minutes in 50% methanol in PBST and stored in 100% methanol (Sigma) at -20° C in 1.5 ml sterile tubes (Eppendorf).

E3 embryo medium:

5.0 mM NaCL (Sigma)
0.17 mM KCL (Sigma)
0.33 mM $CaCL_2$ (Sigma)
0.33 mM $MgSO_4$ (Sigma)
1.0% methylene blue (Sigma)

Tricaine stock solution (15 mM, pH 7.0, 27° C):

0.40 g ethyl 3-aminobenzoate methansulfonate salt (Sigma)

97.9 ml DD water

~2.1 ml 1M Tris HCL (pH 9.0, 27° C; Sigma)

Paraformaldehyde (4%, pH 7.0, 27° C):

1.33 M Paraformaldehyde (Sigma)

1X PBS (Sigma)

The pH was adjusted to 7.0 (27° C) adding 6.0 µl of 10 M NaOH (Sigma).

5.2 *Tcf7l2^{exl} x Et(-1.0otpa:mmGFP)hd1* genotyping

The identification of *tcf7l2^{exl}* (Muncan et al., 2007) homozygote adult and embryo mutants was performed by genotyping.

5.2.1 Genomic DNA extraction

The *tcf7l2^{exl}* x *Et(-1.0otpa:mmGFP)hd1* adult fish and embryos were anesthetized using a lower dose of tricaine and a small portion of the fin tissue was cut with a scalpel or a tweezers respectively and used for the genomic DNA extraction. The adult fish were kipped separately in mouse tanks and sorted in according to the result of each genotyping. For adult fish and embryos as well the excised tissue was incubated in 200 µl of GNT-K buffer containing 100 µg/ml of proteinase K (Sigma) at 56° C for 2 hours and heated at 95° C for 15 minutes. Each sample was briefly spun down and 500 µl of 96% ethanol (Sigma) were added. The solution was centrifuged at room temperature for 30 minutes at 14000 rpm (Eppendorf 5424/5424R), the supernatant was carefully discarded and the pellet was dried in ice for 20 minutes. The genomic DNA was resuspended in 25 µl of Milli-Q DNase/RNase free water and heated at 56° C for 20 minutes. The extracted DNA was stored at -20° C.

GNT-K buffer:

50 mM KCL (Sigma)
1.5 mM $MgCL_2$ (Sigma)
10 mM Tris-HCL pH 8.5 (27° C; Sigma)
0.01% Gelatin (Sigma)
0.45% Nonidet® P-40 (Sigma)
0.45% Tween® 20 (Sigma)

5.2.2 PCR

Purified genomic DNA were amplified by PCR (Qiagen Multiplex PCR Kit) to identify the point mutation in the *tcf7l2* gene using the following primers:

Primer Forward:
5'- AAAATGCCGCAGCTGAAC -3'
Primer Revers:
5'- CAACAACACGGTGCATCG -3'

The PCR reaction mix was prepared for each sample using:

5x Taq Polymerized Buffer	5.0 µl
Q-Solution	10 µl
5.0 mM $MgCL_2$	5.0 µl
Primer Forward [100 µM]	0.50 µl
Primer Revers [100 µM]	0.50 µl
10 mM dNTPs Mix	1.0 µl
Qiagen DNA Taq Polymerase	1.0 U
Extracted Genomic DNA	2.0 µl

The final volume of each reaction was adjusted with Milli-Q DNase/RNase free water to 50 µl.
The polymerase chain reaction was performed under the following condition:

95° C 2 min
95° C 30 sec
63° C 30 sec
72° C 30 sec
go to step 2, repeat the cycle 30 times
72° C 5 min

4.0° C forever

To control the PCR product of each reaction 30 µl of PCR were loaded with 6X loading dye (Fermentas) on 1.5% agarose gel (Sigma).

5.2.3 BsajI restriction analysis

The nonsense point mutation in *tcf7l2* mutant gene disrupts a BsajI restriction site. Therefore, to identify the mutated base pair the BsajI restriction enzyme (New England Biolab, NEB) digestion was performed using:

PCR Product	16 µl
10X Buffer 4 (NEB)	2.0 µl
BsajI (NEB)	2.0 µ (1.0 U)

60° C, 4 hours

The digestion products were loaded with 6X loading dye on 1.5% agarose gel.

5.3 *In-situ* hybridization procedures

5.3.1 Plasmid preparations

DNAs for whole-mount *in-situ* probes were cloned into the TOPO® TA vector (Invitrogen) or in the pBlueScript vector (pBSK, Addgene). *Escherichia coli* chemical competent cells (Invitrogen) were transformed using 0.5-1.0 µl of DNA (~0.50 µg). The solution containing the plasmid DNA and the chemical competent cells was incubated in ice for 30 minutes and heated at 42° C for 40 seconds without shaking. 250 µl of preheated SOC medium (Invitrogen) were added and the cells were grown at 37° C for one hour at 450 rpm (Thermomixer®, Eppendorf). 30-50 µl of each transformation were spread on preheated LB plates containing either 100 mg/ml of ampicillin or 50 mg/ml of kanamycin (Roche). Each plate was incubated at 37° C overnight and to ensure to pick up single colonies, sequential dilutions were prepared for each transformation.

Next day, single colonies were picked up and incubated at 37° C for 6-8 hours in 3.0 ml of LB medium (Sigma) with the appropriate antibiotic containing either 100 mg/ml of ampicillin or 50 mg/ml of kanamycin. The bacterial solution was diluted (1:500) in LB medium containing the antibiotic and grown at 37° C over night at 180 rpm on a shaker incubator (Bionics®). The bacterial culture was centrifuged at 4° C for 20 minutes at 3200 rpm (Eppendorf 5810/5810R) and the plasmid was isolated using the large-scale plasmid purification Qiagen Midi or Maxi Kit.

The plasmid DNA was checked on 0.8-1.0% agarose gels and the concentration/purity was measured using Nanodrop system (Fisher). Each plasmid was stored at -20° C.

LB medium (pH 7.0, 27° C)

1.0% Tryptone (Roth)
0.50% Yeast Extract (Roth)
1.0% NaCL

0.30% Tween 20 (Sigma)
0.30% Glycerol (Sigma)

The mixture was autoclaved on liquid cycle for 20 minutes and stored at 4° C. The antibiotics were added fresh each time.

LB plates

LB Medium
+ 15 g/l LB agar (Roth)

5.3.2 *In-situ* probe transcription and purification

Plasmids for whole mount *in-situ* hybridizations were linearized by restriction enzyme digestion using the following conditions:

Circularized Plasmid DNA	3.0 µl (~1.0 µg)
10X Buffer (NEB)	2.0 µl
Restriction Enzyme (NEB)	2.0 µl (1.0 U)
DD Water	13.0 µl

37° C, 3 hours

The digestion was checked loading 2.0 µl of linearized plasmid with 6X loading dye on 1.0% agarose gel.
To prepare *in-situ* probes, 3.0 µl of linearized plasmid were incubated with 16 U RNAas inhibitors (NEB), 2.0 µl of 10X buffer (NEB) and 2.0 µl of DIG (digoxigenin) or FITC (fluorescein) labelling mix (Roche) in a total volume of 20 µl. RNA transcription was initiated adding 10 U of the appropriated RNA polymerase and the mixture of reaction was incubated at 37° C for 3 hours. The RNA was cleaned up and concentrated using the RNeasy Cleanup Kit (Qiagen) according to the manufacturer's instructions. To ensure higher

concentration levels, the *in-situ* probes were eluted in two steps with 30 ul of Milli-Q DNase/RNase free water. Each *in-situ* probe was checked by agarose gel electrophoresis and the concentration/purity was estimated using the Nanodrop system. The RNA probes were immediately used or stored at -20° C or at -80° C.

In-situ Probes	Linearization Enzyme	RNA Polymerize	References
Kcdt12.1	*EcoRI*	*T7*	*Gamse et al., 2005*
Kcdt8	*XhoI*	*Sp6*	*Gamse et al., 2005*
Cxcr4b	*BamHI*	*T7*	*Roussigné et al., 2009*
Lhx2b	*XbaI*	*T7*	*Peukert et al., 2011* *Seth et al., 2006*
Lhx1a	*BamHI*	*T7*	*Toyama et al., 1995*
Nr4a2a	*HindIII*	*T3*	*Blin et al., 2008* *Filippi et al., 2007*

The *kisspeptin-1* (Ogawa et al., 2012; Servili et al., 2011) *in-situ* probe was obtained by PCR using the following primers:

Primer Forward:
5'- ATGCTGCTTACTGTCATATTGATG -3'
Primer Revers:
5'- GGATCCATTAACCCTCACTAAAGGGAcacctaaaacatgaaggcaaatacc -3'

The lowercase characters on the reversed primer highlight the T3 polymerase DNA binding site.
The RNA was extracted from 10-20 5 dpf (day post fertilization) old embryos using 1.0 ml of trizol reagent (Invitrogen) in 1.5 ml eppendorf tube. The tissue was homogenized by pipetting at room temperature for 5 minutes and 200 µl of chloroform (Sigma) were added. The solution was mixed for 15 seconds

and incubated at room temperature for 3 minutes. The samples were centrifuged at 4° C for 15 minutes at 14000 rpm and the supernatant was transferred in a new sterilized eppendorf tube. 500 µl of isopropanol (Sigma) were added to the mixture and the solution was incubated at room temperature for 10 minutes. Next, the samples were centrifuged at 4° C for 10 minutes at 14000 rpm, the supernatant was carefully discarded and the pellet was washed using 300 µl of 70% ethanol (Sigma). The RNA was isolated by centrifugation and the pellet resuspended in 30 µl of of Milli-Q DNase/RNase free water. 2.0 µl of extracted RNA was loaded with 2X RNA loading dye (Fermentas) on 1.0% agarose gel and the concentration/purity was measured using Nanodrop system. The RNA was stored at -20° C or at -80° C.

The RNA was reverse-transcribed to cDNA using the SuperScript® III Reverse Transcriptase Kit (Invitrogen) in according to the manufacturer's instructions.

The PCR reaction mix was prepared for each sample using:

5x Taq Polymerized Buffer	5.0 µl
Q-Solution	10 µl
5.0 mM MgCl2	5.0 µl
Primer Forward [100 µM]	0.50 µl
Primer Revers [100 µM]	0.50 µl
10 mM dNTPs Mix	1.0 µl
Qiagen DNA Taq Polymerase	1.0 U
Extracted Genomic DNA	2.0 µl

The final volume of each reaction was adjusted with Milli-Q DNase/RNase free water to 50 µl.

The polymerase chain reaction was performed under the following condition:

95° C	2 min
95° C	30 sec

63° C 30 sec
72° C 60 sec
go to step 2, repeat the cycle 29 times
72° C 5 min
4.0° C forever

The PCR product was loaded with 6X loading dye on 1.5% agarose gel. The PCR band with approximately 530 bp (base pair) was gel extracted (Gel Extraction Kit, Qiagen) and the RNA *in-situ* probe was transcribed using the T3 RNA polymerase (NEB) and stored as described above.

5.3.3 *In-situ* hybridization labelling

Whole mount *in-situ* hybridization labelling was performed in 1.5 ml sterilized eppendorf tubes. The embryos were rehydrated in 50% methanol/PBST for 15 minutes and washed two times in PBST for 10 minutes. The embryos were incubated with 10 µg/ml of proteinase K (Sigma) in PBST for a different amount of time in according to the developmental stage.

Developmental Stage	Proteinase K Incubation Time
Prim-5 to Long-pec	20 minutes
Long-pec to Protruding-mouth	40 minutes
4 dpf	1 hour
5 dpf	1 hour and 30 minutes

After proteinase K digestion, the embryos were washed two times in PBST and fixed in 4% PFA for 20 minutes. The fixative was removed and the embryos were washed 5 times for 5 minutes with PBST. All the previous steps were performed at room temperature. Subsequently the embryos were rinsed in 1.0 ml of hybridization mix for 2 hours at 65-68° C. The in-situ probe was diluted 1:100 in hybridization mix and pre-incubated for 10 minutes at 65-68° C. The embryos were incubated with the *in-situ* probe overnight at 65-68 °C.

Next day, the samples were washed for 5 minutes in hybridization mix, incubated for 30 minutes in 50% hybridization mix in 2X SSC and washed two times in 0.2X SSC for 35 minutes. Each step was performed at 65-68° C. Next, the embryos were washed in 1:1 mixture of 0.2X SSC and MAB, equilibrated two times for 5 minutes in MAB and incubated in the blocking solution (MABL) at room temperature for 2 hours. Secondary antibody binding was performed using a mixture of anti-digoxigenin-alkaline phosphatase (1:5000) or anti-fluorescein-isothiocyanate phosphatase (1:1000) diluted in MABL. The binding was completed overnight at 4° C.

The next day, the embryos were washed in MAB 4 times for 30 minutes at room temperature and equilibrated 3 times for 5 minutes in the staining buffer (DIG or FITC). The detection was performed incubating the samples in the developmental substrate at room temperature in the dark until the reaction was completed. For the DIG staining 1.0 ml of pre-mixed NBT/BCIP (Thermo Scientific) was used as developing substrate; for FITC reaction, the embryos were incubated at 28 °C with the Fast Red TR-Naphtol substrate (Sigma) in according to the manufacturer's instructions. Each reaction was stopped by several washing steps in PBST and the staining was fixed in 4% PFA for 1 hour. The stained samples were stored shortly in PBST at room temperature or for long time in 80% glycerol diluted in DD water at 4° C.

Hybridization mix (pH 6.0, 27° C)

50% Formamide (Roth)
5X SSC
250 µg/ml Torula RNA (Sigma)
0.1% Tween 20 (Sigma)
50 µg Heparin (Applichem)

The pH was adjusted to 6.0 (27° C) adding 1.0 M of citric acid.

20X SSC (pH 7.0, 27° C)

0.30 M Sodium Citrate (Sigma)

3.0 M NaCL (Sigma)

MAB (pH 7.5, 27° C)

100 mM Maleic Acid (Sigma)
150 mM NaCL (Sigma)
0.10% Tween 20 (Sigma)

MABL (pH 7.5, 27° C)

MAB
+ 2.0% Blocking Reagent (Roche)

Staining buffer (DIG)

5.0 ml 1.0 M Tris HCL (pH 9.0, 27° C; Sigma)
1.0 ml 5.0M NaCL (Sigma)
2.5 ml 1.0 M $MgCL_2$ (Sigma)
250 µl Tween 20 (Sigma)

The volume was adjusted to 50 ml with DD water.

Staining buffer (FITC)

0.10 M Tris HCL (pH 8.3, 27° C; Sigma)
0.10% Tween 20 (Sigma)

5.3.4 Antibody staining

Whole mount immunohistochemistry was performed in 1.5 ml sterilized eppendorf tubes. Embryo rehydration, proteinase K treatment and fixation were carried out as described in the previous subchapter.

After fixation, the embryos were washed 5 times in PBSTr for 10 minutes (1X PBS + 1.0% Triton-X-100; Roth) and incubated to block the unspecific antibody binding in PBS, 0.80% Triton X-100 (Sigma); 10% NGS (Normal Goat Serum; Invitrogen); 1.0% DMSO (Dimethyl Sulfoxide; Sigma) at room temperature for 2 hours on a shaking plate. The primary antibody was diluted in 500 µl of 1X PBS + 0.80% Triton X-100; 1.0% NGS; 1.0% DMSO and incubated overnight at 4° C on a shaking plate.

Next day, the embryos were washed 5 times for 10 minutes with PBSTr and incubated in blocking solution (0.80% Triton X-100; 10% NGS; 1.0% DMSO) at room temperature for 2 hours. The secondary antibody was diluted in 500 µl of 0.80% Triton X-100; 1.0% NGS; 1.0% DMSO and incubated overnight at 4° C on a shaking plate.

The samples were washed 4 times for 30 minutes with PBSTr and if necessary the nuclei were stained for 30 minutes with Sytox Orange (1:10000, Invitrogen) in PBS, 0.80% Triton X-100; 1.0% NGS. Embryos were washed 3 times for 5 minutes in PBSTr and immediately mounted and imaged by confocal laser scan microscopy (CLSM, see chapter 5.9).

Antibody	Dilution	Brand
Rabbit anti-GFP	1:1000	Torrey Pines Biolabs
Rat anti-GFP	1:500	NacalaiTesque
Mouse α-acetylated tubulin	1:500	Sigma
Rabbit anti-5HT	1:1000	Sigma
Rabbit/Mouse anti-Calretinin	1:1000	Swant
Alexa Fluor 488 Goat Anti Rat	1:200	Molecular Probes
Alexa Fluor 488 Goat Anti Rabbit	1:250	Molecular Probes
AlexaFluor 647 Goat Anti Mouse	1:200	Molecular Probes
AlexaFluor 647 Goat Anti Rabbit	1:200	Molecular Probes

5.3.5 Double fluorescence immuno-*in-situ* labellings

Whole mount of double fluorescence immuno *in-situ* labellings were performed as described previously in the subchapters 5.3.3 and 5.3.4. Between the *in-situ* labelling and the antibody staining, the embryos were fixed at room temperature for maximum 20 minutes and washed 3 times with PBST on a shaking plate (Macdonald et al., 1994; Shanmugalingam et al., 2000 and Carl et al., 2007).

5.4 Long-term 2 photon (2-PM) *in-vivo* microscopy

Long-term 2-PM was applied to overcome the CLSM limitations to follow the entire DDC (dorsal diencephalic conduction) system development in the *Et(-1.0otpa:mmGFP)hd1* transgenic embryos between 32 hpf (hour post fertilization) and at least up to 4 dpf.

5.4.1 Embryo embedding

Dechorionated *Et(-1.0otpa:mmGFP)hd1* transgenic embryos were mounted in the center of a disposable sterile polystyrene petri dish with following dimension: 88 mm of diameter x 12 mm of high. A ring of 1.5% low melting agarose gel (Sigma) with the size of 44 mm x 6.0 mm was built up in the center of each petri dish using a hollow circular mold. The embryos were mounted for an upright 2-PM microscope in a handmade well located in the center of each agarose gel ring with a diameter of 1.0 cm using 200 µl of 0.50% - 0.80% low melting agarose gel preheated at 37° C for 20 minutes. The embryos were placed under the Leica binocular fluorescent microscope (MZ16F) and gently orientated dorsally using a pipet tip (Eppendorf). When the agarose was set (10 minutes), the petri dish was flooded with 15 ml of 0.20 mM 1-phenyl-2 thiourea (PTU); 0.02% of ethyl 3-aminobenzoate methansulfonate (Tricaine) in sterilized E3 medium.

5.4.2 Long-term 2-PM *in-vivo* microscopy - Experimental conditions

The long-term *in-vivo* recording of the *Et(-1.0otpa:mmGFP)hd1* transgenic embryos was performed with an excitation wavelength of 940 nm by LaVision Biotec TriM Scope multi photon upright microscope using the Nikon 16x water immersion long working distance (LWD) objective lens (NA 0.80). Each stack was acquired every 30-40 minutes for a range of time of at least 4 days with a total Z-height between 240 µm and 300 µm. To ensure higher resolution images, the pixel size was set up between 0.30 µm and 0.46 µm (x,y) with a Z-step of 1.0 µm and laser power correction was applied.

To prevent pigment formation and embryo shifting fresh sterilized fish water containing 0.20 mM of 1-phenyl-2 thiourea (PTU) and 0.02% of ethyl 3-aminobenzoate methansulfonate (Tricaine) was added twice per day.

5.4.3 Long-term 2-PM *in-vivo* microscopy vs long-term CLSM *in-vivo* microscopy

To demonstrate the advantages of the 2-PM microscopy, DDC system development was recorded in *Et(-1.0otpa:mmGFP)hd1* transgenic embryos between 32 hpf and 5 dpf using the LaVision Biotec TriM Scope multi photon upright microscope (Figure 3.4) and the inverted CLSM Nikon C2 Plus (Figure 3.3).
The following comparable settings were applied in each experiment:

Parameters	Lavision TriM Scope 2-PM	C2 Plus Nikon
Excitation Wavelength (nm)	940 nm	488 nm
Laser Power (mW)	23 mW to 50 mW	2.0 mW to 6.0 mW
Objective Lens	Nikon 16x (NA 0.80)	Nikon Plan Apo 20x (NA 0.75)
Field of View (µm)	500 x 500 µm	419 x 419 µm
Pixel size (µm)	0.388 µm	0.409 µm
Z-Depth of each stack (µm)	300 µm	300 µm
Z-Step (µm)	1.0 µm	1.0 µm
Time Step (s)	1800 s	1800 s
Total Time (hh:mm:ss)	94:30:00	89:30:00

Laser power correction was used in both cases to compensate for increasing depth. The vitality of the embryos was investigated analyzing the normalized GFP fluorescence emission over the time (data not shown).

5.4.4 2-PM laser ablation in *Et(-1.0otpa:mmGFP)hd1* embryos

2-PM laser ablation of ThEPCs (thalamic early projecting cells) and dHb (dorsal habenula domain) were performed at 32 hpf and 2 dpf respectively by LaVision Biotec TriM Scope multi photon upright microscope at a wavelength of 740 nm with 200-300 mW of laser power using the Nikon 16x water immersion objective lens (NA 0.80).

The position of the cell to be ablated was precisely marked by a point on an acquired image, and the laser parked accordingly by the software (ImSpector Pro, LaVison BioTec GmbH) for point ablation. Ablation was controlled by monitoring the increase of unspecific fluorescence at the treated site: after a certain threshold is reached, the duration of the treatment will define the size of the ablated region. Careful calibration of the laser power allows precise ablations of regions ranging from single cells up to cluster of multiple cells.

Incomplete cell ablations were carried out removing 2-4 cells for 4 times. A stack of approximately 300 µm (Z-step of 1.0 µm) was acquired before and after each step of ThEPC cell ablation.

IPN (interpeduncular nucleus) innervation of living and fixed embryos was imaged using a 60x objective lens (NA 1.0) with a total Z-height of 100-120 µm. For higher resolution images, the pixel size was adjusted between 0.19 µm and 0.20 µm (x,y) with a Z-step of 0.75 µm; laser power correction was applied.

5.4.5 Image colour code analysis

Our 2-PM *in vivo* long-term time-lapse experiments over five days generated datasets up to 800 GB. A customer MIP ColourCode script was written (Appendix 7.3,7.4) and allows us to quickly produce a 2D visualisation of the 3D data, in which the brightness of each pixel is determined by making a maximum intensity projection of the stack, and pixel colours are assigned based upon the depth of the maximum value within the stack. To maximize the number of colours available to planes containing the sample and improving depth discrimination in the main region of interest, the script was

designed to detect automatically the first and last planes within the stack that contain a high density of maxima pixels.

The script is capable of processing automatically 800 GB of data in less than 3 hours using a 2 x 2.26 GHz Quad-Core Intel Xeon processor, after which it was possible to manually track single axons in 2-D images using the manual tracking plugin of the Fiji software (Schindelin et al., 2012). The Colour Code Scale LUT (Look Up Table), the scale bar and the time were inserted using the MIP_ColourCode Script.

The movies were created automatically using the MIP ColourCode script and compressed using the software Wondershare Vide Converter Ultimate (Wondershare, Shenzhen, China). The frame title was added in each movie using iMovie software (Apple Inc., Cupertino, CA).

5.5 H2B photoswitchable monomeric orange (PSmOrange) subcloning

The H2B-PSmOrange encoding DNA (Verkhusha et al., 2011) was subcloned into the pCS2^{+} vector using XbaI/XhoI and NotI/XhoI restriction enzymes respectively (NEB).

The pCS2^{+} vector was initially digested at the 3' end with XbaI restriction enzyme using the following protocol:

pCS2+ Vector	3.0 µl (~1.5 µg)
10X Buffer 4 (NEB)	2.0 µl
100X BSA (NEB)	0.2 µl
XbaI (NEB)	2.0 µl (1.0 U)
DD Water	12.8 µl

37° C, 3 hours

The digested DNA was purified using the PCR Purification Kit (Qiagen) in according to the manufacturer's instructions. The purified product was blunted using the T3 Klenow DNA Polymerase (NEB) under the following conditions:

Gel Extracted DNA	15.5 µl (~100 ng)
Buffer 2 (NEB)	2.0 µl
dNTPs [2.0mM]	2.0 µl
T3 Klenow DNA Polymerize (NEB)	0.5 µl (2.0 U)

37° C, 30 minutes

70° C, 10 minutes

The Klenow treated product was digested at the 5' end with XhoI restriction enzyme using the same reaction conditions described above.

The same approach was used to obtain the H2B-PSmOrange DNA fragment from the pN1 mammalian expression vector using NotI blunted and XhoI restriction enzymes respectively.

The digested products were loaded in 1.5% agarose gel and the expected size bands were gel extracted using the Qiagen Gel Extraction Kit in according to the manufacturer's instructions.

The H2B-PSmOrange DNA fragment was ligated into the pCS2^{+} digested vector using the T4 Ligation Kit (NEB). The ligation conditions were the following:

H2B-PSmOrange DNA Fragment	7.5 µl (5.0 ng)
pCS2+ Digested Vector	1.0 µl (2.0 ng)
T4 Ligation Buffer (NEB)	1.0 µl
T4 Ligase (NEB)	0.5 µl (2.0 U)

16° C, overnight

65° C, 10 minutes

Escherichia Coli chemical competent cells were transformed using 5.0 ng of ligated DNA for plasmid propagation as described in the subchapter 5.3.1 and the isolated clones were sequenced for confirmation (GATC Biotech AG).

5.6 mRNA *in-vitro* transcription, purification and injection

5.6.1 mRNA *in-vitro* transcription

The pCS2^{+} vector was linearized using the NotI restriction enzyme (NEB) and the mRNA for injection was prepared using the mMESSAGE mMACHINE® sp6 Kit (Ambion). 3.0 µl (~1.0 µg) of linearized vector was incubated with 2.0 µl of 2X transcription buffer, 10 µl of 10X ribonucleotides and 2.0 µl of 10X sp6 enzyme mix. The final volume of each reaction was adjusted with Milli-Q DNase/RNase free water to 20 µl and the mixture was incubated at 37° C for 2 hours. After linearization the DNA was digested with 1.0 U of DNase I endonuclease (Fermentas) at 37° C for 10 minutes.
The mRNA was cleaned up using the RNeasy Cleanup kit and additionally purified by mRNA precipitation. 6.0 µl of sodium acetate (3.0 M, pH 5.2, Sigma) and 150 µl of 96 % ethanol were added to mRNA solution. The mixture was incubated at -20° C for 30 minutes and centrifuged at 4° C for 30 minutes at 14000 rpm. The pellet was dried and resuspended in 150 µl of 70% ethanol. The solution was centrifuged at 4° C for 5 minutes at 14000 rpm and the pellet was dissolved in 20 µl of Milli-Q DNase/RNase free water. The mRNA was checked by agarose gel electrophoresis and the concentration/purity was estimated using Nanodrop system. The mRNA solution was immediately diluted for injection or stored at -20° C or at -80° C.

5.6.2 mRNA injection in zebrafish embryos

Using a microinjection machine (Eppendorf) 260 pg *H2B-PSmOrange* mRNA were injected into one cell stage embryos. The expression of H2B-PSmOrange was monitored using a Leica binocular fluorescent microscope (MZ16F). 80% (n=150) of injected zebrafish embryos showed strong expression of the nuclear H2B-PSmOrange protein for up to at least 4 dpf.
For *in vivo* nuclei labellings 130 pg *H2A-CFP* mRNA were injected in one cell stage old zebrafish embryos. Using the 2-PM, it was possible to visualise the H2A-CFP protein for up to at least 3 dpf.

5.7 H2B-PSmOrange photoconversion and image analysis

50 hpf *H2B-PSmOrange* mRNA injected embryos were imaged using the inverted confocal microscope Nikon A1R. Before and after photoconversion, an image was acquired using the sequential scanning mode for the 488 nm, 561 nm and 637 nm channels with the Nikon 20x air objective lens (NA 0.20). The pinhole was set to 24.7 µm (637 nm) to prevent spectral overlapping.

For H2B-mOrange photoswitching, the photoconversion NIS-Elements AR software tool was used: 17-20 mW of 488 nm excitation laser power; 1/2 scan speed frequency; 20 to 28 rounds of stimulation. The photoconverted protein was visible up to at least 3 days after treatment. To determine the position of ThEPC cells, a Z-stack was acquired at 4 dpf with Z-intervals of 1.0-2.0 µm.

The stacks were analyzed with our newly generated automatic FiJi ImageJ Macro (Appendix 7.5). To highlight the regions of interest (ROIs), different automatic thresholds were applied in the green and the far-red channel stacks. Each threshold area was detected with a fitting setting using the analyze particles tool and the overlapping ROIs displayed in yellow using the image calculator plugin. To speed up each analysis, the original stacks were convolved using the GaussianBlur plugin, the resulting smooth stacks were subtracted to the original stacks and the BachMode was set to “true” (Appendix 7.5).

5.8 Confocal Laser Scan Microscope (CLSM), image analysis and neuroanatomy

For CLSM, embryos were mounted in 1.0% low melting agarose (Sigma) in a glass bottom dish (MatTek or LabTek). Confocal images and stacks were acquired with a Nikon A1R using the Nikon 20x air objective lens (NA 0.20) and with a Leica TCS SP5 using Leica 20x air objective (NA 0.70) or the Leica 40x oil immersion objective (NA 1.3). Each Z-stack was acquired with intervals between 0.5 µm and 2.0 µm.

3D reconstructions, stack analysis and image corrections were performed using the software FiJi, NIS-Element AR and Adobe Photoshop CS4.

For the annotation of brain areas, we used traditional terminology consistent with the embryonic zebrafish atlas (Mueller and Wullimann, 2005) and took into account literature related to the markers used (Amo et al., 2010; Castro et al., 2006; Peukert et al., 2011; Puelles and Rubenstein, 2003).

6 REFERENCES

Agetsuma, M., Aizawa, H., Aoki, T., Nakayama, R., Takahoko, M., Goto, M., Okamoto, H. (2010). The habenula is crucial for experience-dependent modification of fear responses in zebrafish. Nat Neurosci, 13(11), 1354-1356.

Amo, R., Aizawa, H., Takahoko, M., Kobayashi, M., Takahashi, R., Aoki, T., and Okamoto, H. Identification of the zebrafish ventral habenula as a homolog of the mammaliam lateral habenula. (2010). Journal of Neuroscience 30(4), 1566-1574.

Aizawa, H., Bianco, I. H., Hamaoka, T., Miyashita, T., Uemura, O., Concha, M. L., Russell, C., Wilson, S. W., Okamoto, H. (2005). Laterotopic representation of left-right information onto the dorso-ventral axis of a zebrafish midbrain target nucleus. Curr Biol 15, 238 -243.

Aizawa, H., Bianco, I. H., Hamaoka, T., Miyashita, T., Uemura, O., Concha, M. L., Russell, C., Wilson, S. W. and Okamoto, H. (2006). Laterotopic Representation of Left-Right Information onto the Dorso-Ventral Axis of a Zebrafish Midbrain Target Nucleus. Current Biology 15, 238-243.

Aizawa, H., Goto, M., Sato, T. and Okamoto, H. (2007). Temporally regulated asymmetric neurogenesis causes left-right difference in the zebrafish habenular structures. Dev Cell 12, 87-98.

Altman, J., Bayer S. A. (1979). Development of the diencephalon in the rat. IV. Quantitative study of the time of origin of neurons and the internuclear chronological gradients in the thalamus. J Comp Neurol. 188(3), 455-71.

Ando, R., Hama, H., Yamamoto-Hino, M., Mizuno, H., Miyawaki, A. (2002). An optical marker based on the UV-induced green-to-red photoconversion of a fluorescent protein. Proc. Natl Acad. Sci. U. S. A. 99(20), 12651-6.

Aramaki, S. and Hatta, H. (2006). Visualizing neurons one-by-one in vivo: optical dissection and reconstruction of neural networks with reversible fluorescent proteins. Dev Dyn. 235(8), 2192-9.

Barresi, M. J., Hutson, L. D., Chien, C. B., Karlstrom, R. O. (2005). Hedgehog regulated Slit expression determines commissure and glial cell position in the zebrafish forebrain. Development 132, 3643-3656.

Bastiani, M. J., Raper, J. A., Goodman, C. S. 1984. Pathfinding by neuronal growth cones in grasshopper embryos. III. Selective affinity of the G growth cone for the P cells within the A/P fascicle. J Neurosci 4: 2311–1228.

Bate, C. M. (1976). Pioneer neurones in an insect embryo. Nature 260, 54-56.

Bell, G., and Sons (1897). A Treatiseon Painting. London: ElibronClassics.

Bentley, D., Caudy, M. (1983). Pioneer axons lose directed growth after selective killing of guidepost cells. Nature 304, 62-65.

Beretta, C. A., Dross, N., Gutierrez-Triana, J. A., Ryu, S., and Carl, M. (2012). Habenula circuit development: past, present and future. Frontiers in Neuroscience. Volume 6, Article 51.

Bianco, I. H., Carl, M., Russell, C., Clark, J. and Wilson, S. W. (2008). Brain asymmetry is encoded at the level of axon terminal morphology. Neural Development 3, 9.

Bianco, I. H. and Wilson, S. W. (2009). The habenular nuclei: a conserved asymmetric relay station in the vertebrate brain. Phil. Trans. R. Soc. B 364, 1005-1020.

Blin, M., Norton, W., Bally-Cuif, L., and Vernier, P. (2008). NR4A2 controls the differentiation of selective dopaminergic nuclei in the zebrafish brain. Mol Cell Neurosci 39, 592-604.

Bonnin, A., Torii, M., Wang, L., Rakic, P., and Levitt, P. (2007). Serotonin modulates the response of embryonic thalamocortical axons to netrin-1. Nature Neuroscience 10, 588-597.

Breasted, J. H. (1980). The Edwin Smith surgical papyrus. Chicago: University Press.

Broca, P. P. (1861). Remarques sur la siège de la faculté du langage ariticulè, suivies d'une observation d'apèmie. Bulletin de la Société anatomique de Paris 2, 330-357.

Bromberg-Martin, E.S., and Hikosaka, O. (2011). Lateral habenula neurons signal errors in the prediction of reward information. Nature Neuroscience 14, 1209-1216.

Brulli, J. D. and Easter, S. S. jr. (1995). The first retinal axons and their microenvironment in zebrafish cryptic pioneers and the pretract. The Journal of Neuroscience 15(4), 2935-2947.

Cajal y Ramon (1995) Histology of nervous system of a man and vertebrate. (trans. N Swanson and LW Swanson), Vol 1: 532. Oxford University Press, New York.

Caldecott-Hazard, S. (1988). Interictal changes in behavior and cerebral metabolism in the rat: opioid involvement. Exp Neurol, 99(1), 73-83.

Carl, M., Bianco, I. H., Bajoghli, B., Aghaallaei, N., Czerny, T. and Wilson, S. W. (2007). Wnt/Axin1/beta-Catenin Signaling Regulates Asymmetric Nodal Activation, Elaboration, and Concordance of CNS Asymmetries. Neuron 55, 393-405.

Castro, A., Becerra, M., Manso, M. J., and Anadón, R. (2006). Calretinin immunoreactivity in the brain of the zebrafish, Danio rerio: distribution and comparison with some neuropeptides and neurotransmitter-synthesizing enzymes. I. Olfactory organ and forebrain. Journal of Comparative Neurology 494, 435-459.

Centonze, V. E. and White, J. G. (1998). Multiphoton excitation provides optical sections from deeper within scattering specimens than confocal imaging. Biophys. J. 75, 2015-2024.

Chalupa, L. M., Meissirel, C., and Lia, B. (1996). Specificity of retinal ganglion cell projections in the embryonic rhesus monkey. Perspect Dev Neurobiol. 3(3), 223-231.

Cheng, H. J., Nakamoto, M., Bergemann, A. D., Flanagan, J.G., (1995). Complementary gradients in expression and binding of ELF-1 and Mek4 in development of the topographic retinotectal projection map. Cell 82, 371-381.

Chen, P. L., Clandinin, T. R. (2008). The cadherin Flamingo mediates level-dependent interactions that guide photoreceptor target choice in Drosophila. Neuron 58, 26-33.

Chitnis, A. B, Kuwada, J. Y. (1990). Axonogenesis in the brain of zebrafish embryos. J Neurosci 10, 1892-1905.

Colamarino, S. A., Tessier-Lavigne, M. (1995). The axonal chemoattractant netrin-1 is also a chemorepellent for trochlear motor axons. Cell 81, 621-629.

Concha, M. L., & Wilson, S. W. (2001). Asymmetry in the epithalamus of vertebrates. J Anat, 199 (Pt 1-2), 63-84.

Conchello, J. A. and Lichtman, J. W. (2005). Optical sectioning microscopy. Nature Methods 2, 920-931.

Connolly, J. L., Seeley, P. J., Greene, L. A. (1985). Regulation of growth cone morphology by nerve growth factor: A comparative study by scanning electron microscopy. J Neurosci Res 13, 183-198.

Cragg, B. G. (1961). The connections of the habenula in the rabbit. Experimental Neurology 3, 388-409.

Denk, W., Strickler, J. & Webb, W. Two-photon laser scanning fluorescence microscopy. Science 248, 73-76 (1990)],

Doll, C. A., Burkart, J. T., Hope, K. D., Halpern, M. E., and Gamse, J. T. (2011). Subnuclear development of the zebrafish habenular nuclei requires ER translocon function. Developmental Biology 360, 44-57.

Dontchev, V. D., Letourneau, P. C. (2002). Nerve growth factor and semaphorin 3A signaling pathways interact in regulating sensory neuronal growth cone motility. J Neurosci 22, 6659-6669.

Dufour, A., Seibt, J., Passante, L., Depaepe, V., Ciossek, T., Frisén, J., Kullander, K., Flanagan, J.G., Polleux, F., and Vanderhaeghen, P. (2003). Area specificity and topography of thalamocortical projections are controlled by ephrin/Eph genes. Neuron 39, 453-465.

Durbin, R. M. (1987). Studies on the development and organization of the nervous system of Caenorhabditis elegans. PhD thesis, University of Cambridge.

Edwards, J. S. (1977). Pathfinding by arthropod sensory nerves. In Identified neurons and behavior of arthropods (ed.) G Hoyle), pp. 484-493, Plenum, New York.

Edwards, J. S, Chen, S. W, Berns, M. W. (1981). Cercal sensory development following laser microlesions of embryonic apical cells in Acheta domesticus. J Neurosci 1, 250-258.

Ellison, G. (2002). Neural degeneration following chronic stimulant abuse reveals a weak link in brain, fasciculus retroflexus, implying the loss of forebrain control circuitry. Eur Neuropsychopharmacol, 12(4), 287-297.

Falcon, J. (1999). Cellular circadian clocks in the pineal. Prog Neurobiol, 58(2), 121-162.

Fazeli, A., Dickinson, S. L., Hermiston, M. L., Tighe, R. V., Steen, R. G., Small, C. G., Stoeckli, E. T, Keino-Masu, K., Masu, M., Rayburn, H. (1997). Phenotype of mice lacking functional Deleted in colorectal cancer (Dcc) gene. Nature 386, 796-804.

Feldheim, D. A, Kim, Y. I., Bergemann, A. D., Frise´n, J., Barbacid, M., Flanagan, J. G. (2000). Genetic analysis of ephrin-A2 and ephrin-A5 shows their requirement in multiple aspects of retinocollicular mapping. Neuron 25, 563-574.

Filippi, A., Dürr, K., Ryu, S., Willaredt, M., Holzschuh, J., and Driever, W. (2007). Expression and function of nr4a2, lmx1b, and pitx3 in zebrafish dopaminergic and noradrenergic neuronal development. BMC Developmental Biology 7:135.

Gamse, J. T., Thisse, C., Thisse, B. and Halpern, M. E. (2003). The parapineal mediates left-right asymmetry in the zebrafish diencephalon. Development 130, 1059-1068.

Gamse, J. T., Kuan, Y. S., Macurak, M., Brosamle, C., Thisse, B., Thisse, C., and Halpern, M. E. (2005). Directional asymmetry of the zebrafish epithalamus guides dorsoventral innervation of the midbrain target. Development 132, 4869-4881.

Goronowitsch, N. (1883). Das gehirn und die cranialnerven von Acipenser ruthenus. Morph. Jahrb. 13, 427-574.

Guglielmotti, V. and Cristino, L. (2006). The interplay between the pineal complex and the habenular nuclei in lower vertebrates in the context of the evolution of cerebral asymmetry. Brain Research Bulletin 69, 475-488.

Guillery, R. W. (1959). Afferent fibers to the dorso-medial thalamic nucleus in the cat. Journal of Anatomy 93, 403-419.

Halpern, M. E., Liang, J. O., and Gamse, J. T. (2003). Leaning to the left: laterality in the zebrafish forebrain. Trends Neurosci. 26, 308-313.

Hattori, T., McGeer, E. G., Singh, V. K. and McGeer, P. L. (1977). Cholinergic synapse of the interpeduncular nucleus. Experimental Neurology 55, 666-679.

Heisenberg, C. P., Houart, C., Take-uchi, M., Rauch, G. J., Young, N., Coutinho, P., Masai, I., Caneparo, L., Concha, M. L., Geisler, R., et al. (2001). A mutation in the Gsk3-binding domain of zebrafish Masterblind/Axin1 leads to a fate transformation of telencephalon and eyes to diencephalon. Genes & Development 15, 1427-1434.

Helmchen, F. and Denk, W. (2005). Deep tissue two-photon microscopy. Nature Methods 2, 932-940.

Hendricks, M., and Jesuthasan, S. (2007). Asymmetric Innervation of the Habenula in Zebrafish. Journal of Comparative Neurology 502, 611-619.

Hendricks, M., Mathuru, A. S., Wang, H., Silander, O., Kee, M. Z. L., and Jesuthasan, S. (2008). Disruption of Esrom and Ryk identifies the roof plate boundary as an intermediate target for commissure formation. Molecular and Cellular Neuroscience 37, 271-283.

Herrera, E., Marcus, R., Li, S., Williams S., Erskine, L., Lai, E., and Mason, C. (2004). Foxd1 is required for proper formation of the optic chiasm. Development 131, 5727-5739.

Mizunu, H., Hirano, T., and Tagawa, T. (2007). Evidence for Activity-Dependent Cortical Wiring: Formation of Interhemispheric Connections in Neonatal Mouse Visual Cortex Requires Projection Neuron Activity. Journal of Neuroscience 27(25), 6760-6770.

Hikosaka, O. (2010). The habenula: from stress evasion to value-based decision-making. Nature Neuroscience 11, 503-513.

Hindges, R., McLaughlin, T., Genoud, N., Henkemeyer, M., O'Leary, D., D. (2002). EphB forward signaling controls directional branch extension and arborization required for dorsal-ventral retinotopic mapping. Neuron 35, 475-487.

Hirano, S., Yan, Q., Suzuki, S. T. (1999). Expression of a novel protocadherin, OL-protocadherin, in a subset of functional systems of the developing mouse brain. J Neurosci 19, 995-1005.

Hutter, H. (2003). Extracellular cues and pioneers act together to guide axons in the ventral cord of C. elegans. Development 130, 5307-5318.

Kamei, M. and Weinstein, B. M. (2005). Long-term time-lapse fluorescence imaging of developing zebrafish. Zebrafish 2, 113-123.

Keleman, K., Rajagopalan, S., Cleppien, D., Teis, D., Paiha, K., Huber, L. A., Technau, G. M., Dickson, B. J. (2002) Comm sorts robo to control axon guidance at the Drosophila midline. Cell 110(4), 415-427

Keshishian, H. (1980). The origin and morphogenesis of pioneer neurons in the grasshopper metathoracic leg. Dev Biol 80: 388-397.

Klein, D. C., & Moore, R. Y. (1979). Pineal N-acetyltransferase and hydroxyindole-O-methyltransferase: control by the retinohypothalamic tract and the suprachiasmatic nucleus. Brain Res, 174(2), 245-262.

Kobat, D., Durst, M. E., Nishimura, N., Wong, A. W., Schaffer, C. B. and Xu, C. (2009). Deep tissue multiphoton microscopy using longer wavelength excitation. Optic express 17, 13354-13364.

Kuan, Y. S., Yu, H. H., Moens, C. B. and Halpern, M. E. (2007). Neuropilin asymmetry mediates a left-right difference in habenular connectivity. Development 134, 857-865.

Imai, T., and Sakano, H. (2011). Axon-axon interactions in neuronal circuit assembly: lessons from olfactory map formation. European Journal of Neuroscience 34, 1647-1654.

Lakhina, V., Falnikar, A., Bhatnagar, L., and Tole, S. (2007). Early thalamocortical tract guidance and topographic sorting of thalamic projections requires LIM-homeodomain gene Lhx2. Developmental Biology 306, 703-713.

Lecourtier, L., Neijt, H. C., & Kelly, P. H. (2004). Habenula lesions cause impaired cognitive performance in rats: implications for schizophrenia. Eur J Neurosci, 19(9), 2551-2560.

Lecourtier, L., & Kelly, P. H. (2005). Bilateral lesions of the habenula induce attentional disturbances in rats. Neuropsychopharmacology, 30(3), 484-496.

Lee, E. H., & Huang, S. L. (1988). Role of lateral habenula in the regulation of exploratory behavior and its relationship to stress in rats. Behav Brain Res, 30(3), 265-271.

Lee, A., Mathuru, A. S., Teh, C., Kibat, C., Korzh, V., Penney, T. B. and Jesuthasan, S. (2010). The habenula prevents helpless behavior in larval zebrafish. Curr. Biol. 20, 1-6.

Lindell, A. K. (2011). Lateral thinkers are not so laterally minded: hemispheric asymmetry, interaction, and creativity. Laterality 16, 479-498.

Lindwall ,C., Fothergill, T., Richards, L. J. (2007). Commissure formation in the mammalian forebrain. Curr. Opin. Neurobiol. 17, 3-14.

Lisoprawski, A., Herve, D., Blanc, G., Glowinski, J., & Tassin, J. P. (1980). Selective activation of the mesocortico-frontal dopaminergic neurons induced by lesion of the habenula in the rat. Brain Res, 183(1), 229-234.

Marcus, R. C., Blazeski, R., Godement, P., Mason, C. A. (1995). Retinal axon divergence in the optic chiasm: Uncrossed axons diverge from crossed axons within a midline glial specialization. J Neurosci 15, 3716-3729.

Marcus, R. C., Mason, C. A. (1995). The first retinal axon growth in the mouse optic chiasm: Axon patterning and the cellular environment. J Neurosci 15, 6389-6402.

Marshak, S., Nikolakopoulou, A. M., Dirks, R., Martens, G. J., Cohen-Cory, S. (2007). Cell-autonomous TrkB signaling in presynaptic retinal ganglion cells mediates axon arbor growth and synapse maturation during the establishment of retinotectal synaptic connectivity. J Neurosci 27, 2444-2456.

Matsumoto, M., and Hikosaka, O. (2007). Lateral habenula as a source of negative reward signals in dopamine neurons. Nature 447, 1111-1115.

Matsumoto, M., and Hikosaka, O. (2009a). Representation of negative motivational value in the primate lateral habenula. Nature Neuroscience 12, 77-84.

Matsumoto, M., and Hikosaka, O. (2009b). Two types of dopamine neuron distinctly convey positive and negative motivational signals. Nature 459, 837-841.

Macdonald, R., Xu, Q., Barth, K. A., Mikkola, I., Holder, N., Fjose, A., Krauss, S.,Wilson, S. W., 1994. Regulatory gene expression boundaries demarcate sites of neuronal differentiation in the embryonic zebrafish forebrain. Neuron 13, 1039–1053.

McLaughlin, T., Hindges, R., Yates, P. A., O'Leary, D. D. (2003). Bifunctional action of ephrin-B1 as a repellent and attractant to control bidirectional branch extension in dorsal-ventral retinotopic mapping. Development 130, 2407-2418.

Minsky, M. 1957. U.S. Patent no. 3013467. Microscopy apparatus, Dec.19, 1961 (Filed Nov. 7, 1957)

Miyasaka, N., Wanner, A. A., Li, J., Mack-Bucher, J., Genoud, C., Yoshihara, Y., and Friedrich, R. W. (2012). Functional development of the olfactory system in zebrafish. Mechanisms of Development.

Morgane, P. J., Galler, J. R. and Mokler, D. J. (2005). A review of systems and networks of the limbic forebrain/limbic midbrain. Progress in Neurobiology 75, 143-160.

Mueller, T., and Wullimann, M. (2005). Atlas of Early Zebrafish Brain Development. A Tool for Molecular Neurogenetics. 1st edition, Elsevier.

Muncan, V., Faro, A., Haramis, A. P. G., Hurlstone, A. F. L., Wienholds, E., van Es, J., Korving, J., Begthel, H., Zivkovic, D., and Clevers, H. (2007). T-cell factor 4 (Tcf7l2) maintains proliferative compartments in zebrafish intestine. EMBO reports 8, 966-973.

Nawabi, H., and Castellani, V. (2011). Axonal commissures in the central nervous system: how to cross the midline? Cell Mol Life Sci 68, 2539-2553.

Nishikawa, T., Scatton, B. (1985). Inhibitory influence of GABA on central serotonergic transmission. Involvement of the habenulo-raphe pathways in the GABAergic inhibition of ascending cerebral serotonergic neurons. Brain Res 331, 81-90.

O'Connor, R., Tessier-Lavigne, M. (1999). Identification ofmaxillary factor, a maxillary process-derived chemoat-tractant for developing trigeminal sensory axons. Neuron 24: 165-178.

Ogawa, S., Ramadasan, P. N., Goschorska, M., Anantharajah, A., Ng, K. W., and Parhar, I. S. (2012). Cloning and Expression of Tachykinins and Their Association With Kisspeptins in the Brains of Zebrafish. Journal of Comparative Neurology 520, 2991-3012.

Peukert, D., Weber, S., Lumsden, A., and Scholpp, S. (2011). Lhx2 and Lhx9 Determine Neuronal Differentiation and Compartition in the Caudal Forebrain by Regulating Wnt Signaling. PLOS Biology 9(12).

Pike, S. H., Melancon, E. F., Eisen, J. S. (1992). Pathfinding by zebrafish motoneurons in the absence of normal pioneer axons. Development 114, 825,831.

Pittman, A. J., Law, M. Y., and Chien, C. B. (2008). Pathfinding in a large vertebrate axon tract: Isotypic interactions guide retinotectal axons at multiple choice points. Development 135, 2865-2871.

Powell, A. W., Sassa, T., Wu, Y., Tessier-Lavigne, M., and Polleux, F. (2008). Topography of thalamic projections requires attractive and repulsive functions of Netrin-1 in the ventral telencephalon. PLoS Biology 6(5).

Puelles, L., and Rubenstein, J. L. (2003). Forebrain gene expression domains and the evolving prosomeric model. Trends Neurosci 26, 469-476.

Raper, J. A, Bastiani, M. J, Goodman, C. S. 1984. Pathfinding by neuronal growth cones in grasshopper embryos. IV. The effects of ablating the A and P axons upon the behavior of the G growth cone. J Neurosci 4, 2329-2345.

Raper, J., and Mason, C. (2010). Cellular strategies of axonal pathfinding. Cold Spring Harb Perspect Biol 2.

Regan, J. C., Concha, M. L., Roussigne, M., Russell, C., & Wilson, S. W. (2009). An Fgf8-dependent bistable cell migratory event establishes CNS asymmetry. Neuron, 61(1), 27-34.

Ross, L. S., Parrett, T., Easter, S. S. Jr. (1992). Axonogenesis and morphogenesis in the embryonic zebrafish brain. J Neurosci 12, 467-482.

Roussigne' Myriam, Bianco H. Isaac, Wilson W. Stephen and Blader Patrick (2009). Nodal signialling imposes left-right asymmetry upon neurogenesis in the habenular nuclei. Development 136, 1549-1557.

Schindelin, J., Arganda-Carreras, I., Frise, E., Kaynig, V., Longair, M., Pietzsch, T., Preibisch, S., Rueden, C., Saalfeld, S., Schmid, B., Tinevez J. Y.,, White, D. J., Hartenstein, V., Eliceiri, K., Tomancak, P., and Cardona, A. (2012) Fiji: an open-source platform for biological-image analysis, Nature Methods 9(7), 676-682.

Schmid, R. S., Maness P. F. (2008). L1 and NCAM adhesion molecules as signaling coreceptors in neuronal migration and process outgrowth. Curr Opin Neurobiol 18, 245-250.

Shanmugalingam, S., Houart, C., Picker, A., Reifers, F., Macdonald, R., Barth, A., Griffin, K., Brand, M., and Wilson, S.W. (2000). Ace/Fgf8 is required for forebrain commissure formation and patterning of the telencephalon. Development 127, 2549-2561.

Serafini, T., Colamarino, S. A., Leonardo, E. D., Wang, H., Beddington, R.,

Skarnes, W. C., Tessier-Lavigne, M. (1996). Netrin-1 is required for commissural axon guidance in the developing vertebrate nervous system. Cell 87, 1001-1014.

Servili, A., Le Page, Y., Leprince, J., Caraty, A., Escobar, S., Parhar, I. S., Seong, JY., Vaudry, H., Kah, O. (2011). Organization of two independent kisspeptin systems derived from evolutionary-ancient kiss genes in the brain of zebrafish. Endocrinology 152(4), 1527-1540.

Seth, A., Culverwell, J., Walkowicz, M., Toro, S., Rick, J. M., Neuhauss, S. C., Varga, Z. M., and Karlstrom, R. O. (2006). belladonna/(lhx2) is required for neural patterning and midline axon guidance in the zebrafish forebrain. Development 133, 725-735.

Squirrell, J. M., Wokosin, D. L., White, J. G. and Bavister, B. D. (1999). Long-term two-photon fluorescence imaging of mammalian embryos without compromising viability. Nat. Biotechnol. 17, 763-767.

Sretavan, D. W., Feng, L., Pure, E., Reichardt, L. F. (1994). Embryonic neurons of the developing optic chiasm express L1 and CD44, cell surface molecules with opposing effects on retinal axon growth. Neuron 12, 957-975.

Staines, W. A., Nagy, J. I., Vincent, S. R. and Fibiger, H. C. (1980). Neurotransmitters contained in the efferents of the striatum. Brain Research 194, 391-402.

Stosiek, C., Garaschuk, O., Holthoff, K. and Konnerth, A. (2003). In vivo two-photon calcium imaging of neuronal networks. PNAS 100, 7319-7324.

Svoboda, K. and Yasuda, R. (2006). Principles of two-photon excitation microscopy and its applications to neuroscience. Neuron 50, 823-839.

Subach, O. M., Patterson, G. H., Ting, L. M., Wang, Y., Condeelis, J. S., and Verkhusha, V. V. (2011). A photoswitchable orange-to-far-red fluorescent protein, PSmOrange. Nature Methods 8, 771-777.

Sutherland, R. J. (1982). The dorsal diencephalic conduction system: A review of the anatomy and functions of the habenular complex. Neurosci. Biobehav. Rev. 6, 1-13.

Tello, F. (1923). Les diffe´renciations neuronales dans l'embryon du poulet, pendant les premiers jours de l'incubation. Trav Lab Invest biol Univ Madrid 21, 1-93.

Toyama, R., O'Connell, M.L., Wright, C.V., Kuehn, M.R., and Dawid, I.B. (1995). Nodal induces ectopic goosecoid and lim1 expression and axis duplication in zebrafish. Development 121, 383-391.

Valjakka, A., Vartiainen, J., Tuomisto, L., Tuomisto, J. T., Olkkonen, H., & Airaksinen, M. M. (1998). The fasciculus retroflexus controls the integrity of REM sleep by supporting the generation of hippocampal theta rhythm and rapid eye movements in rats. Brain Res Bull, 47(2), 171-184.

van der Knaap, L. J., and van der Ham, I. J. (2011). How does the corpus callosum mediate interhemispheric transfer? A review. Behav Brain Res 223, 211-221.

Wen, L., Wei, W., Gu, W., Huang, P., Ren, X., Zhang, Z., Zhu, Z., Lin, S. and Zhang, B. (2008). Visualization of monoaminergic neurons and neurotoxicity of MPTP in live transgenic zebrafish. Developmental Biology 314, 84-92.

Westerfield, M., 1995. The Zebrafish Book. The University of Oregon Press, Eugene.

Whitlock, K. E., and Westerfield, M. (1998). A transient population of neurons pioneers the olfactory pathway in the zebrafish. Journal of Neuroscience 18, 8919-8927.

Whitlock, K. E., and Westerfield, M. (2000). The olfactory placodes of the zebrafish form by convergence of cellular fields at the edge of the neural plate. Development *127*, 3645-3653.

Wilson, S. W., Ross, L. S., Parrett, T., Easter, S. S. Jr. (1990). The development of a simple scaffold of axon tracts in the brain of the embryonic zebrafish, Brachydanio rerio. Development 108, 121-145.

Wilson, S. I., Shafer, B., Lee, K. J., and Dodd, J. (2008). A molecular program for contralateral trajectory: Rig-1 control by LIM homeodomain transcription factors. Neuron 59, 413-424.

Yang, L. M., Hu, B., Xia, Y. H., Zhang, B. L., & Zhao, H. (2008). Lateral habenula lesions improve the behavioral response in depressed rats via increasing the serotonin level in dorsal raphe nucleus. Behav Brain Res, 188(1), 84-90. doi: 10.1016/j.bbr.2007.10.022

Young, R., Reyes, A., and Allende, M. (2002). Expression and splice variant analysis of the zebrafish tcf4 transcription factor. Mech. Dev. 117, 269-273.

7 Appendix

7.1 List of Abbreviations

A-P	anterior-posterior
BC	before Christ
bp	base pairs
CANs	cell adhesion molecules
cDNA	complementary DNA
CFP	cyan fluorescent protein
CLSM	confocal laser scan microscopy
cxcr4b	C-X-C chemochin receptor 4b
d	dorsal
DCC	deleted in colon-rectal carcinoma
DDC	dorsal diencephalic conduction system
dHb	dorsal habenula
dHbl	lateral dorsal habenula
dHbm	medial dorsal habenula
DIG	digoxigenin alkaline
DMSO	dimethylsulfoxide
DNA	deoxyribonucleic acid
dNTP	deoxyribonucleosidtriphosphate
dpf	day post fertilization
D-V	dorso-ventral
EDTA	ethylenediaminetetraacetate
EPC	early projecting cell
FITC	fluorescein isothiocyanate
FP	floor plate
FR	fasciculus retroflexus
Gb	gigabyte
GFP	green fluorescent protein
GHz	gigahertz
H2A	histone H2A protein

H2B	histone H2B protein
hd1	heidelberg1
hpf	hour post fertilization
KCTD	potassium channel tetramerization domain
IPN	interpeduncular nucleus
LB	luria bertani
LH	lateral hypothalamic
LPO	lateral preotic
LUT	look up table
LWD	long working distance
M	molarity
mbl	masterblind
MFB	medial forebrain bundle
MIP	maximum intensity projection
mmGFP	mammalian membrane GFP
MR	median raphe
mW	milliwatt
NA	numerical aperture
NGS	normal goat serum
NIC	Nikon imaging center
nm	nanometer
OA	olfactory areas
OB	olfactory bulb
OE	olfactory epithelium
P	Pineal
PBS	phosphate buffer saline
PCR	polymerase chain reaction
PFA	paraformaldehyde
pg	picogram
2-PM	2 photon microscopy
pp	parapineal
PSmOrange	photoswitchable monomeric orange protein
PTU	1-phenyl-2 thiourea
RNA	ribonucleic acid

ROI	region of interest
rpm	revolutions per minute
SCNs	spinal cord neurons
SM	stria medullaris
Taq	Thermophilus aquaticus
TCF	T-cell specific transcription factor
Tec	optic tectum
Tg	transgen
Th	thalamus
Tr	triton X-100
Tricain	ethyl 3-aminobenzoate methansulfonate
Tris	Tris(hydroximethil)aminomethan
v	ventral
vHb	ventral habenula
VTA	ventral tegmental area
wt	wildtype
µm	micrometer
WM	white matter

7.2 List of figure and movie legends

Figure 1.1: DDC neuronal network complexity in the mammalian brain. 13

Figure 1.2: Habenular neuronal network in the zebrafish brain. 18

Figure 3.1: All habenular domains and efferent projections innervating the ventral mid- and hindbrain are labelled in *Et(-1.0otpa:mmGFP)hd1* transgenic embryos. 31

Figure 3.2: Marker gene analysis of the ThEPC. 32

Figure 3.3: CLSM cannot be used to follow DDC system formation for more then 30 hours. 34

Figure 3.4: Long-term 2-PM *in-vivo* recording identifies interhemispheric axonal connections during habenular neural circuit development. 35

Figure 3.5: ThEPC early axonal tracking. 38

Figure 3.6: Unilateral ThEPC cell ablation causes the arrest of dHb efferent axons on both brain hemispheres. 39

Figure 3.7: Habenular neuronal circuit development in normal and ThEPC ablated embryos. 42

Figure 3.8: Failed ThEPC ablation does not affect ThEPC and dHb axon pathfinding. 43

Figure 3.9: Incomplete unilateral ThEPC cell ablation causes dHb axon pathfinding errors. 45

Figure 3.10: Unilateral dHb cell ablation does not affect axonal targeting on the contralateral side. 47

Figure 3.11: Unilateral dHb and ThEPC ablation experiments suggest a contribution of ThEPC cells to the final habenula architecture. 49

Figure 3.12: ThEPC neurons contribute to the vHb architecture. 51

Figure 3.13: *Tcf7l2* mediated Wnt/beta-catenin signaling is required for vHb development. 53

Figure 3.14: ThEPC neurons contribute to the vHb architecture under the influence of Wnt/beta-catenin pathway activity, tcf7l2 mediated. 54

MovieS1: Long-term 2-PM *in-vivo* recording of habenular neuronal circuit development, related to Figure 3.4 and 3.5. 56

MovieS2: Long-term 2-PM *in-vivo* recording of habenular neuronal circuit development (black and white), related to Figure 3.4 and 3.5. 56

MovieS3: Complete unilateral ThEPC laser ablation followed by long-term 2-PM *in-vivo* recording of habenular neuronal circuit development, related to Figure 3.6. 56

MovieS4: Complete unilateral ThEPC laser ablation followed by 2-PM *in-vivo* recording of habenular neuronal circuit development (black and white), related to Figure 3.6. 57

MovieS5: Sequential unilateral ThEPC cell laser ablation followed by 2-PM *in-vivo* recording of habenular neuronal circuit development, related to Figure 3.7. 57

MovieS6: Sequential unilateral ThEPC cell laser ablation followed by long-term 2-PM *in-vivo* recording of habenular neuronal circuit development, related to Figure 3.7. . 57

MovieS7: The ThEPCs are composed of mixed populations of deviding cells and postmitotic neurons, related to Figure 3.1 and 3.2. 57

MovieS8: A population of ThEPC cells contribute to the vHb and is absent in embryos mutant for *tcf7l2*, related to Figure 3.12 and 3.14. 58

7.3 Imagej Script: MIP_ColourCode.ijm

```
// MIP_ColourCode Script
// Create the MIP and the Slice from the original stacks

	showMessage("Running MIP", "<html>"
	    +"<font size=+2>MIP Script");

	beep();
	showStatus("Choose the INPUT directory");
	dir_in = getDirectory("Choose the INPUT directory containing the source images");
	if (lengthOf(dir_in) == 0) {
	   exit();
	}
	beep();
	showStatus("Create the OUTPUT root directory, i.e.:MIP");
	dir_out = getDirectory("Choose the OUTPUT root directory");
	if (lengthOf(dir_out) == 0) {
	   exit();
	}

	dir_max = dir_out;
	dir_slices = dir_out;

// Get a list of files in the input directory

	file_list = getFileList(dir_in);
	setBatchMode(true);

// Loop through the files

	print("Number of files: " + file_list.length);
	for (i=0; i<file_list.length; i++) {
	   if (endsWith(file_list[i], '.tif')) {

	   // Open the image

			open(dir_in + file_list[i]);

			//-----
			if (i == 0) {
				setBatchMode(false);
				run("Properties...");
				getVoxelSize(width, height, depth, unit);
				setBatchMode(true);
			} else {
				setVoxelSize(width, height, depth, unit);
			}
			//-----

			id_stack = getImageID();

	   // Compute the maximum projection

			run("Z Project...", " projection=[Max Intensity]");
			id_max = getImageID();
			title_max = getTitle();

	   // Find the first slices containing the maxima

			selectImage(id_stack);
			run("NIC find values", "compare=["+title_max+"] choose=First");
			id_slices = getImageID();
			setVoxelSize(width, height, depth, unit);

	   // Write the Slices

			saveAs("Tiff", dir_slices+"Slices_"+file_list[i]);
			selectImage(id_max);

	   // Write the MIP

			saveAs("Tiff", dir_max+"Max_"+file_list[i]);
```

```
        // Close the images, reclaim memory, and update the log
                run("Close All");
                call("java.lang.System.gc");
                showStatus("Completed");
                print("Completed: " + file_list[i]);
        }
    }
    setBatchMode(false);
    beep();
    showMessage("Running MIP", "<html>"
        +"<font size=+2>Finished MIP!");

// Apply the ColurCode to the MIP

    ColourCode = getBoolean("Do you want to run the Colour Code Script on the MIP?");
    if (ColourCode) {
        beep();
        showStatus("Choose the INPUT directory");
        dir_in = getDirectory("Choose the INPUT directory containing the source images");
        if (lengthOf(dir_in) == 0) {
        exit();
        }

        beep();
        showStatus("Create the OUTPUT root directory, i.e.:ColourMIP");
        dir_out = getDirectory("Choose the OUTPUT root directory");
        if (lengthOf(dir_out) == 0) {
        exit();
        }

// Read the maximum projection and slice stacks
// Give these unique titles, so that they can be identified by Calculator Plus later

        run("Image Sequence...", "open=[" + dir_in + "] scale=100 or=Max_.*.tif or=[] sort");
        id_max = getImageID();
        title_max = "Slices_"+abs(id_max)+getTitle();
        rename(title_max);
        run("Image Sequence...", "open=[" + dir_in + "] scale=100 or=Slices_.*.tif or=[] sort");
        id_slices = getImageID();
        title_slices = "Slices_"+abs(id_slices)+getTitle();
        rename(title_slices);

// Compute the neighbourhood range for slices
// If a region is part of the specimen, it will tend to contain values in the MIP all obtained from the
// same slice of the stack. However, background regions containing noise only will usually have
// maxima from different slices. For better visual discrimination of depths, we want the LUT colours
// to be distributed between slices in which the specimen is visible, with any extra slices acquired
// above or below (containing noise/blur only) to be given the first or last LUT colours.
// The following code achieves this automatically by looking for the highest and lowest slices in which// there
are any regions containing stack maxima from the same slice or its immediate neighbours.

        run("Duplicate...", "title=[Min slices] duplicate");
        run("Minimum...", "radius=1 stack");
        id_slices_min = getImageID();
        selectImage(id_slices);
        run("Duplicate...", "title=[Range slices] duplicate");
        run("Maximum...", "radius=1 stack");
        id_slices_range = getImageID();
        imageCalculator("Subtract stack", id_slices_range, id_slices_min);

// Get where the range is <= 3

        setThreshold(0, 3);
        run("Convert to Mask", "black");
        run("Max...", "value=1 stack");
        imageCalculator("Divide create 32-bit stack", id_slices, id_slices_range);
        Stack.getStatistics(voxelCount, mean, slice_first, slice_last, stdDev);

// Close images that are no longer needed

        close();
        selectImage(id_slices_min);
        close();
        selectImage(id_slices_range);
```

```
    close();

// Set the LUT

    selectImage(id_slices);
    setMinAndMax(slice_first, slice_last);
    run("ColourCode");
    run("RGB Color");

// Create 8-bit version of maximum projection, and make it RGB to match the colour image

    selectImage(id_max);
    run("Enhance Contrast", "saturated=0.4 use");
    run("Gamma...", "value=0.75 stack");
    run("Enhance Contrast", "saturated=0.4 use");
    run("8-bit");
    run("RGB Color");

// Multiply the two images
// Calculator Plus makes it possible to scale the result (by 1/255) to ensure it fits into a 24-bit RGB result

    scale = 1/255;
    getVoxelSize(width, height, depth, unit);
    run("Calculator Plus", "i1=" + title_max + " i2=" + title_slices + " operation=[Multiply: i2 = (i1*i2) x k1 + k2]
k1="+scale+" k2=0 create");
    setVoxelSize(width, height, depth, unit);

// Add ScaleBar and TimeFrame on the ColourCodeMIP

    run("Properties...");
    run("Gamma...", "value=0.75 stack");
    run("Scale Bar...", "width=50 height=4 font=24 color=White background=None location=[Lower Right] bold
label");
    run("Label...");

// Save the result as ColourMIP.tiff and .avi

    fileName = dir_out+"ColourMIP_Time_" + slice_first + "-" + slice_last;
    saveAs("Tiff", fileName + ".tiff");
    saveAs("avi", dir_out + "ColourMIP.avi");
    close();

// Close LUT Image

    selectImage(id_slices);
    close();

// Add ScaleBar and TimeFrame on the MIP

    run("Properties...");
    run("Scale Bar...", "width=50 height=4 font=24 color=White background=None location=[Lower Right] bold
label");
    run("Label...");

// Save the result as MIP.tiff and avi

    fileName = dir_out+"MIP_Time_" + slice_first + "-" + slice_last;
    saveAs("Tiff", fileName + ".tiff");
    saveAs("avi", dir_out + "MIP.avi");
    close();

// Print out the slices that were used

    print("First coloured slice: " + slice_first);
    print("Last coloured slice: " + slice_last);
    print("Total coloured slices: " + (slice_last - slice_first)+1);

    beep();
    showMessage("ColourMIP", "<html>"
    +"<font size=+2>Finished the Colour Code Script");
} else {
    exit
}

// Add Spectrum Colour Bar to ColourCode.avi
```

```
beep();
ColourCodeBar = getBoolean("Do you want to add the ColourCodeBar?");
if (ColourCodeBar) {
   newImage("ColourCodeBar", "8-bit Ramp", 1024, 25, 1);
   run("ColourCode");
   run("Rotate 90 Degrees Right");
   beep();
   showStatus("Open ColourCode LUT");
   open(dir_out + "ColourMIP.avi");
   run("Add Image...", "opacity=100");
```

// Save the result as ColourCodeMIPBar.avi

```
saveAs("avi", dir_out + "ColourCodeMIPBar.avi");
run("Close All");
print("Completed");
} else {
   run("Close All");
   print("Completed");
}
```

7.4 NIC Find Maxima Plugin

```
import java.util.Vector;

import ij.gui.GenericDialog;
import ij.gui.NewImage;
import ij.plugin.PlugIn;
import ij.process.ImageProcessor;
import ij.IJ;
import ij.ImagePlus;
import ij.ImageStack;
import ij.WindowManager;


/**
 * Plugin to identify the first or last slices in a stack in which particular values occur.
 * The values being searched for can be constants, or vary according to each x,y coordinate.
 *
 * This is useful to help create a depth-colour-coded maximum intensity projection (MIP).
 * The general process is as follows:
 * - Compute the MIP using ImageJ's Z Project... command
 * - Use find values plugin to identify the slices on which the maximum values occurred
 * - Assign a suitable, colourful LUT to the slice image
 * - Scale the brightness of the pixels in the slices image according to the MIP image values
 *
 * @author Peter Bankhead
 *
 */
public class NIC_find_values implements PlugIn {

	protected ImagePlus imp;
	protected boolean compareConstant = false;
	protected float constant;
	protected ImagePlus impCompare;
	protected boolean findLast = false;

	@Override
	public void run(String arg) {
		// Get the image stack to compare
		imp = IJ.getImage();
		if (imp == null) {
			IJ.noImage();
			return;
		}

		// Create dialog to choose 2D image/constant with which to compare
		int width = imp.getWidth();
		int height = imp.getHeight();
		WindowManager.getIDList();
		Vector<String> namesCompare = new Vector<String>();
		namesCompare.add("Use Constant Value");
		int[] ids = WindowManager.getIDList();
		// Make a list of all the open images that have the same width and height, but
a z and time depth of 1
		for (int i = 0; i < ids.length; i++) {
			ImagePlus impTemp = WindowManager.getImage(ids[i]);
			if (impTemp != imp && impTemp.getWidth() == width &&
impTemp.getHeight() == height &&
```

```
                                        impTemp.getNSlices() == 1 &&
impTemp.getNFrames() == 1 &&
                                        impTemp.getNChannels() == 1) {
                                namesCompare.add(impTemp.getTitle());
                        }
                }
                GenericDialog gd = new GenericDialog("Find values along dimension");
                gd.addMessage("Dimension search for " + imp.getTitle());
                String[] strCompare = new String[namesCompare.size()];
                namesCompare.toArray(strCompare);
                gd.addChoice("Compare with image", strCompare, strCompare[0]);
                gd.addNumericField("Constant Value", 0, 5);
                gd.addMessage("Constant Value will be ignored if comparing with an
image");
                String[] strOccurrence = new String[]{"First", "Last"};
                gd.addChoice("Choose occurrence", strOccurrence, strOccurrence[0]);

                // Show dialog
                gd.showDialog();
                if (gd.wasCanceled())
                        return;

                // Get the image or constant with which to compare
                String titleCompare = gd.getNextChoice();
                constant = (float)gd.getNextNumber();
                if (titleCompare.equals(strCompare[0]))
                        compareConstant = true;
                else
                        impCompare = WindowManager.getImage(titleCompare);
                // Determine whether are looking for the first or last instance of the values in
the stack
                findLast = gd.getNextChoice().equals("Last");

                // Create an output image - use 8-bit if the stack contains < 256 slices,
otherwise 16-bit
                ImagePlus impOutput;
                if (imp.getStackSize() / imp.getNChannels() <= 255)
                        impOutput = NewImage.createByteImage("Find_" + imp.getTitle(),
width, height, 1, NewImage.FILL_BLACK);
                else
                        impOutput = NewImage.createShortImage("Find_" + imp.getTitle(),
width, height, 1, NewImage.FILL_BLACK);

                // Loop through the original image stack looking for the comparison values,

                // and write the slices on which they occur to the output image
                ImageStack stack = imp.getStack();
                ImageProcessor ipCompare = null;
                if (!compareConstant)
                        ipCompare = impCompare.getProcessor();
                ImageProcessor ipOutput = impOutput.getProcessor();
                for (int s = 1; s <= stack.getSize(); s++) {
                        IJ.showProgress(s, stack.getSize());
                        ImageProcessor ip = stack.getProcessor(s);
                        for (int i = 0; i < width * height; i++) {
                                float comp = compareConstant ? constant :
ipCompare.getf(i);
                                if (ip.getf(i) == comp) {
                                        if (findLast || ipOutput.getf(i) == 0)
                                                ipOutput.set(i, s);
```

```
                                        }
                                }
                        }
                        // Show the output image
                        impOutput.show();
                }
        }
```

7.5 Imagej Macro: Colocalisation_H2B-PSmOrange.ijm

```
// Colocalisation H2B-PSmOrange

	setBatchMode(true);

	dir_out = getDirectory("Choose the OUTPUT root directory");
	if (lengthOf(dir_out) == 0) {
	   exit();
	}

	run("Bio-Formats Importer", "color_mode=Default view=Hyperstack stack_order=XYCZT");

	idOrig = getImageID();
	run("Duplicate...", "duplicate channels=1");
	idCh1 = getImageID();
	run("Enhance Contrast", "saturated=0.35 stack");

// Detect on Channel 1 to make ROIs

	run("Duplicate...", "duplicate");
	run("32-bit");
	idCh1Filtered = getImageID();
	run("Gaussian Blur 3D...", "x=6 y=6 z=1");
	imageCalculator("Subtract stack", idCh1Filtered, idCh1);
	run("Multiply...", "value=-1 stack");
	run("Gaussian Blur 3D...", "x=1 y=1 z=0.5");
	setAutoThreshold("Triangle dark stack");

// Analyze Particles Channel 1
// Exclude very small detections (< 5 pixels)

	run("Analyze Particles...", "size=5-Infinity circularity=0.00-1.00 show=Masks add in_situ stack");
	roiManager("Show All without labels");
	roiManager("Show All");
	roiManager("Set Color", "green");
	roiManager("Save", dir_out + "488_ROI.zip");

// Open Channel 3 and add the Channel 1 overlay

	selectImage(idOrig);
	run("Duplicate...", "duplicate channels=3");
	idCh3 = getImageID();
	roiManager("Show All without labels");
	roiManager("Show All");
	run("From ROI Manager");
	run("Enhance Contrast", "saturated=0.35 stack");
	saveAs("Tiff", dir_out + "C3_488_ROI.tif");
	roiManager("Delete");

// Detect on Channel 3 to make ROIs

	run("Duplicate...", "duplicate");
	idCh3Filtered = getImageID();
	run("32-bit");
	run("Gaussian Blur 3D...", "x=16 y=16 z=1");
	imageCalculator("Subtract stack", idCh3Filtered, idCh3);
	run("Multiply...", "value=-1 stack");
	run("Gaussian Blur 3D...", "x=1 y=1 z=0.5");
	setAutoThreshold("Moments dark stack");

// Analyze Particles Channel 3
// Exclude very small detections (< 3 pixels)

	run("Analyze Particles...", "size=3-Infinity circularity=0.00-1.00 show=Masks add in_situ stack");
	roiManager("Set Color", "red");
	roiManager("Save", dir_out + "637_ROI.zip");

// Select Channel 1 and add the Channel 3 overlay

	selectImage(idCh1);
	roiManager("Show All without labels");
	roiManager("Show All");
```

```
run("From ROI Manager");
saveAs("Tiff", dir_out + "C1_637_ROI.tif");
close();
```

// Find the detected regions overlapping in Channel 1 and Channel 3

```
imageCalculator("AND stack", idCh1Filtered, idCh3Filtered);
idOverlaps = idCh1Filtered;
selectImage(idOverlaps);
roiManager("Delete");
run("Analyze Particles...", "size=3-Infinity circularity=0.00-1.00 show=Nothing add stack");
roiManager("Set Color", "yellow");
roiManager("Save", dir_out + "Overlay_ROIs.zip");
roiManager("Delete");
```

// Add ROI C1/C3 in C2 Channel

```
selectImage(idOrig);
run("Duplicate...", "duplicate channels=2");

list = getFileList(dir_out);
for (i=0; i<list.length; i++) {
   if (endsWith(list[i], ".zip"))
                roiManager("open", dir_out +list[i]);
}

roiManager("Show All without labels");
roiManager("Show All");
run("From ROI Manager");
run("Enhance Contrast", "saturated=0.35 stack");
saveAs("Tiff", dir_out + "Overlay_C2_ROIs.tif");
run("Close All");
call("java.lang.System.gc");
showStatus("Completed");
```

Acknowledgment

Someone, called Albert Einstein, said: ”Not everything that can be counted counts, and not everything that counts can be counted”. Is the verb *count* just related to a specific quantification of a certain event? In my opinion, the meaning of the word *count* is quite ambiguous within the numbers and probably more difficult if applied to people all over the time. However, during my PhD I recognized that *count* on people is basically the key to success.

I want to especially thank my supervisor, Dr. Matthias Carl, whose guidance was essential to my scientific growth. He was always enthusiastically interested in my work and he never locked up the door of his office even if he was already overextended with his own business. Second, I would like to acknowledge my advisors Professor Dr. Joachim Wittbrodt and Professor Dr. Michael Boutros for supporting my PhD project and for critically discussing each result carried out in the last three years.

A special thank you to Dr. Nicolas Dross that spent hours in the dark with me to measure samples and taught me whatever I wanted to know about 2 photon microscopy and CLSM. Dr. Peter Bankhead, that contributes to my scientific growth investing his working and spare time to answer all of my questions on ImageJ macro language, Fiji and image analysis. Ulrike Engels has given me the opportunity to perform my experiments in a stimulating environment, such as the Nikon Imaging Center (NIC) and she carefully followed every single step of my project. Further, thanks to all of the members and users of NIC, to tolerate the large amount of data stored on the Bioqunat server without too many complainings. I promise, as soon as possible I will delete all of them.

The past and the present members of the Zbio, Dkfz and Poggi’s lab; a special thank you to Ulrike Hüsken, Juan Manuel Gomez, Jun Zhou and Alessio Paolini for the time together in the lab but also for the nights of complaining about the bloody experiments and our bosses.

Leaving behind the scientific environment, I would like to thank my girlfriend Leila Kraft. In the last months, I could count on her any single moment and she was so kind not to break up with me due too all my endless complainings

about the writing, the lab and the “final” experiments. Finally, I thank all of my relatives; in the last three years, they unconditionally advised, motivated and supported every my single decision.

In conclusion, probably not everything can be counted but *count* on people can always be a way to broaden the personal horizons. At least this one is my own experience.